TAMPEREEN TEKNILLINEN YLIOPISTO
TAMPERE UNIVERSITY OF TECHNOLOGY
Julkaisu 731 • Publication 731

Lasse Orsila

Optical Thin Film Technology for Ultrafast Fiber Lasers

Tampere 2008

Tampereen teknillinen yliopisto. Julkaisu 731
Tampere University of Technology. Publication 731

Lasse Orsila

Optical Thin Film Technology for Ultrafast Fiber Lasers

Thesis for the degree of Doctor of Technology to be presented with due permission for public examination and criticism in Tietotalo Building, Auditorium TB104, at Tampere University of Technology, on the 25th of April 2008, at 12 noon.

Tampereen teknillinen yliopisto - Tampere University of Technology
Tampere 2008

ISBN 978-952-15-1955-0 (printed)
ISBN 978-952-15-2018-1 (PDF)
ISSN 1459-2045

ABSTRACT

This thesis investigates novel dispersion compensation methods for mode-locked fiber lasers and the dynamical properties of ytterbium and thulium-holmium gain materials. The emphasis is on dielectric thin film structures and their integration into fiber cavities to control laser performance.

A Gires–Tournois interferometer (GTI) made with electron beam evaporation was used for the first time to compensate for the dispersion of a fiber cavity and thus achieve ultrashort mode-locked pulses. Another thin film dispersion compensator, a Fabry-Pérot etalon, demonstrated in a mode-locked fiber laser, allowed for continuously tunable short pulse operation of an ytterbium fiber laser over a broad wavelength range.

In addition to dispersive thin film structures, the thesis also presents a new type of dichroic coating deposited directly onto an optical fiber end. The dichroic coating acts as an output coupler and pump combiner, simultaneously. This enables laser cavities which are substantially shorter than would be possible with conventional fiber components. The compact all-fiber ytterbium fiber laser presented had a record high fundamental repetition rate of 571 MHz with ultrashort, 572 fs, pulses.

The energy level scheme of ytterbium and thulium-holmium gain materials was studied for the first time in this thesis by analyzing the laser relaxation oscillations. Both materials exhibited a change in transition mechanism from three-level to four-level laser operation in the long-wavelength tail of the gain bandwidth.

ACKNOWLEDGMENTS

The work presented in this thesis was carried out at the Optoelectronics Research Centre (ORC) at Tampere University of Technology from 2003 to 2007. I gratefully acknowledge the financial support provided by the Graduate school of Electronics, Telecommunication and Automation (GETA), by the Finnish Foundation for Advanced Sciences (TES), by the Finnish Academy of Science and Letter's Vilho, Yrjö and Kalle Väisälä Foundation, by the Jenny and Antti Wihuri Foundation, by the Magnus Ehrnrooth Foundation, by the European Commission through the URANUS and NATAL projects, and by the Academy of Finland through the Tule-QUEST project.

I would like to thank my supervisor Professor Oleg Okhotnikov for his important role in the research carried out in this thesis and his enthusiastic guidance of my work at ORC, Professor Markus Pessa for giving me the opportunity to work at ORC and for the continuous support along the way and Dr. Mircea Guina for guidance and valuable discussions during the thesis. I must also remember to thank Anne Viherkoski for her great help along the way and for leveling bureaucratic obstacles.

I thank my excellent current and former colleagues Dr. Robert Herda, Dr. Matei Rusu, Dr. Antti Isomäki, Dr. Luís Gomes, Dr. Claudio Porzi, M.Sc. Tommi Hakulinen, M.Sc. Samuli Kivistö, M.Sc. Esa Saarinen, M.Sc. Jussi Rautiainen and M.Sc. Juho Kerttula for fruitful co-operation during these many years. Moreover, I want to especially thank Dr. Antti Härkönen for being my office mate and a friend during my time at ORC.

I also want to thank the whole ORC research staff for supporting my work. Particularly I want to mention the processing people Pirjo Leinonen and Jukka Viheriälä, MBE growers Jari Lyytikäinen, Tomi Leinonen and Soile Suomalainen, and Antti Tukiainen concerning material characterization. I also remember the help from my former colleague Markus Peltola with the electron beam evaporator in the early stages of the work and also Jari Näppi for valuable discussions and hints for thin film problems.

My work at ORC has also benefited from co-operation with several companies including EpiCrystals, Fianium, Modulight, Nokia, Planar and RefleKron.

I thank Dr. Charis Reith for proofreading the thesis and giving valuable suggestions and pre-examiners Dr. John Clowes and Dr. Sergey Vainshtein for comments and review of my thesis.

I also want to thank my family and relatives, especially my parents-in-law, my parents, my wife Reetta and little Aino for support and motivation for my work.

Tampere, Finland, April 2008

Lasse Orsila

TABLE OF CONTENTS

Abstract i

Acknowledgments iii

Table of Contents v

List of Publications vii

Author's contribution ix

List of Abbreviations xi

1. Introduction 1

1.1 A brief history of optical thin films and fiber lasers 1

1.1.1 Thin films 1

1.1.2 Lasers 2

1.1.3 Fiber lasers 3

1.2 State of the art 4

1.3 Incentives and outline 5

2. Optical thin films 7

2.1 Introduction to thin films 7

2.2 Thin film properties 8

2.3 Mechanical properties of optical thin films 10

2.4 Manufacturing thin films 11

2.5 Electron beam evaporation 12

2.6 Basic optical thin film theory 13

2.7 Thin film design 19

2.7.1 Anti-reflection coatings 20

2.7.2 High reflective coatings 26
2.7.3 Dichroic coatings 29
2.7.4 Dispersive mirrors 31
2.8 Summary 37
3. Ytterbium mode-locked fiber lasers 39
3.1 Mode locking 39
3.1.1 Active mode locking 39
3.1.2 Passive mode locking 40
3.2 Ytterbium fiber lasers 41
3.2.1 Saturable absorbers 42
3.2.2 Fiber components 43
3.3 Dispersion compensation techniques for the 1 μm region 44
3.4 GTI dispersion compensation 47
3.5 Fabry–Pérot etalons for dispersion compensation 51
3.6 Summary 53
4. Fiber laser dynamics and relaxation oscillations 55
4.1 Dynamics 55
4.2 Relaxation oscillations 56
4.3 Ytterbium 58
4.4 Thulium-holmium 60
4.5 Summary 62
5. High repetition rate short pulse fiber lasers 63
5.1 Why high repetition rate? 63
5.2 Dichroic fiber end facet coatings 64
5.3 Compact fiber laser with photonic crystal fiber 68
5.4 Summary 70
6. Conclusions 71
Bibliography 73

LIST OF PUBLICATIONS

This thesis contains the following six publications, which are included as appendices. In the text, these publications are referred to as [P1]...[P6]. In addition to this, the thesis contains new, unpublished material e.g. dispersion measurements that verify the modeled dispersion curves presented in [P1] and [P2], and a novel dispersion compensation scheme integrating a dispersive mirror into a prism.

[P1] L. A. Gomes, L. Orsila, T. Jouhti, and O. G. Okhotnikov, "Picosecond SESAM based ytterbium mode-locked fiber lasers," *IEEE Journal of Selected Topics in Quantum Electronics*, vol. 10, no. 1, issue on Ultrafast Science and Technology, pp. 129–136, 2004.

[P2] L. Orsila, L. A. Gomes, N. Xiang, T. Jouhti, and O. G. Okhotnikov, "Mode-locked ytterbium fiber lasers," *Applied Optics*, vol. 43, no. 9, pp. 1902–1906, 2004.

[P3] L. Orsila and O. G. Okhotnikov, "Three- and four-level transition dynamics in Yb-fiber laser," *Optics Express*, vol. 13, no. 9, pp. 3218–3223, 2005.

[P4] L. Orsila, R. Herda, T. Hakulinen and O. G. Okhotnikov, "Thin-film Fabry–Pérot dispersion compensator for mode-locked fiber lasers," *IEEE Photonics Technology Letters* vol. 19, no. 1, pp. 6–8, 2007.

[P5] L. Orsila, S. Kivistö, R. Herda and O. G. Okhotnikov, "Spectroscopy of the relaxation dynamics in Tm-Ho-fiber lasers," in *Conference Digest of European Conference on Lasers and Electro-Optics 2007,* München, 20–25 June, 2007, p. CE-24-TUE.

[P6] L. Orsila, R. Herda and O. G. Okhotnikov, "Monolithic fiber mirror and photonic crystal technology for high repetition rate all-fiber soliton lasers," *IEEE Photonics Technology Letters*, vol. 19, no. 24, pp. 2009–2011, 2007.

In addition to the papers included in this thesis, the following supplementary papers are related to this work but are not appended to this dissertation. In the text, these publications are referred to as [S1]...[S3]. I have also made contributions to other publications concerning thin films [1–12], optoelectronics [13–24] and fiber technology [25–27] but they are beyond the scope of this thesis.

[S1] L. Orsila, L. Gomes, O. G. Okhotnikov, "Mode-locked ytterbium fiber laser dispersion compensation with Gires–Tournois interferometer," in *Proceedings of the Optics Days 2004,* Turku, Finland, 6–7 May, 2004, p. 49.

[S2] L. Orsila, "Economic thin film in-situ monitoring in electron-beam evaporation using optical fiber back reflection," in *Proceedings of the Optics Days 2004,* Turku, Finland, 6–7 May, 2004, p. 48.

[S3] L. Orsila, R. Herda, T. Hakulinen and O. G. Okhotnikov, "Thin-film dispersion compensator for mode-locked fiber lasers," in *Conference Digest of European Conference on Lasers and Electro-Optics,* 2007, München, 20–25 June, 2007, p. CF-21-MON.

AUTHOR'S CONTRIBUTION

This thesis includes six papers published in international peer-reviewed journals and scientific conferences. It also contains material from supplementary publications and new unpublished results.

The work presented here is a result of teamwork. I have been directly responsible for designing and manufacturing the optical thin films presented in this thesis and building several of the measurement systems presented here. I have also had a major role in writing the papers and carrying out most of the measurements presented in this thesis and the included publications.

A summary of my contribution to the included papers is listed in Table 1 below.

Table 1: *Author's contribution to the papers and to the experimental research work.*

Paper	Contribution in experimental work	Contribution in writing the paper
[P1]	Group work (30 %)	Co-author (20 %)
[P2]	Group work (80 %)	Co-author (30 %)
[P3]	Main author	Co-author (50 %)
[P4]	Group work (80 %)	Co-author (60 %)
[P5]	Group work (80 %)	Main author
[P6]	Group work (90 %)	Main author

LIST OF ABBREVIATIONS

APC	Angle polished Physical Contact
APM	Additive Pulse Mode locking
AR	Anti-Reflection
ASE	Amplified Spontaneous Emission
CARS	Coherent Anti-Stokes Raman Scattering
CDBR	Chirped DBR
CFBG	Chirped Fiber Bragg Grating
COD	Catastrophic Optical Damage
CPA	Chirped Pulse Amplification
CVD	Chemical Vapor Deposition
cw	continuous wave
DBR	Distributed Bragg Reflector
DCM	Double Chirped Mirror
DND	Direct Nanoparticle Deposition
D-SAM	Dispersion-compensating Saturable Absorber Mirror
EB	Electron Beam
ESA	Electrical Spectrum Analyzer
FOM	Figure Of Merit
FC/PC	FC type / Physical Contact

FP	Fabry–Pérot
FWHM	Full Width at Half Maximum
GD	Group Delay
GDD	Group Delay Dispersion
GTI	Gires–Tournois Interferometer
GTIP	Gires–Tournois Interferometer Prism
GVD	Group Velocity Dispersion
HR	High Reflective
IR	Infrared
KLM	Kerr-Lens Mode locking
LIDAR	Light Detection And Ranging
MBE	Molecular Beam Epitaxy
ML	Mode Locking
MM	Multi-Mode
MOPA	Master Oscillator Power Amplifier
NALM	Nonlinear Amplifying Loop Mirror
NLSE	NonLinear Schrödinger Equation
PBGF	Photonic Band Gap Fiber
PCF	Photonic Crystal Fiber
PVD	Physical Vapor Deposition
QSML	Q-Switched Mode Locking
QW	Quantum Well
RF	Radio Frequency
RSAM	Resonant Saturable Absorber Mirror

RTA	Rapid Thermal Annealing
SAM	Saturable Absorber Mirror
SBS	Stimulated Brillouin Scattering
SC-PBGF	Solid-Core Photonic Bandgap Fiber
sech	Hyperbolic secant, $sech(x) = \frac{1}{cosh(x)} = \frac{2}{e^x + e^{-x}}$
SESAM	SEmiconductor Saturable Absorber Mirror
SM	Single-Mode
SPM	Self-Phase Modulation
SRS	Stimulated Raman Scattering
TE	Transverse Electric
TM	Transverse Magnetic
TOD	Third Order Dispersion
TPA	Two-Photon Absorption
TPE	Two-Photon fluorescence Excitation
UV	Ultraviolet
VECSEL	Vertical-External-Cavity Surface-Emitting Laser
WDM	Wavelength Division Multiplexer

1. INTRODUCTION

> *Optical coatings are traditionally thought to be rather mysterious with the unexpected the norm and success dependent on skill and experience and a certain degree of good fortune. However there are excellent reasons for even the extremely bizarre behavior of coatings and it is an understanding of these reasons that is the key to real, effective, expertise in the subject.*
>
> Professor H. Angus Macleod

1.1 A brief history of optical thin films and fiber lasers

1.1.1 Thin films

Thin film optics has a very long history dating back to the prehistoric era, when man could have observed thin films of oil on calm water. Man-made thin films became possible around 1600 B.C., when amalgam was discovered and could be laid on thin gold films. Ever since, the colors of thin films have fascinated people and a great number of descriptions has been written on the subject. [28]

The earliest scientific observations of thin films date back to the 17th century, when Robert Hooke (1635–1703) [29] and Robert Boyle (1627–1691) [30] independently discovered the phenomenon know as 'Newton's rings.' This phenomenon can nowadays easily be explained by interference in a single film with varying thickness. However, at the time, the nature of light was not sufficiently well understood to explain the first observations or experiments made later by Sir Isaac Newton (1642–1727) [31, 32]. Nevertheless, Newton's experiments went far beyond qualitative description when he published his findings in his Optiks (1704). He related the colors so accurately to the thicknesses of the films that Thomas Young (1773–1829) [33] could, some hundred years later, calculate accurately the associated wavelengths of light from the data [28]. In his findings Young introduced the principle of interference and gave the first satisfactory explanation for the effect. His wave theory

was strongly opposed at first but then became slowly recognized after Augustin Jean Fresnel's (1788–1827) work on diffraction patterns arising from various obstacles and apertures [33].

The next significant step in thin film history was the discovery of the anti-reflecting properties of low refractive index layers by Joseph von Fraunhofer (1787–1826) [34], even though he did not realize that, not only was the reflection reduced, but also that the transmission was increased. However, this wasn't significant at the time because optical components were not complicated enough to make the need obvious. Once the wave theory was widely accepted and optical technology started to develop, great progress was made during the remainder of the nineteenth century and early twentieth century.

The most significant development in terms of thin film technology was the Fabry–Pérot interferometer invented in 1897 [35] by Charles Fabry (1867–1945) [36, 37] and Jean-Baptiste Alfred Pérot (1863–1925) [38], which became one of the basic structures for thin film filters. Despite the theoretical progress, thin film development did not start its radical upswing until the invention of suitable vacuum pumps and the work of Cecil Reginald Burch (1901–1983) [39] on diffusion pump oil in the 1920s [40]. Ever since, progress has been enormous, and the work of thousands of thin film scientists has produced a large number of new applications covering all areas of life. These days complex layer structures having over 100 layers are not uncommon and almost all products available to buy incorporate some kind of thin films. [32]

1.1.2 Lasers

The basic principle of the laser was presented in 1954, when Charles Townes and Arthur Schawlow invented the maser (**m**icrowave **a**mplification by **s**timulated **e**mission of **r**adiation), using ammonia gas and microwave radiation. The same research was also conducted elsewhere, which led to the Nobel Prize for this work being shared between Charles H. Townes (1915–), Nikolai G. Basov (1922–2001) and Aleksandr M. Prokhorov (1916–2002) in 1964 [41]. A logical continuation of the maser was the laser (**l**ight **a**mplification by the **s**timulated **e**mission of **r**adiation) and it was first presented by Theodore Harold Maiman (1927–2007) [42] in 1960. His ruby laser [43] is considered to be the first successful optical or light coherent source even though similar work was carried out by Gordon Gould (1920–2005). The laser consisted of a ruby rod with silvered ends as mirrors and was pumped with a flashlamp. The ruby laser was not capable of continuous wave (cw) operation but just before the end of

1960 the first gas laser using helium and neon appeared. This type of laser (a He-Ne laser) was the dominant laser for the next 20 years until cheap semiconductor lasers appeared.

Thin film technology was boosted by the emergence of the microprocessor industry in the 1960s and 1970s, since they share several technical aspects. However, the surge in demand for optical thin films came after semiconductor laser diode mass production started and all fields of optics started growing rapidly. Nowadays hundreds of millions of semiconductor laser diodes are produced annually and they are all coated with optical thin films.

1.1.3 Fiber lasers

Optical fiber gain experiments were performed already in 1961 [44, 45] and the first fiber laser was demonstrated in 1964 [46], but cw single-mode fiber lasers only appeared in the mid 1980s as a result of dramatic improvement in optical fiber quality [47] and doping technology [48]. At first the emphasis was on telecom applications like fiber amplifiers with simple fiber coupler configuration to deliver the pump light to the amplifying fiber [49]. A few years later short pulse fiber lasers were demonstrated [50]. The pulsed fiber laser presented in 1986 was a Q-switch laser [51] delivering 200 ns pulses. Soon after the laser was mode-locked [52] and the pulse duration was shortened by two orders of magnitude down to ns-level. However, the operation was flawed due to intracavity reflections at the fiber end facets and pulse widths shorter than 1 ns were not obtained [53]. The laser design was further improved and 100 ps pulses were reported by several research groups in 1988 [54, 55]. Significant progress followed in the next years as well-defined mode locking with 20 ps pulses was demonstrated in 1989 [56] and in the same year soliton-shaping was first used by Kafka et al. to push the pulse widths below 5 ps [57].

Subpicosecond fiber laser configurations were already suggested by Kafka and Baer in 1987 (patent [58] issued in 1989) but the era of ultrashort pulse fiber lasers only started in 1990 as subpicosecond pulses were first presented by Fermann et al. in an actively mode-locked Nd-doped fiber laser with additional soliton shaping [59]. The laser produced 430 fs pulses and the next year the technique was further optimized to produce 125 fs pulses [60]. This laser was the first truly passively mode-locked fiber laser. However, until then ultrashort pulse fiber lasers contained a large amount of bulk components and complicated active components, not to mention the often inconvenient pumping systems. In parallel to Fermann, Duling demonstrated an all-fiber laser design, which was the first self-starting passively mode-locked fiber laser and

produced at first 3.3 ps pulses [61] and soon after 314 fs pulses [62]. This demonstration was among the first lasers in which fiber laser advantages over bulk solid state lasers started to appear. In the following years, fiber materials and lasers continued to improve, but the main applications remained in the telecom sector until 2001 when the sudden economic downfall shifted the emphasis to high power lasers. The shift is best depicted by the fact that cw single-mode fiber laser output power increased from 30 W to 135 W in the time period from 1996 to 2002 and then dramatically to 1.4 kW (10 kW in multi-mode, MM) by the end of 2004 [63]. Moreover, in 2007 the highest commercial MM output powers were already 50 kW. Similar advances have also been made with pulsed lasers, mainly due to the technique called chirped pulse amplification (CPA) and large mode-area fibers.

1.2 State of the art

This thesis deals with ultrashort pulse fiber lasers and concentrates on intra-cavity dispersion compensation and other components affecting fiber laser pulse behavior. This section contains a brief overview of state of the art lasers and applications relevant to this work.

Modern lasers have come a long way from the first demonstrations and are present in various everyday consumer products. The selection of lasers covers wavelengths from UV to far infrared and from cw operation to pulsed lasers with pulse widths as short as a few optical cycles [64], i.e. on the order of a few femtoseconds. However, substantial pulse shortening typically requires complex and costly components. In order to use ultrashort pulses in many applications, the laser needs to be portable and environmentally stable. Also the pumping of the laser should preferably be done with a fiber pigtailed light source or directly electrically. Currently, electrically pumped short pulse sources like mode-locked semiconductor lasers are able to produce ultrashort pulses [65] but they typically exhibit multiple pulses within a period due to residual intracavity reflections [66]. More recently, passively mode-locked vertical-external-cavity surface-emitting lasers (VECSELs) [67] with electric pumping [68, 69] have become a promising candidate for optical clock signal generation.

The highest fiber laser output powers, that are commercially available, have reached 50 kilowatts in multi-mode operation [70]. Single-mode (SM) continuous wave output power from fiber systems can exceed five kilowatt level with diffraction-limited beam quality. In 2007 the highest claimed SM fiber laser output power was 2 kW and

in January 2008 the power already leaped over the 5 kW level [71]. This progress is enabled by the good power-scalability of fiber lasers [72]. However, such laser systems are largely based on a number of free space components and only the gain medium and power amplifier are fiber based. This configuration is often called a master oscillator power amplifier (MOPA). The output from a mode-locked seed laser of a few mW can be scaled in a fiber amplifier according to the need. That is why this thesis concentrates on compact, simple solutions for ultrafast light sources, and more precisely, presents new, alternative solutions to fiber laser challenges like cavity dispersion.

By producing compact and low cost sources of ultrashort pulses, probing of materials for characterization becomes practical and optical ranging becomes more precise [66]. Other applications of ultrashort pulses include ultrafast time-gated and nonlinear microscopy, ultrafast optical sampling and imagining, optical tweezers, high resolution imaging of live cells by second harmonic generation, surgery, micropatterning and laser ablation [73]. These applications typically require pulse widths from some tens of fs to a few ps with moderate peak power. Current lasers that meet these requirements are bulky systems comprising of a number of free space components.

1.3 Incentives and outline

Ultrashort optical pulses have become an important tool for scientific measurements. An obvious motivation for producing shorter light pulses is to improve the temporal resolution of experiments. Another motivation comes from scientists' desire to explore the limits of mode locking and the laser itself. However, ultrashort pulses are nowadays used in many other fields besides scientific measurements. With the emergence of reliable, cost-effective short pulsed fiber sources, ultrafast lasers have the potential to be used as medical instruments in eye [74] and dental [75] surgery, tissue welding [76] and micromachining [77]. From this perspective, the development of a compact and reliable source of ultrashort pulses is all the more meaningful. The goal of this thesis is to promote fiber laser development by investigating novel dispersion compensation methods for mode-locked fiber lasers and the dynamical properties of ytterbium and thulium-holmium gain materials.

This PhD thesis consists of an introduction followed by four main chapters and conclusions. Chapter 2 reviews the optical thin film properties, design and technology relevant to this thesis and related work. This chapter explains the coating types that

were implemented during this thesis work and some other general thin film structures. The objective of this chapter is to equip readers with no previous knowledge about thin films properties or design with the tools necessary to understand how the experimental results in this thesis were achieved. The fact that thin films have spread to all areas of life and technology should emphasize the importance of thin films even more.

Chapter 3 introduces mode-locked ytterbium fiber lasers and concentrates on different dispersion compensation techniques. The last two sections of the chapter explain the pros and cons of the novel thin film dispersion compensation methods introduced in this thesis. These methods enable new possibilities and compactness in fiber laser design.

Chapter 4 gives a short review of fiber laser dynamics and laser relaxation oscillations. Relaxation oscillation results are summarized for ytterbium and thulium-holmium gain materials. The motivation to study these materials lies with the fact that there is only a limited number of suitable dopant materials for active fibers. A basic knowledge of operation levels and their dynamics is valuable for thorough understanding of fiber lasers using these gain materials. As discussed earlier, ytterbium fiber lasers are used in various applications requiring high power in the 1.0–1.1 μm wavelength range or frequency conversion to visible light, whereas thulium-doped silica fiber has proved to be a good solution for light generation near 2 μm wavelength. Lasers based on this gain medium have been shown to be capable of producing high powers with a broad tuning range and have clear potential for ultra short pulse generation [78]. These features make thulium a promising material for spectroscopic, medical and LIDAR (Light Detection And Ranging) applications [79].

Chapter 5 presents high repetition rate fiber lasers with ultrashort pulses and explains how novel optical thin film coatings developed in this thesis have improved their performance. High repetition rates are needed, for example, in industrial inspection systems, for monitoring fast moving processes like chemical reactions, micromachining and two photon microscopy.

The main achievements and final conclusions are presented in chapter 6.

2. OPTICAL THIN FILMS

This chapter first gives a short overview of optical thin films, their manufacturing, modeling and design. Specific optical thin films that are relevant to this thesis and applications are then discussed in more detail. The thesis covers a lot of the necessary basic knowledge about thin films properties and design, which should help the reader to understand how the experimental results in this thesis were achieved.

2.1 Introduction to thin films

Thin films can be described as thin, parallel, smooth layers or layer structures, with thicknesses varying from a few Å to about 20 μm. For optical thin films we also require thin film materials to be transparent at the wavelength of interest. In addition, special care needs to be taken when we define 'thin' for an optical layer. Macleod [32] offers the definition that "A film is thin when interference effects can be detected in the reflected or transmitted light, that is, when the path difference between the beams is less than the coherence length of the light, and thick when the path difference is greater than the coherence length." In this definition the film's thickness is compared to the incident light coherence length, which typically is far greater than the thin film thickness. However, with ultrashort pulses the coherence length is the pulse length, and thus conventional dielectric mirrors don't necessarily work with few femtosecond pulses as expected from the basic theory. For example, a 10 fs pulse is only 3 μm long, and thus significantly shorter than the beam path difference in a complex interference filter. One should also remember that even if the thin film structure is only a few micrometers thick, in a resonant structure the beam path difference can be significantly longer, even up to several orders of magnitude.

These days optical thin films are used almost everywhere, even though most consumers do not realize it. Obvious everyday applications range from eye glass antireflection coatings for improved transmission and enhanced scratch resistance to mobile phone screen coatings. In addition to obvious applications in full view of everyone, a lot of sophisticated coatings are needed for color separation (image projectors,

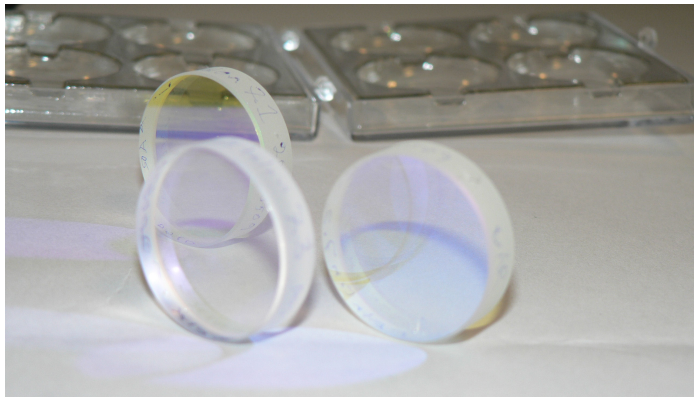

Fig. 2.1: *Typical optical thin film structures on top of fused silica substrates. The 25 mm diameter substrates are coated on both sides: the front surfaces have Fabry–Pérot etalon structures and the rear sides have been anti-reflection coated for improved transmission in the infrared.*

cameras), spectral bandpass filtering (medical, environmental diagnostics and monitoring), high reflection (mirrors, lasers) and other specialized applications [80]. Fig. 2.1 shows typical thin film laser mirrors for laboratory purposes.

In consumer products the films are integrated into the components and cannot often be seen. A good example where a consumer can see the integrated optical thin film coating is a laptop DVD- or CD-drive, where the drive's high numerical aperture lens on top of the laser diode is coated. The coating is an anti-reflection coating for the DVD wavelength range 635–650 nm (red) and CD wavelength range 770–830 nm (near infrared). This coating usually appears bluish since it is characteristic of broad band anti-reflection coatings to have elevated reflectivity below their low reflectivity wavelength region. In reality, the situation in a DVD-drive is more complicated since the focusing lens is followed by a corner mirror (high reflective for red, transmission in blue can be seen), lenses, two beam splitters, a wave plate and finally the laser diodes and photodetectors. All these are coated for improved performance and altogether the drive could have about 26 optically coated surfaces.

2.2 Thin film properties

Thin films are used to improve surface properties in various everyday applications like cutting tools, eyeglasses, monitor screens, mobile phones covers, fishing lures etc. Here we concentrate mainly on optical properties, but we cannot ignore environmental stability [81], adhesion, heat conduction, thermal expansion, scratch re-

sistance, hardness and other mechanical, chemical or thermal properties. The most important optical properties are refractive index (n), absorption (α), scattering and material dispersion ($dn/d\lambda$). Other parameters that sometimes need to be considered are refractive index temperature dependence (dn/dT) and material filling factor, i.e. how densely the evaporated material is packed. These parameters become significant when we monitor thin film evaporation or growth at high temperatures or if we expect that the filling of void with air will affect the properties considerably. This is often the case with in situ monitored anti-reflection coatings [S2]. In some rare cases materials have excellent mechanical and optical properties but they are either toxic or radioactive making the material useless for most common applications. In table 2.1 the most important optical thin film materials relevant to the laser industry are listed.

Table 2.1: *Optical properties of common thin film materials in the laser industry. These materials are deposited by electron beam by default but some materials behave better with other deposition techniques and this is mentioned in the remarks.*

Material	Symbol	Refractive index	Region of high transparency	References
Aluminum oxide[1]	Al_2O_3	1.62 at 600 nm 1.59 at 1.6 μm	UV to IR	[82, 83]
Germanium	Ge	4.05 at 3 μm	1.9–14 μm	[84–86]
Hafnium oxide	HfO_2	2.00 at 500 nm	220 nm–12 μm	[87–89]
Magnesium fluoride[2]	MgF_2	1.37 at 1 μm	210 nm–8 μm	[90]
Silicon	Si	3.5 at 1200 nm	1.2–14 μm	[84–86]
Silicon monoxide[3]	SiO	1.9 at 1 μm	500 nm–8μm	[91]
Silicon dioxide[4]	SiO_2	1.45 at 1 μm	<200 nm–8 μm	[32, 82, 92]
Tantalum pentoxide	Ta_2O_5	2.16 at 550 nm	300 nm–10 μm	[87, 88]
Titanium dioxide[5]	TiO_2	1.75–2.4 at 550 nm 2.15[4] at 1 μm	350 nm–12 μm	[93–96]
Zirconium oxide	ZrO_2	2.163 at 1 μm	340 nm–12 μm	[87, 88]

Remarks
1 Hard, good adhesion
2 High tensile stress
3 Tantalum boat resistive deposition
4 Typical in this thesis
5 Requires extra O_2

Dielectric materials are usually the best choice for a coating material even though they may not have the right absolute value of refractive index for the coating or the highest refractive index difference. However, their broad range of low absorption, small scattering and fairly constant refractive index, i.e. low material dispersion, are more important characteristics. A good example of combining the best properties of different kinds of materials is a distributed Bragg reflector (DBR) made of Al_2O_3 and Si. The dielectric Al_2O_3 is hard, has a low refractive index of about 1.6, good adhe-

sion to many surfaces, higher thermal conduction than most other dielectric materials and is easy to evaporate. Silicon on the other hand is a semiconductor and has a much higher refractive index than dielectrics, about 3.4 at 1000 nm, and due to the large index difference a fairly high reflectance mirror can be achieved with a reasonably small number of pairs. Such a mirror can of course never have ultra high reflectivity, because of Si absorption and scattering with a large number of pairs. However, this is usually not required with, for example, edge-emitting diode laser rear side high reflective coatings.

2.3 Mechanical properties of optical thin films

The physical and chemical properties of thin films are determined by evaporation conditions as they are condensed and grown into solid films. Thin film deposition technology needs to consider the harsh environmental conditions that the thin films might need to endure. Common examples of high-durability coatings are anti-reflection coatings on eyeglasses, automobile windscreens and aircraft canopies. The durability of coatings is mainly determined by their cohesive and adhesive strength and hardness, which depend on the material and deposition process. Durability under the influence of mechanical forces is determined by the microstructural growth of the layers during their condensation on the substrate surface. The microstructure, in turn, determines the magnitude and sign of the residual stress built into the thin film multi-layer system. [97]

Even though we can only do so much to improve the cohesive and adhesive strengths in a thin film structure, we can still devise a durable coating by compensating for the stress i.e. by balancing the tensive and compressive strain. With tensive stresses the forces lie in the plane of the film and substrate; this is why stress causes a thin substrate to bend from planar to concave. Fluoride compounds generally exhibit tensive stress. This is especially important for MgF_2 [98], which is a common material for the UV region [99]. SiO_2, on the other hand, has compressive stress with characteristic buckling due to expansion forces parallel to the substrate. In contrast, high-index oxide-compound films generally exhibit tensive stress properties giving thin substrates a concave shape. Typical tensive materials are ZrO_2, TiO_2, HfO_2 etc. This is why these materials are typically combined with SiO_2 to reduce the intrinsic stress that accumulates with thickness. At the same time, extrinsic stresses increase with thermal expansion differences between the substrate and the coating.

The main thin film technological approaches to preserve the desirable optical and

mechanical properties are:

- Selection of the appropriate deposition process,
- Modification of process parameters,
- Search for alternative material compositions,
- Introducing stress compensation between layers and substrate
- Post-deposition treatment.

Forces holding the thin film to the substrate are described by *adhesion*. Adhesion energies between the substrate and the film vary from sub-eV to over 10 eV. The main adhesion mechanisms are physisorption, with weak van der Waals interaction between the film and the substrate, and chemisoption, where electrons are shared between film atoms and substrate atoms giving rise to strong adhesion [100]. Naturally, good adhesion requires an ultra clean surface and therefore contaminants and adsorbed gas layers should be removed prior to evaporation.

2.4 Manufacturing thin films

Modern design techniques allow for the design of optical coatings with quite complicated spectral characteristics. The main problem nowadays is not to obtain a design with the reasonable required spectral properties but to find the one which is the most manufacturable [28].

In this thesis I concentrate on the electron beam (EB) evaporation method but it is important to realize that there are a large number of different methods with their own pros and cons. Thin films can be formed on solid substrates by various wet and dry chemical and physical deposition methods. The applied process together with the deposition environment pressure and composition have a large effect on the end result. Chemical vapor deposition (CVD) usually produces less homogenous and smooth films than physical vapor deposition (PVD) and hence PVD methods dominate in interference optics production.

In physical vapor deposition there are two fundamental processes that transfer the coating material into the vapor phase: evaporation and sputtering. In all cases the vaporized material is transported through a reduced pressure atmosphere to the target sample and condensed on the surface. Samples can be heated and are often rotated. Typical process pressure is between 10^{-2} and 10^{-4} mbar but lower pressure, on the order of 10^{-6} mbar, is required for high quality films with high purity and low scattering.

2.5 Electron beam evaporation

In this thesis electron beam evaporation was used to manufacture the thin film structures. Since the technique is widely described in the literature [28] and routinely available around the world, I only briefly introduce the basic principle of the method and discuss the most important practical aspects.

Typical uses for electron beam evaporation are processes for coating lenses and filters with anti-reflection, scratch-resistant or other specialized coatings. The process is also commonly used for coating insulating and resistor films on electronic components [101].

An electron beam evaporation system typically consists of the following components:

- Vacuum chamber,
- Pumping system,
- Electron beam gun,
- Control rack,
- Power supply,
- Vacuum monitor,
- Thickness monitor,
- Shutter,
- Sample heater or cooler linked to a pyrometer,
- Process gasses and gas lines,
- Liners in a crucible for the evaporation material,
- Materials for evaporation and
- Sample (substrate) to be coated.

The entire process takes place inside a vacuum chamber. The basic principle is to launch an intense electron beam from a hot filament with an 6–10 kV acceleration voltage to a selected material. The beam heats up the material which is loaded into a liner with an extremely high melting point. Common liner materials are graphite, aluminum oxide and tantalum. A typical electron beam gun can contain 4–8 liners and they are positioned in a water cooled copper crucible indexer which is rotated to select the material. The evaporated material travels upwards forming a smooth layer on a target sample. The evaporation rate is controlled with the electron beam current which is typically on the order of 10–150 mA. The beam shape is varied depending on the evaporated material and often a spiral beam sweeping is used to

prevent the beam from drilling a hole into the material. The layer uniformity can be improved by various techniques, for example rotating the sample. A typical electron beam evaporation chamber is depicted in Fig. 2.2 (b) and the EB machine used in this thesis can be seen in Fig. 2.2 (a).

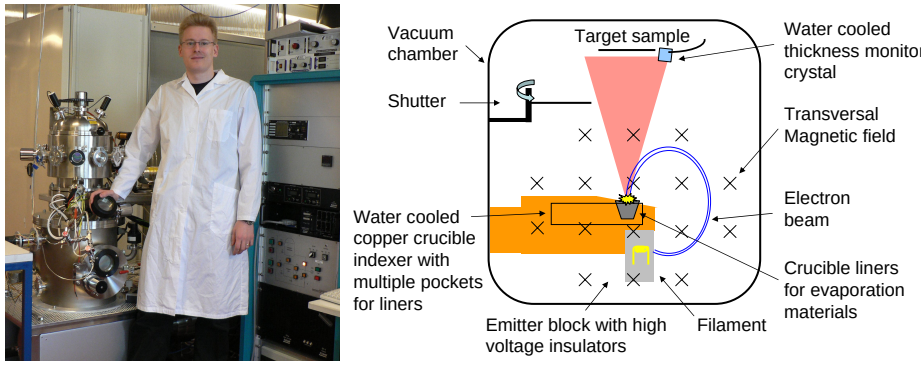

(a) (b)

Fig. 2.2: *(a) A typical electron beam evaporator alongside the user. The sample chamber on the top is separated from the electron beam gun chamber with the evaporation materials by a port valve to avoid material contamination while loading new samples. (b) Schematic of an electron beam evaporator.*

2.6 Basic optical thin film theory

In order to understand optical thin films and their behavior we need to use a formalism which is accurate, yet simple enough to enable analytical and fast numerical simulations. For this purpose we use wave optics, where light propagation in a thin film can be described by a light beam consisting of discrete frequency components ω_i. A wave packet is given by [33]:

$$\Psi(\bar{r},t) = \sum_i A_i e^{i[\omega_i t - n(\omega_i)\bar{k}\cdot\bar{r}]}, \tag{2.1}$$

where t is time, $\bar{k}$ represents the propagation constant vector, $\bar{r}$ is the coordinate vector, $n(\omega_i)$ is the refractive index corresponding to a frequency ω_i, and A_i is the amplitude of the frequency component ω_i. In optical thin film structures the phase term $\phi_i = \omega_i t - n(\omega_i)\bar{k}\cdot\bar{r}$ is what enables the complex behavior of an optical coating. Usually we look at the problems in the wavelength domain i.e. we need to write $\bar{k} = 2\pi/\lambda\,\hat{k}$, where $\hat{k}$ is the propagation constant unity vector. We also know that high

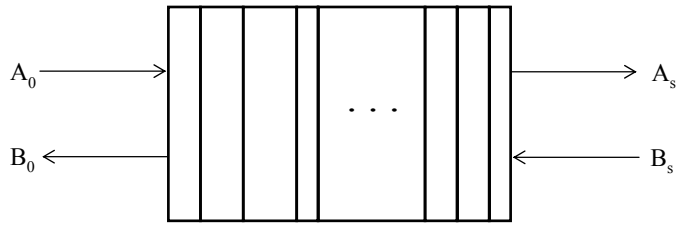

Fig. 2.3: *A schematic representation of a transfer matrix system.*

frequency oscillations ($f \sim 10^{14}$ Hz) average out in detection so we can neglect the time term. Furthermore, when we analyze thin films along the single axis (z) perpendicular to the thin film structure, we use the propagation constant's perpendicular component $k_\perp$ and avoid the vector form. As a result, we can write the phase term as

$$\phi = n(\omega)\, k_\perp\, z = n(\omega)\, k\, \cos(\theta)\, z = \frac{2\pi\, n(\lambda)}{\lambda}\, z\, \cos(\theta), \tag{2.2}$$

where θ is the angle of incidence. After simplifying the phase term, we need to remember that in the general case the optical wave has two opposite components – forward and backward propagation. To account for this, we divide the wave function in two components, with amplitude A for forward and B for backward propagation, and get

$$\Psi = Ae^{i\phi} + Be^{-i\phi}. \tag{2.3}$$

In this thesis linear algebra tools like Matlab were used for thin film simulations. Calculations followed the transfer matrix formalism described by Yeh [102]. This requires that we write the equation (2.3) in matrix form as

$$Ae^{i\phi} + Be^{-i\phi} \mapsto \begin{pmatrix} e^{i\phi} & 0 \\ 0 & e^{-i\phi} \end{pmatrix} \begin{pmatrix} A \\ B \end{pmatrix}. \tag{2.4}$$

Next we define the basis for multilayer thin film analysis by setting the forward propagation direction from intermediate media (usually air) to substrate. This rule is depicted in Fig. 2.3, where $\binom{A_0}{B_0}$ and $\binom{A_s}{B_s}$ represent the forward and backwards propagating components at the layer structure interfaces. Index 0 describes the boundary on top of the layer structure and s the boundary to the substrate. The structure is chosen to have N individual layers with parallel interfaces. Tilted layers require more advanced analysis.

Transfer matrix formalism

The idea of transfer matrix formalism is that each section or layer can be described by a set of 2×2 matrices and the total effect of a multilayered system is given by their product matrix M. The wave function at the outer boundary can be written with the help of M and the wave function at the substrate boundary as

$$\begin{pmatrix} A_0 \\ B_0 \end{pmatrix} = \begin{pmatrix} M_{11} & M_{12} \\ M_{21} & M_{22} \end{pmatrix} \begin{pmatrix} A_s \\ B_s \end{pmatrix}. \tag{2.5}$$

The thin film structures can be described using boundaries and straight propagation. The propagation accumulates the phase term but it can also include the absorption if one takes into account the refractive index imaginary part. The transfer matrix for the light propagating in a layer l is given by a propagation matrix

$$P_l = \begin{pmatrix} e^{i\phi_l} & 0 \\ 0 & e^{-i\phi_l} \end{pmatrix}, \tag{2.6}$$

where ϕ_l is the phase shift given as

$$\phi_l = k_l\, d_l = \frac{2\pi\, n_l(\lambda)}{\lambda}\, d_l\, \cos(\theta_l). \tag{2.7}$$

Here k_l is the propagation constant, d_l is the physical layer thickness, θ_l is the propagation angle in the layer and $n_l(\lambda)$ is the refractive index at the calculation wavelength λ. After constant propagation in a layer the light meets a boundary, i.e. the refractive index changes significantly. Typically, small inhomogeneities or even very thin layers can be neglected as mentioned before. Typical layers that are often ignored are semiconductor wafer native oxides on top of a polished semiconductor surface, because their thicknesses are on the order of a few Å. However, in ellipsometric analysis such simplifications cannot be made. At the interface between the adjacent layers the light refracts and reflects. Refraction is described by the Snell's law:

$$n_a \sin(\theta_a) = n_b \sin(\theta_b), \tag{2.8}$$

where n_a and n_b are the refractive indices for the opposite sides of the boundary and θ_a and θ_b are the incident and the refraction angles. In transfer matrix formalism this can be described by boundary matrices D_l [102]. $D_{l,s}$ is for s-polarization i.e. for transverse electric (TE) polarization, where the electric field is transversal to the

surface interface. The matrix for s-polarization is

$$D_{l,s} = \begin{pmatrix} 1 & 1 \\ n_l \cos\theta_l & -n_l \cos\theta_l \end{pmatrix} \tag{2.9}$$

and for p-polarization i.e. transverse magnetic (TM) polarization, where the magnetic field is normal to the surface level, boundary refraction is described by

$$D_{l,p} = \begin{pmatrix} \cos\theta_l & \cos\theta_l \\ n_l & -n_l \end{pmatrix}. \tag{2.10}$$

In this thesis the layers are often assumed to be lossless, which simplifies the analysis. With complex refractive indices, the calculations for angles, boundary conditions and wave propagation in thin film layers are much more complicated. We concentrate here on lossless thin films and, therefore, we can write the equation for θ_l directly as

$$\theta_l = \arcsin\left(\frac{n_0(\lambda)}{n_l(\lambda)} \sin\theta_0\right). \tag{2.11}$$

If the layer's absorption were included, the complex refractive index N would be

$$N = n - i k_{ex}, \tag{2.12}$$

where k_{ex} is the extinction coefficient (often [32] marked k but in this thesis we want to distinguish it from the propagation coefficient k) and n is the real part of refractive index as used before. In many cases absorption is not expressed by the extinction coefficient but by the absorption coefficient α. Their relation is

$$\alpha = \frac{4\pi k_{ex}}{\lambda}. \tag{2.13}$$

The complex refractive index can be used in calculations with this formalism as long as the absorption is relatively small, and the propagation angles can be estimated from the real part of the eq. (2.12), while the imaginary part is used in the propagation matrix phase term to describe the attenuation of the field.

Now the formalism allows us to combine the matrices to account for all layers in the thin film structure

$$\begin{pmatrix} M_{11} & M_{12} \\ M_{21} & M_{22} \end{pmatrix} = D_0^{-1} \left[\prod_{l=1}^{N} D_l P_l D_l^{-1}\right] D_s. \tag{2.14}$$

This formalism can also be applied to layers with a graded refractive index profile by dividing the graded index layers into thinner sublayers with constant refractive index and their own boundaries. It should be noted that this model is based on wave optics and hence it works best for layer thicknesses from several nanometers to a few micrometers. In this range optical thin film imperfections remain small and the theory is consistent with the experiments. When the thin films are patterned, one needs to use Fourier optics to account for three dimensional effects.

Optical thin film reflectors

So far we have considered thin films in relation to their general properties and analyzed wave function behavior inside the optical thin film but we have not yet derived the reflectivity (R) or transmission (T) of a layer structure. If we assume that the films are flat and smooth and all boundaries are parallel to each other, we can calculate the reflectivity with high accuracy. However, reflectivity can be reduced by absorption, scattering [103], surface roughness and impurities in the layers. These factors are usually irrelevant to typical thin films and they become significant only in more extreme cases like when one tries to reach or measure ultra high reflectivities [104].

From the transfer matrix notation, eq. (2.5), we can derive an expression for the reflectivity of a thin film. By definition, the amplitude reflectance r is the ratio of an electric field reflected from a surface and the field directed towards it. In our formalism these fields are A_0 and B_0, respectively (see Fig. 2.3). When we also assume that no light is arriving from the substrate side, i.e. $B_s = 0$, the amplitude reflectance is given by

$$r = \frac{B_0}{A_0}. \tag{2.15}$$

Equation (2.5) can now be written in the form

$$\begin{pmatrix} A_0 \\ B_0 \end{pmatrix} = \begin{pmatrix} M_{11} A_s \\ M_{21} A_s \end{pmatrix}. \tag{2.16}$$

Finally, the reflectivity for our thin film structure is the absolute value of the amplitude reflectance squared:

$$R = |r|^2 = \left|\frac{B_0}{A_0}\right|^2 = \left|\frac{M_{21} A_s}{M_{11} A_s}\right|^2 = \left|\frac{M_{21}}{M_{11}}\right|^2. \tag{2.17}$$

All components of M are naturally functions of wavelength and they depend on refractive index. However, when we calculate a large number of wavelength components and form a spectrum, it is often useful to calculate the accumulated phase φ or phase change in the thin film structure. This can be calculated by extracting [105] the phase angle of the complex ratio of electric field components as

$$\varphi = -phase\,angle(r) = -phase\,angle\left(\frac{M_{21}}{M_{11}}\right). \tag{2.18}$$

In addition to this, one also needs to correct the discontinuation of phase function by adding or subtracting 2π cumulatively to every discontinuous phase value. When the phase calculations are handled properly, calculating the group delay (GD) and group delay dispersion (GDD) becomes trivial. Group delay τ_g means the rate of change of the total phase shift with respect to angular frequency. It is given by

$$\tau_g = \frac{d\varphi}{d\omega} = \varphi', \tag{2.19}$$

and can be directly calculated from our phase by remembering that $\omega = 2\pi c/\lambda$ and $d\omega = (-2\pi c/\lambda^2)d\lambda$. We get

$$\tau_g = \frac{d\varphi}{d\omega} = -\frac{\lambda^2}{2\pi c}\frac{d\varphi}{d\lambda}. \tag{2.20}$$

Using the group delay, calculating the group delay dispersion is straightforward. A usual measure of GDD is the dispersion parameter D, which is defined as

$$D = \frac{d\tau_g}{d\lambda}. \tag{2.21}$$

Typical values for group delay are a few ps for resonant structures and some fs for others. The dispersion parameter D is often given in units ps/nm or fs/nm but specifically for dispersive optical thin films the unit fs^2 is much more common. Unit conversion is obtained by $\mathrm{GDD[fs^2]} = -\mathrm{GDD[fs/nm]}\cdot\lambda[\mathrm{nm}]^2/(2\pi c[\mathrm{m/s}])\cdot 10^6$.

It is worth noting that this formalism has the disadvantage that analytical calculations easily become tedious. However, this algorithm can be easily implemented using any software that has linear algebra tools. The formalism becomes more complex in the case of short pulse propagation due to the effect of nonlinearities and higher order dispersion terms [106]. We also need to remember that ultra short pulses have a

very short coherence length and our analysis assumes that films are 'thin'. Therefore, transfer matrix results should not be carelessly interpreted with femtosecond pulses.

2.7 Thin film design

Thin film design tries to fulfill set targets as well as possible for surface properties. These properties can include adhesion, thermal properties, homogeneity, manufacturing robustness, dispersion etc. but most important are the reflectivities and transmissions at target wavelengths.

As was shown in the previous sections, calculation of the optical properties of a given thin film coating is a straightforward task. However, film design for desired optical properties is rather more difficult and requires a deeper understanding of thin film structures. This section presents the different kinds of coating structures and techniques that are used in this thesis. Good design skills are also important requirements for thin film structure reverse engineering, which attempts to identify the errors responsible for manufacturing failures. Reverse engineering is similar to design but requires a much greater level of understanding. In contrast to the pre-computer era, where thin film design was limited to only the most simples cases and few layers, modern computer aided design tools are easy to use and even a novice can design simple structures. However, a skilled and experienced designer will most likely end up with a better design that meets the set requirements more accurately and is easier to manufacture. That is why the structure's designer should preferably have a lot of hands-on experience of depositing and characterizing coatings. Pure theoreticians tend to design too thick layer structures that are difficult or impossible to make.

Regardless of one's own expertise with thin films, one can use thin film structures to advance system performance or create completely new devices without deeper understanding of thin films. Good examples of the diverse optical coatings that are possible are presented e.g. by Dobrowolski et. al. [107]. These include designing complex, arbitrary reflectance profiles with an inverse Fourier transform method with as much as 152 layers [108] to classical thin film problems with elegant solutions using only a few layers. The possibilities seem endless if a large amount of layers can be used while still keeping the interaction distance below the coherence length. The fundamental limits set by scattering and quantum effects impose a certain limit for linear optics [109].

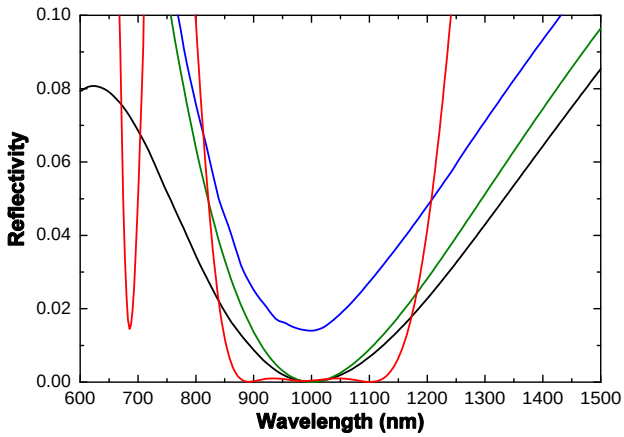

Fig. 2.4: *Typical anti-reflection coating designs on silicon surface. As the complexity increases the performance improves. The simples case (blue curve) is a single TiO_2 layer on top of a Si-surface producing reflectivity below a few percent. An ideal single layer coating on Si would have a refractive index of about 1.884 (green curve), but an even better result can be achieved by a double layer structure (black curve) with conventional materials (TiO_2 and SiO_2). When maximum reflectivity is set to about 0.1 % one can achieve an anti-reflection band from 875 nm to 1125 nm with six layers (red curve).*

2.7.1 Anti-reflection coatings

Anti-reflection (AR) coatings are the most common optical coatings. They reduce the surface reflectivity and are usually designed for a particular wavelength range and angle of incidence or range of incidence angles. Broad band, broad angle AR coatings are used for example for eyeglasses. Theoretically, AR coatings with zero reflectivity at one wavelength can be attained by one or two lossless dielectric layers of the proper refractive index. However, broadband anti-reflection coatings require use of complicated multi-layer structures, and do not reach absolute zero reflectivity at any point but instead remain below a certain level over a broad range of wavelengths. In certain cases not even a large number of layers can give a good result. Then the only chance is to look for solutions with patterning the coating which can enhance e.g. behavior in a wide range of angles [110]. In Fig. 2.4 a few examples of simple and more complicated AR designs are presented.

In the following we describe the most common types of AR coatings. The first and

most simple structure is a single layer with thickness $d = \lambda/(4n)$ and $n_0 < n < n_s$, where λ is the target wavelength, n_0 is the refractive index of the propagation medium, n the coating refractive index, and n_s the substrate refractive index. A particular case for a single layer coating is when $n = \sqrt{n_0 n_s}$. In this case the reflectivity goes to zero at a wavelength $\lambda = d \cdot 4 \cdot n(\lambda)$. Usually it is difficult to find a material to match this condition but in some common cases, such as air to glass interfaces, reflection can be reduced below 1 % over a broad wavelength range with a MgF_2 layer. This is due to the fact that MgF_2 has an exceptionally low refractive index in the visible and near IR wavelength ranges ($n \approx 1.37$ at 1 μm) and a low absorption coefficient. This coating is probably the most popular monolayer anti-reflection coating.

The second category is two layer coatings, also known as V-coatings due to their V-shaped reflectivity spectra in the AR-region, with $n_0 < n_1 < n_2 < n_s$. V-coatings are very useful for the laser industry because of their simplicity and low reflectivity over a narrow bandwidth. An example of a V-coating is presented in Fig. 2.4. A V-coating is easy to design since it can be analytically calculated [32] as follows. The phase thickness for a thin film is

$$\varphi_i = \frac{2\pi}{\lambda_t} n_i d_i, \tag{2.22}$$

where d_i is the thickness and n_i the layer refractive index of the i-th layer. λ_t is the target wavelength. The evaporated layer phase thicknesses squared need to be

$$\tan^2 \varphi_1 = \frac{(n_s - n_0)(n_2^2 - n_0 n_s) n_1^2}{(n_1^2 n_s - n_0 n_2^2)(n_0 n_s - n_1^2)} \tag{2.23}$$

and

$$\tan^2 \varphi_2 = \frac{(n_s - n_0)(n_s n_0 - n_1^2) n_2^2}{(n_1^2 n_s - n_0 n_2^2)(n_2^2 - n_0 n_s)}, \tag{2.24}$$

where n_0 is the intermediate material refractive index, usually air, n_1 is for the first layer from the top and n_2 for the second layer i.e. first evaporated layer here. This order of indexing layers in used throughout the thesis and is quite common in thin film literature. Of course this order needs to be reversed when one writes the evaporation recipe for the thin film structure. The usable thicknesses can now be solved from equation (2.22). The thickness d_i is

$$d_i = \arctan\left(\sqrt{tan^2 \varphi_i}\right) \frac{\lambda_t}{2\pi n_i}. \tag{2.25}$$

However, even if one follows this design accurately, it doesn't necessarily work in

reality, and there can be two separate solutions due to the different roots of the square root and different quadrants with the tangent function. According to Macleod [32], for a solution to exist, i.e. layer admittances to match, either all three of the following expressions must be positive, or two negative and one positive:

$$n_2^2 - n_0 n_s, \tag{2.26}$$

$$n_1^2 n_s - n_0 n_2^2 \tag{2.27}$$

and

$$n_0 n_s - n_1^2. \tag{2.28}$$

When analyzing all the expression combinations, we see that this rule can be further simplified mathematically by multiplying the expressions and requiring the product to be positive:

$$\left(n_2^2 - n_0 n_s\right)\left(n_1^2 n_s - n_0 n_2^2\right)\left(n_0 n_s - n_1^2\right) > 0. \tag{2.29}$$

The V-coatings performance depends somewhat on the substrate and the available materials, but for example, on a semiconductor surface, one can reach reflectivity levels below 10^{-4} [111]. However, accurate direct measurements of such reflectivity is challenging because of substrate rear side backreflections and unwanted reflections from measurement the instrument's optical boundaries.

When coating silicon or similar semiconductor samples one can evaluate the evaporation result with a witness, or monitor, sample. The monitor sample rear side can then be filed or scratched to significantly reduce the backreflection and we can obtain a better reading of the actual coating. This is especially important when we operate in a region where the substrate's absorption changes rapidly: e.g. silicon in the range of 1000–1300 nm, where the Si substrate absorption drops dramatically due to the bandgap, absorbs a lot of the light entering the substrate near 1 μm, but is fairly transparent beyond 1300 nm. Such substrate absorption inequality appears as a shift in the monitor sample's reflectivity spectrum compared to a monitor sample whose the rear surface has been roughened. This phenomenon is shown in Fig. 2.5.

A third category of AR coatings is multilayer coatings, where high (n_H) and low (n_L) refractive index materials alternate: $n_0|n_L|n_H|\cdots|n_L|n_H|n_s$, and the order of materials is determined by the refractive indices of the substrate and intermediate media.

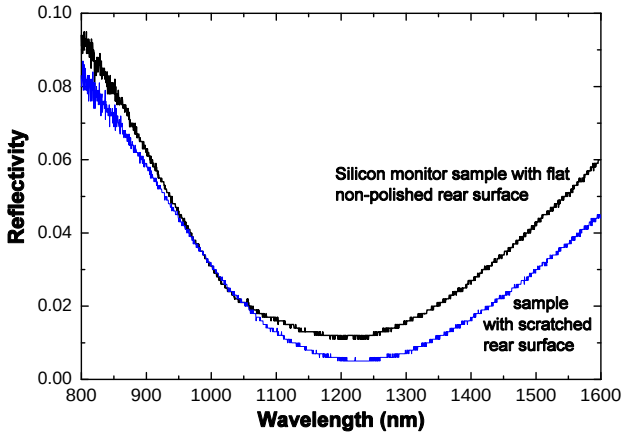

Fig. 2.5: *A typical two layer anti-reflection coating on a silicon surface. The monitor sample was first measured without preparations and then the silicon rear side was scratched heavily to reduce backreflections. Notable is the shift not just in the minimum reflectivity level, but also the minimum wavelength position.*

Generally, the layer order should minimize the index change at the first and the last boundary. Also, more than two materials can be used to reduce the total thickness, or to adapt to more complicated spectral requirements. Overall performance, i.e. transmission bandwidth and level, is limited by material properties and manufacturing technology, which dictate the maximum total thickness and number of layers.

Each layer is designed for a customized thickness. In the pre-computer era smart analytical designs and design practices like those presented in [112, 113] were used. Nowadays broad band anti-reflection coatings are designed with powerful computer tools that refine the initial structure within certain constraints to match the set targets. One can write one's own program with any programming language or use commercial software like "The Essential Macleod" [114]. The initial structure should consist of a basic structure which uses materials and a layer number which are approximately correct, and thus allows the problem at hand to be at least partially solved. This is where expertise is most valuable and the biggest mistakes can be made. A good designer chooses a suitable structure basis and modifies it before refinement so that refining leads to convergence to a optimal solution. Targets are values of e.g. reflectivity, transmission, dispersion or phase at specified wavelengths, angles and polarizations. Each target should also be weighted to distinguish the important targets from the less significant ones. Setting the targets is an important step of the design since too dif-

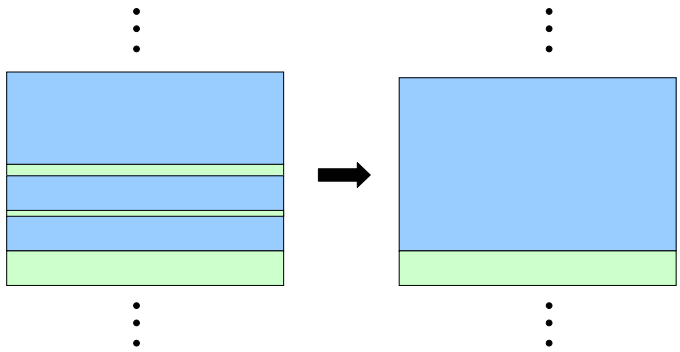

Fig. 2.6: *An example of simplifying a complex layer structure without significantly increasing the figure of merit. Different colors represent different materials with different refractive indices. The physical thickness changes slightly and the direction of change depends on whether we replace high refractive index material with low refractive index or vice versa.*

ficult targets are impossible to reach and refinement might not find a good solution at all if the targets are ill-considered. On the other hand, setting the targets too low doesn't utilize the full potential of the layer structure, and one might end up with an unnecessarily thick structure for the target performance. Naturally the first targets set can be modified during the design process and the end result may vary significantly from the first version. In order to limit the refinement process to reasonable parameters the design needs constraints for e.g. the maximum number of layers and the total maximum thickness of layers or certain materials. Finally, when the design is ready one should always check if it contains very thick layers or ultra thin (few nm) layers. Very thick layers are sometimes a sign of a non-optimal solution to the design problem and ultra thin layers, e.g. $1/200\ \lambda_t$, can often be removed without changing the reflectivity spectrum significantly and removing such a layer simplifies the evaporation process, saving time. The layer removal is done by adding an optically equivalent thickness of material to the next, thicker layer, i.e. by merging it with another layer. If the structure has two alternating materials, the process effectively merges three, or a higher odd number of layers as presented in Fig. 2.6.

Another category of anti-reflection coatings includes coatings with absorbing layers. These don't transmit light at the absorbing wavelength region and hence they emphasize the anti-reflection or filtering properties in the coatings at the expense of high transmission, which makes them less useful than purely dielectric coatings. In this thesis we don't deal with this kind of coatings to any great extent but they are a significant type of coating and worth mentioning. A common use of absorbing layers is

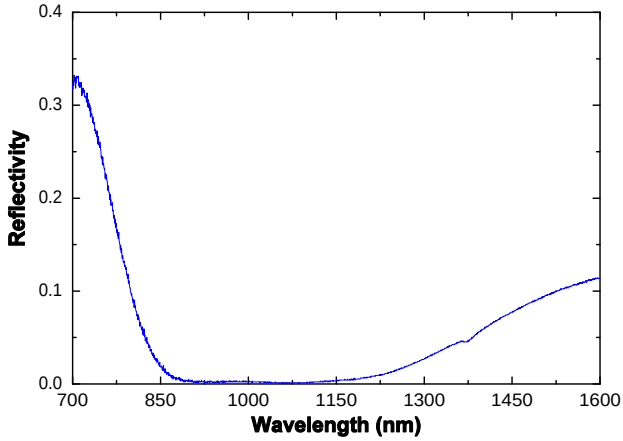

Fig. 2.7: *An example of an AR coating that is highly transparent at 0.9–1.1 μm from publication P4. The coating consists of 30.4 / 76.0 / 166.8 / 34.8 / 102.1 / 46.4 / 159.5 / 181.8 nm of* $TiO_2 (n = 2.15)$ */* $SiO_2 (n = 1.45)$ */* $\cdots$ */* TiO_2*. The substrate was fused silica.*

in telescopes and binoculars, where a special layer absorbs the yellow sodium lines typical of most city lights. With a proper dopant one can reach very high absorption at particular wavelengths, but sharp changes from one wavelength region to another are impossible for absorption filters.

A reflectivity spectrum of a typical AR coating in this thesis is presented in Fig. 2.7. In this example the coating consists of four pairs of SiO_2/TiO_2 layers. The structure was designed with a Matlab based computer program that utilized the algorithm described in [115].

As a summary of AR coatings, they are at the most common optical thin films and irreplaceable in most modern optical systems. The difficulty in producing or designing AR coatings depends largely on the required performance and situation. A lot of information about the coating environment, system requirements and design constraints is needed in order to realize an optimum AR coating. An optimal solution is a compromise between the absolute value of the reflectivity, transmission bandwidth, robustness of the structure, cost, manufacturing time, adhesion, scratch resistance etc. Limiting factors are available materials and their refractive indices, absorption coefficients and the accuracy of controlling the thickness of each film during the deposition.

2.7.2 High reflective coatings

High reflective (HR) coatings are a highly important group of thin film coatings. The simplest ones consist of a single layer of aluminum, silver, gold or chromium deposited on a flat plastic or glass surface. They are not much different from antique metal mirrors with polished silver plates. The simplicity of such a mirror is due to the basic Fresnel equations [33]: the amplitude reflection coefficient, when electric field is perpendicular to the plane of incidence, is

$$r_\perp \equiv \left(\frac{E_{0r}}{E_{0i}}\right)_\perp = \frac{n_i \cos\theta_i - n_t \cos\theta_t}{n_i \cos\theta_i + n_t \cos\theta_t}, \tag{2.30}$$

where E is the electric field, indices i, r and t refer to intermediate, reflected and transmitted angles (θ) and corresponding refractive indices (n). Similarly, the amplitude reflection coefficient for the field parallel to the plane of incidence is given by

$$r_\parallel = \frac{n_t \cos\theta_i - n_i \cos\theta_t}{n_i \cos\theta_t + n_t \cos\theta_i}. \tag{2.31}$$

The equation for the amplitude reflection coefficient can be substituted for the left part of eq. (2.17) and for the case, where $n_i = 1$ in normal incidence, we get

$$R = \left(\frac{n_t - 1}{n_t - 1}\right)\left(\frac{n_t - 1}{n_t + 1}\right)^*. \tag{2.32}$$

Therefore, since the complex refractive index can be split into real and imaginary components $n_t = n_R - i n_I$,

$$R = \frac{(n_R - 1)^2 + n_I^2}{(n_R + 1)^2 + n_I^2}. \tag{2.33}$$

This form of equation, with the knowledge that for metals the refractive index imaginary component is significantly higher than the real part, reveals the origin of shiny metal surfaces. For example for silver it gives a reflectivity higher than 99 % over a broad reflectivity spectrum from 900 nm to 10 μm. However, silver oxidizes easily resulting in reduced reflectivity. This is why gold coatings are more common above 0.7 μm [116]. The harmful oxidation process can be reduced by a protective dielectric layer which is typically a 10–30 nm layer of Al_2O_3. Moreover, in the UV region most metals make poor mirrors but Al is an exception. Al mirrors reflect over 80 % at 200 nm whereas other typical metal mirrors reflect less than 50 %. Al mirror are also easy to manufacture and have a fairly high reflectivity over the whole UV-VIS-IR-range making it one of the most popular HR mirror materials.

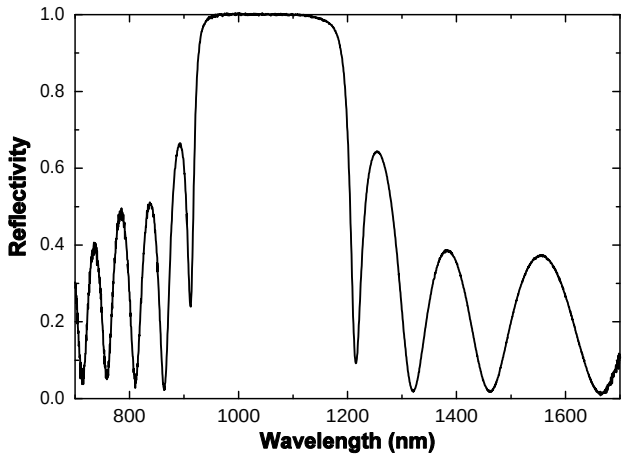

Fig. 2.8: *An example of a high reflective DBR layer structure on GaAs substrate. The DBR was made of SiO_2 and TiO_2 using an electron beam evaporator.*

Even though metal coatings are simple and quite highly reflective, they absorb part of the incident light and hence cannot be used in situations where low loss is required. Absorption in the mirror can also lead to catastrophic optical damage (COD), usually originating from a defect inside the mirror. Metal mirrors have a tendency to oxidize and they are usually protected with a thin dielectric layer, e.g. with a few tens of nanometers of Al_2O_3.

In contrast to metallic mirrors, dielectric HR mirrors, like the one shown in Fig. 2.8, are nearly lossless and can achieve higher reflectivities through use of a proper periodic structure. Dielectric HR mirrors are based on cumulative interference at every second interface of the layer structure. The reflected wave is designed to be at the same phase as the one arriving deeper from the structure. In this way the residual transmission gets smaller and smaller as the periodic structure becomes thicker.

An optimal type of dielectric reflector, called a distributed Bragg reflector (DBR), consists of a substrate with a refractive index n_s followed by multiple (N) pairs of alternating low (n_L) and high (n_H) refractive index layers, each with a thickness (d) dependent on the target center wavelength (λ_B):

$$d = \frac{\lambda_B}{4\,n(\lambda_B)}. \tag{2.34}$$

λ_B is also called the Bragg wavelength. This structure can be written in transfer matrix form with eq. (2.6)–(2.11) and (2.14). We obtain the propagation matrix

$$P_l = \begin{pmatrix} e^{i\phi_l} & 0 \\ 0 & e^{-i\phi_l} \end{pmatrix} = \begin{pmatrix} i & 0 \\ 0 & -i \end{pmatrix} \tag{2.35}$$

and the system matrix for a single quarter-wave layer is

$$D_l P_l D_l^{-1} = \begin{pmatrix} 1 & 1 \\ n_l & -n_l \end{pmatrix} \begin{pmatrix} i & 0 \\ 0 & -i \end{pmatrix} \frac{1}{2} \begin{pmatrix} 1 & \frac{1}{n_l} \\ 1 & -\frac{1}{n_l} \end{pmatrix} = i \begin{pmatrix} 0 & \frac{1}{n_l} \\ n_l & 0 \end{pmatrix}. \tag{2.36}$$

Thereby, the transfer matrix for the whole DBR structure is

$$\begin{aligned} M &= D_0^{-1} \left[\prod^{N} D_H P_H D_H^{-1} D_L P_L D_L^{-1} \right] D_s \\ &= \frac{(-1)^N}{2} \begin{pmatrix} 1 & \frac{1}{n_0} \\ 1 & -\frac{1}{n_0} \end{pmatrix} \left[\prod^{N} \begin{pmatrix} 0 & \frac{1}{n_H} \\ n_H & 0 \end{pmatrix} \begin{pmatrix} 0 & \frac{1}{n_L} \\ n_L & 0 \end{pmatrix} \right] \begin{pmatrix} 1 & 1 \\ n_s & -n_s \end{pmatrix} \\ &= \frac{1}{2}(-1)^N \begin{pmatrix} \left(\frac{n_L}{n_H}\right)^N + \frac{n_s}{n_0}\left(\frac{n_H}{n_L}\right)^N & \left(\frac{n_L}{n_H}\right)^N - \frac{n_s}{n_0}\left(\frac{n_H}{n_L}\right)^N \\ \left(\frac{n_L}{n_H}\right)^N - \frac{n_s}{n_0}\left(\frac{n_H}{n_L}\right)^N & \left(\frac{n_L}{n_H}\right)^N + \frac{n_s}{n_0}\left(\frac{n_H}{n_L}\right)^N \end{pmatrix}. \end{aligned} \tag{2.37}$$

This can then be substituted into eq. (2.17) to get the DBR's reflectivity at λ_B at normal incidence:

$$R = \left| \frac{M_{21}}{M_{11}} \right|^2 = \left| \frac{\frac{n_s}{n_0} - \left(\frac{n_L}{n_H}\right)^{2N}}{\frac{n_s}{n_0} + \left(\frac{n_L}{n_H}\right)^{2N}} \right|^2. \tag{2.38}$$

This result can also be found in other equivalent forms [102, 117]. Nonetheless, it is important to realize that a reflectivity of 1 can never be reached. Using typical dielectric materials, mirrors that reflect at least 99.99984 % [104] have been reliably demonstrated. The ultimate limiting factors for mirror reflectivity are scattering, material losses [118] and DBR stack adhesion (too thick layer structures are not stable enough). A typical reflectivity curve is presented in Fig. 2.8. This DBR was used in [P2] in the bottom section of the Gires–Tournois interferometer (GTI). More details of DBR manufacturing can be found from my Master's thesis [119]. The usable

DBR width $\Delta\lambda$, i.e. the high reflective region, increases with refractive index contrast, $\Delta n = n_H - n_L$, of the DBR layers. Typical dielectric materials for DBRs are TiO_2(n = 1.9–2.6, in this thesis about 2.15), Ti_3O_5, TiO, Al_2O_3($n = 1.59$) and SiO_2(n = 1.44–1.46). For the semiconductor mirrors covered in this thesis, AlAs ($n \approx 2.9$ at 1.5 μm) and GaAs ($n = 3.5$ at 1 μm) were typical compound semiconductor materials for DBRs. Semiconductors in this thesis were grown by molecular beam epitaxy (MBE). The advantage of MBE is that it offers the possibility to grow both lattice-matched and strained crystal layers, which have varied refractive index. However, semiconductors have low losses only for certain wavelength regions above their bandgap and even then, DBRs with lattice matched materials have relatively low Δn. As a consequence, the high reflectivity bandwidth of a semiconductor DBR is narrow, and a large number of pairs, on the order of 20–40, is typically needed to reach reflectivities over 99.9 %.

2.7.3 Dichroic coatings

Numerous applications require separation of different wavelengths of a light beam. Typical examples of such applications are sunglasses, video projectors and laser output couplers. In some cases only one wavelength range is needed and the other is redirected away. This task can be handled with a dichroic mirror. In this thesis dichroic coatings are used in laser cavities with closely separated wavelengths, making the coatings fairly challenging.

Wavelength separation is typically achieved by designing an interference edge filter with a DBR structure that reflects one of the wavelengths well and modifying it such that it transmits the other wavelength or wavelength range. The high transmission region naturally requires us to suppress the DBR sidebands. This can be achieved by choosing a modified DBR-based starting structure and refining it to match the required reflection and transmission targets.

Common edge filter starting structures [32] on top of a substrate are of the form $\frac{H}{2}LHLH\ldots L\frac{H}{2}$ or $\frac{L}{2}HLHL\ldots H\frac{L}{2}$, where H stands for high refractive index quarter wave layer (see eq. (2.34)) and L for low index quarter wave layer, i.e. the structure is the same as that of the DBR, but it starts and ends with the same material, and those layers are only half the thickness of a normal quarter wave layer. This starting point already reduces the sideband reflections and additional optimization based on the targets further significantly improves the result. The starting structure can also have a phase-matching section to dampen the sidebands even more: for example adding a low refractive index layer (L) outside the $H/2$ layer dampens the sidebands for a

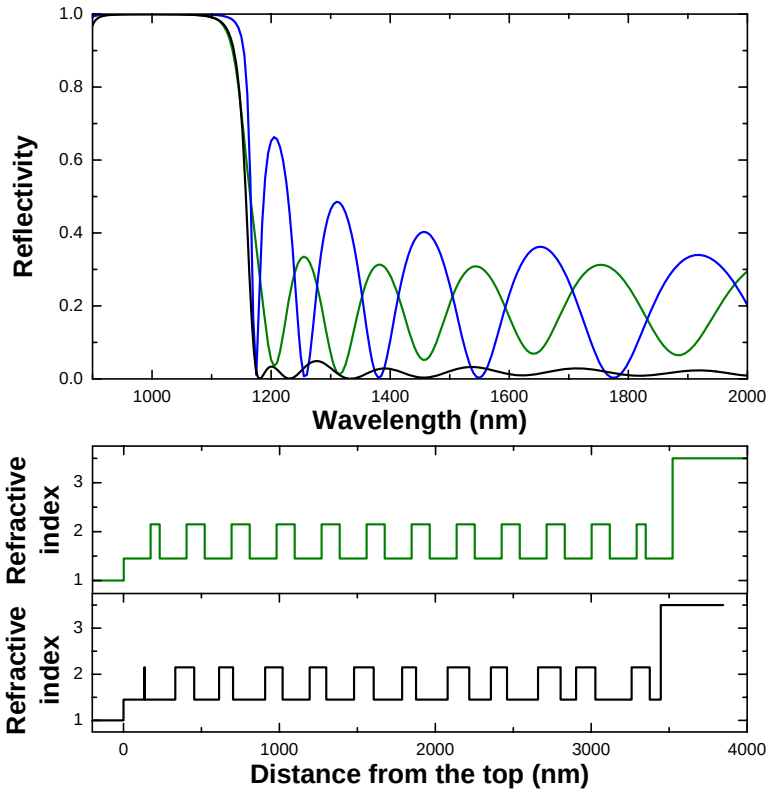

Fig. 2.9: *(top) An example of a SiO_2/TiO_2 long-wave pass filter (black). The target was to reflect over 99 % in the 950–1100 nm wavelength range and transmit over 98 % in the range 1200–2000 nm. The starting structure before layer optimization (green) and a normal DBR (blue) are also presented for comparison. Refractive index profiles of the starting structure (middle) and the long-wave pass filter (bottom) reveal that the filter profile remains highly periodic in the optimization i.e. it is only slightly modified from the starting point, but the figure of merit is improved by a factor of 2807.*

long-wave pass edge filter. Such a starting structure is used in the example depicted in Fig. 2.9. Of course the number of layers in the structure is important and as a rule of thumb we can say that the more layers we have, the sharper the transition from the high reflection to high transmission regions can be. Naturally, if we choose too high a number of layers, the optimization becomes more complicated and we face adhesion and manufacturing problems with the result. In our example the targets were fairly well matched, but the optimization with Matlab's Nelder-Mead simplex algorithm took already 5.3 hours.

2.7.4 Dispersive mirrors

Dispersive mirrors are a major part of this thesis and their advantages and disadvantages are discussed in more detail in publications [P1], [P2] and [P4] and in chapter 3. In the following subsections we describe the background and introduce the general structures of the basic dispersive mirrors. Fabry-Pérot etalons and Gires–Tournois interferometers are more relevant to this thesis but double-chirped mirrors are also discussed due to their great significance for low-dispersion compensation in ultra broad band femtosecond solid-state lasers. However, chirped mirrors are not suitable for fiber laser dispersion compensation because of their very small dispersion.

Fabry–Pérot etalons

The Fabry–Pérot (FP) etalon is a form of multiple-beam interferometer [35], where the interference occurs not in separate interferometer branches like in a Mach-Zehnder two-beam device, but instead inside a resonant structure with two high-quality parallel mirrors, usually DBRs, spaced by a lossless cavity, typically made of fused silica or evaporated SiO_2. The term FP interferometer and etalon are often used interchangeably, but here we attempt to emphasize that "etalon" refers to a single, solid device, whereas "interferometer" is more general classification and can include devices and setups which have e.g. an air cavity. FP etalons are particularly important for optics since they are used in filters to pick narrow spectral lines. However, a single FP cavity results in a triangle-shaped transmission spectrum and the shape can be made more rectangular by combining two or more etalons spaced by a coupling layer in between.

The full transmission at the resonant wavelengths occurs when the parallel mirrors have equal reflectivities (perfect mode matching is assumed). FP etalon properties for different mirror reflectivities are depicted in Fig. 2.10. This shows that the higher the reflectivities (R) are, the sharper the resonance lines are, i.e. the finesse is higher. Dispersive properties are discussed in section 3.5. Finesse is defined as "the free spectral range divided by the full width at half maximum (FWHM) width of resonances of an optical resonator." [120] The FP etalon finesse is given by

$$F = \frac{\pi (R_1 R_2)^{1/4}}{1 - (R_1 R_2)^{1/2}}, \tag{2.39}$$

where R_1 and R_2 are mirror reflectivities. In an ideal etalon the mirror reflectivities

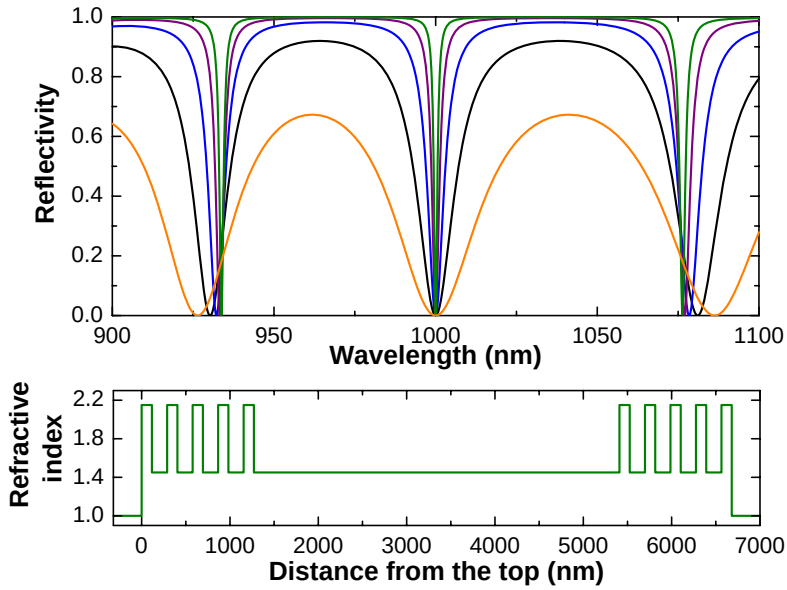

Fig. 2.10: *(top) Examples of reflectivity spectra from Fabry–Pérot etalons consisting of a 4137.9 nm SiO_2 cavity between dielectric DBRs with different numbers of pairs. The DBRs with 1000 nm Bragg wavelength have half a pair (orange, $R = 0.273$), 1.5 pairs (black, $R = 0.563$), 2.5 pairs (blue, $R = 0.771$) 3.5 pairs (purple, $R = 0.889$) and 4.5 pairs (green, $R = 0.948$). (bottom) The FP etalon with 4.5 pairs at each side of the cavity has a finesse of about 58.5 and its refractive index profile is shown in the lower graph.*

are identical, R, but this is seldom the case. Equal mirror reflectivities result in a simplified finesse formula

$$F = \frac{\pi\sqrt{R}}{1-R}. \tag{2.40}$$

However, the etalon finesse can degrade with roughness of the optical surfaces of the mirrors [121]. The surface quality is measured as the roughness, $\Delta x_{surface}$, which is the deviation from the planarity and is compared to the wavelength of the light, λ_{light}:

$$\Delta x_{surface} = \frac{1}{m}\lambda_{light}. \tag{2.41}$$

The deviator m in the equation is typically in the range 2–100 and relates to the roughness finesse as

$$F_{roughness} = \frac{m}{2}, \tag{2.42}$$

and thus the total finesse F_{total} is given by

$$\frac{1}{F_{total}} = \frac{1}{F} + \frac{1}{F_{roughness}}. \tag{2.43}$$

Gires–Tournois interferometers

A Gires–Tournois interferometer (GTI) is a resonant structure consisting of two parallel mirrors spaced by a low loss cavity. Therefore it is similar to a FP etalon but the top mirror should be only partially reflective, while the bottom mirror should reflect as much as possible to avoid losses. Hence, we can call a GTI an asymmetric FP etalon. The basic structure is presented in Fig. 2.11.

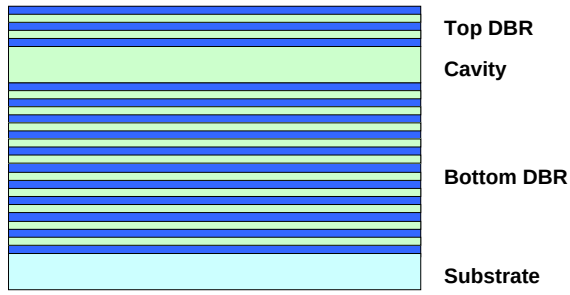

Fig. 2.11: *Basic GTI structure for dispersion compensation.*

If the cavity is lossless and the bottom mirror has several orders of magnitude less reflection losses than the top mirror, the GTI reflectivity stays high for all wavelengths, but the phase of the reflected light is strongly frequency-dependent due to the resonance effect. This causes group delay dispersion (GDD). However, in practice the bottom mirror always leaks a certain amount of light to the substrate which results in an effective cavity loss. The effect is especially pronounced near the resonance wavelength where the light propagates multiple round-trips and this appears as a resonance dip in the reflectivity spectrum. An example is shown in Fig. 2.12.

The original design was first introduced by Francois Gires and Pierre Tournois in 1964 [122]. They suggested that the structure provides a large group delay at resonance frequencies, which depend on the cavity optical thickness. Later, the GTI

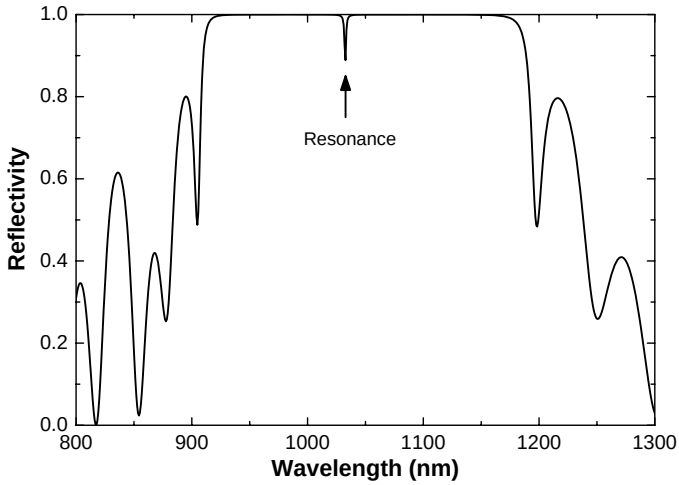

Fig. 2.12: *An example of a dielectric GTI with visible losses at the resonance wavelength of 1032.8 nm. However, the dispersion is zero at the resonance, where the losses are highest, and the short pulse laser should be operated slightly below the resonance, where losses are smaller.*

group delay was used to introduce a small group delay dispersion for a dielectric mirror [123] and a few years later, a GTI design was used to generate 44-fs and soon after already 14-fs pulses [124, 125]. However, these lasers were solid state lasers with a short crystal and required only a very small amount of dispersion compensation to operate. Moreover, these lasers were pumped with bulky gas lasers, making them less practical than modern fiber lasers. Afterwards multi-cavity thin film GTIs were introduced as an alternative approach to realize anomalous dispersion mirrors [126, 127], but these mirrors could generate only little dispersion and they could not be used for fiber laser dispersion compensation.

Large dispersion values can be achieved near the GTI cavity resonance, but the operation bandwidth becomes narrower as the mirror finesse increases and the effect of higher order dispersion can not be neglected. Typical dielectric GTI reflectivity, group delay and dispersion values are presented in Fig. 2.13. The design's dispersive properties are discussed further in section 3.4.

Double-chirped mirrors

Double-chirped mirrors (DCM) appeared in the 1990s to meet the need to compensate for the gain crystal dispersion of solid state lasers in a broad wavelength range. Compared to earlier dispersion compensation techniques, they enabled remarkable

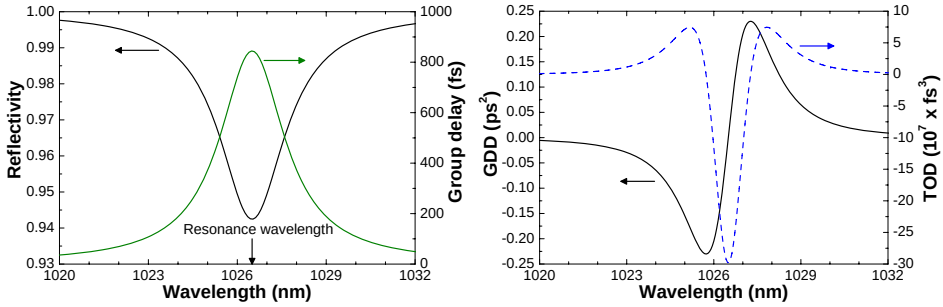

(a) (b)

Fig. 2.13: *(a) A typical GTI reflectivity (black) spectrum around the resonance wavelength with corresponding group delay (green). (b) The GTI's group delay dispersion (solid line) and third order dispersion (dashed line).*

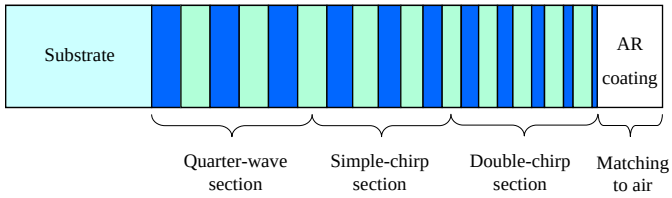

Fig. 2.14: *Example of double-chirped mirror sections. All the sections are merged in the end result, and sections other than the DCM section are not necessarily required. However, including them in the initial structure gives a good starting point for subsequent design optimization.*

improvements in the field of generating ultra-short pulses [128, 129]. The required reflectivity needs to be high over a wide spectral range because these lasers, e.g. Ti-sapphire, do not tolerate high cavity losses [130]. This can be achieved with a DBR-like structure with some modifications concerning the phase shift and consequently mirror dispersion. Naturally, mirrors need to be dielectric due to material dispersion and loss issues, but the structures nevertheless become very thick. A common DCM (see Fig. 2.14) consists of a DBR on a substrate followed by a chirped DBR (CDBR) section.

The chirping means that the center wavelength for the DBR stopband progressively decreases or increases, depending on the target dispersion sign, as the layer number (j) increases (1 being the first layer from the top). The CDBR can be followed or replaced by a double-chirp section [131, 132] if compensation of the higher order dispersions is required [133] or if the dispersion profile for the second order disper-

sion needs to be of a certain shape e.g. particularly flat. The entire structure should finally be matched to air or another intermediate medium with an anti-reflection coating to ensure optimal DCM behavior. An unmatched structure will have unwanted roughness in the dispersion characteristics. These problems can also be reduced by operating the mirror from the substrate side and making the anti-reflection coating at the rear side of the component [134].

A DCM with a large GDD, on the order of several hundreds of fs^2, cannot be flat over a broad spectral range. Mirrors with GDD values on the order of ± 1000 fs^2 are commercially available in a limited range, but large bandwidths of several hundreds of nanometers typically have a dispersion of about 50 ± 50 fs^2. Such mirrors are often used in pairs, where the GDD oscillations cancel out each other to give an overall flat dispersion profile. The DCM's limited dispersion is often enhanced by placing several, or even a dozen, DCMs into the laser cavity, making the technique complex and expensive.

Double-chirped mirror design strategy

The DCM mirrors are typically very time-consuming and challenging to design but a reasonable result can be achieved with, for example, the following design strategy. First we need to define parameters to vary the local Bragg wavelength (λ_B) and duty cycle (r) as follows:

$$\lambda_B(j) = b_0 + b_1 j + b_2 j^2 + b_3 j^3, \tag{2.44}$$

where j is the number of the layer ($j = 1$ for the layer at the air interface), b_{0-3} are optimization coefficients and

$$r(j) = \frac{1 + \tanh\left(\frac{j-P}{D}\right)}{4}, \tag{2.45}$$

where P and D are optimization coefficients for the duty cycle. Next we need to define a figure of merit (FOM), which accounts for deviations from the target dispersion level as well as reflection losses. An ideal design would have FOM $= 0$. In the design program a preliminary Monte-Carlo optimization is done for the 6 parameters P, D and b_{0-3} within predefined upper and lower limits. The last step is the full optimization of all layers to utilize the full potential of the layer structure and smooth the dispersion characteristics. Usually this algorithm needs to be repeated multiple

times in order for the designer to learn proper starting parameters and their boundaries for the refractive index pair in use. As a rule, the higher the relative refractive index change for the used materials is, the broader the wavelength range that can be achieved.

2.8 Summary

In this thesis work we have studied the available material selection for optical thin films and chosen the optimal materials for each purpose. Our thin film design is based on mature design practises which we have developed further in this work to aid ultrafast fiber laser development. The most important thin film structures in this thesis are Gires–Tournois interferometers, Fabry–Pérot etalons, dichroic mirrors and anti-reflection coatings.

3. YTTERBIUM MODE-LOCKED FIBER LASERS

This chapter gives a short overview of ytterbium fiber laser mode locking and the main components for mode-locked fiber lasers. We then discuss the work done in this thesis to improve Yb-fiber laser performance using alternative, advanced solutions. The main emphasis is on fiber laser dispersion compensation, showing new options to be reckoned with for anyone wanting to design a simple short pulse fiber laser. The main advances deal with compensating for cavity fiber dispersion with electron beam evaporated dielectric thin film structures.

3.1 Mode locking

Though short pulses can be achieved with the Q-switching technique [135], the shortest laser pulses can be generated exclusively via mode locking (ML). It is based on multiple modes exited in the laser cavity with coupled phases. This sets a number of requirements for the laser dynamics and dispersion properties in order for the mode locking to be started and sustained. Self-starting requires that the laser cavity favors short pulses over cw light. After that the mode-locked pulse evolves for some hundreds to a few thousand round trips [136] until it reaches the steady-state. However, the pulse duration doesn't evolve to the ultrashort regime unless the dispersion and pulse shaping mechanisms are properly adjusted. The small anomalous dispersion required for soliton formation usually enables even shorter pulses by balancing the cavity GDD and the nonlinear refractive index change from self-phase modulation (SPM).

3.1.1 Active mode locking

Fiber lasers can be mode-locked either actively or passively [137]. Active ML, where a modulator introduces amplitude or phase modulation to the laser cavity, requires an external signal to sustain the mode locking. The modulation frequency, ω_m, needs

to be matched closely to the laser's mode separation frequency $\Delta\omega_e$ [138], which is determined by the cavity round trip time, T_R, as

$$\Delta\omega_e = 2\pi \frac{1}{T_R}. \tag{3.1}$$

This modulation causes the laser axial mode with frequency ω_e to form sidebands at frequencies $\omega_e \pm n \cdot \omega_m$. These sidebands then enable the axial modes to lock their phases together. As a result of this mode coupling, the multiple spectral components form a Gaussian pulse [139]

$$E(t) = E_0 \, exp\left(-t^2/\tau^2\right), \tag{3.2}$$

where the τ is proportional to the pulse duration and is given by

$$\tau = \sqrt[4]{\frac{8\,g}{m\,\omega_m\,\omega_g}}, \tag{3.3}$$

where m is the modulation depth, ω_m is the modulation frequency and ω_g is the gain bandwidth. However, it is important to note here that the pulse width is not limited merely by the gain bandwidth and modulation but also by the dispersion.

3.1.2 Passive mode locking

Ever since the first picosecond pulses were generated with only the help of a passive, saturable absorber element, e.g. semiconductor, [140, 141], passive mode locking has been the means for generating the shortest pulses [139]. Nonlinear optical methods for passive mode locking [137, 139] include use of fast or slow saturable absorbers, additive pulse mode locking (APM), polarization APM, Kerr-Lens mode locking (KLM) and nonlinear amplifying loop mirrors (NALM) as artificial saturable absorbers.

When dealing with fiber lasers, we need to remember that they are also susceptible to Q-switching and Q-switched mode locking (QSML) due to their long upper-state lifetimes. This can be avoided by using a saturable absorber with low modulation depth even though this makes laser self-starting more difficult [138].

As with active mode locking, a broad spectrum is needed to support short pulses. In an ideal case, i.e. the best pulse quality, the relationship between the pulse width $\Delta\tau_p$ and the spectral width $\Delta\omega_s$ is governed by the Fourier transform limitation, which

tells us that for a Gaussian pulse the time-bandwidth product [142] is

$$\Delta\tau_p \, \Delta\omega_s \geq 0.441. \tag{3.4}$$

This product for a hyperbolic secant (sech) pulse shape is about 0.315. This means that, for example, the shortest pulse durations that can be generated at 1030 nm with a spectral bandwidth of 2 nm are 727 fs for Gaussian pulses or 557 fs for sech pulses.

3.2 Ytterbium fiber lasers

Ytterbium (Yb) is a rare-earth element that is nowadays a common optical fiber dopant. Ytterbium fiber can provide a broad-gain bandwidth with excellent power conversion efficiency, enabling high output power from a laser or amplifier [143]. Yb can also be inserted at high doping levels with e.g. the direct nanoparticle deposition (DND) process [144], leading to high gain in a short length of fiber [P2]. The broad gain bandwidth is required for ultrashort pulse amplification while the high saturation fluence allows for high pulse energies. The ytterbium absorption and emission cross section and energy level diagram are presented in Fig. 3.1. Ytterbium's remarkable gain bandwidth is also demonstrated in [P1], where Yb provides gain for picosecond pulses in the whole range from 980 nm up to 1105 nm.

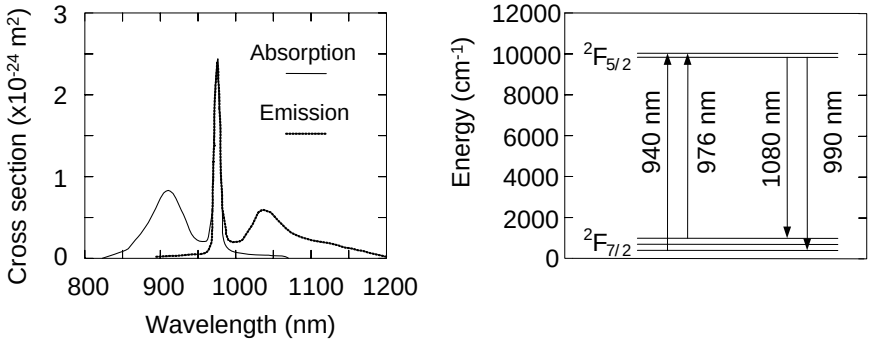

Fig. 3.1: *(left) Ytterbium-doped fiber absorption and emission cross section and (right) energy level diagram [145].*

As a result of ytterbium's high conversion efficiency and good thermal dissipation techniques, Yb-fiber lasers with amazing power levels have been demonstrated in both cw and ultrafast regimes [70, 72]. The efficient heat dissipation of the fiber owing to its large surface to active volume ratio and the superb beam quality of the

guided mode determined only by the fiber core characteristics are the well-known advantages of single-mode fibers. High power is also supported by the long interaction length. This is especially helpful when using double-clad fiber since the pump light is launched into the outer cladding and is gradually absorbed to the inner core over the entire fiber length. However, the long interaction length also brings problems to ultrafast lasers with fiber nonlinearities like SPM, which originates from the third-order susceptibility $\chi^{(3)}$, and is responsible for the intensity-dependent refractive index in the form of $n = n_0 + n_2 I$. Another fiber nonlinearity issue is stimulated inelastic scattering [146], where the light transfers a part of its energy to the glass host material in the form of excited vibrational modes. A frequency shift of about 13 THz is observed with the excitation of optical phonons. This process is called stimulated Raman scattering (SRS). A smaller shift occurs with stimulated Brillouin scattering (SBS) when an acoustical phonon is excited and the shift is on the order of 17 GHz. Both SRS and SBS could provide a notable power loss mechanism in high intensity fiber lasers but when dealing with ultrashort pulses in fibers, the large spectral width is much broader than the Brillouin gain bandwidth and the effect of SBS is negligible.

Ytterbium fiber lasers have various applications ranging from laser welding [147] and supercontinuum generation [148–150] to more sophisticated applications like coherent anti-Stokes Raman scattering (CARS) microspectroscopy [151].

3.2.1 Saturable absorbers

The upper-state lifetimes of rare-earth-doped fibers are long (ms level), implying that the gain does not recover within the cavity round-trip time, which is typically below 1 μs. Therefore, a fast nonlinear device is needed to clean up both the leading and trailing edges of the pulse and a fast saturable absorber is one solution.

Saturable absorbers are divided in two categories depending on their recovery time, fast and slow. Semiconductor, carbon nanotube and dye have been used in ultrafast lasers, but this thesis concentrates on semiconductor saturable absorber mirrors (SESAMs) for mode locking. The absorbers used in this study are described in many publications and a more complete overview of SESAM design and their parameters can be found from [138, 152].

There are four important parameters for SESAMs. They are

- recovery time (τ_A),

- saturation fluence ($F_{sat,A}$), which is the saturation energy ($E_{sat,A}$) per unit area that reduces the initial low-intensity reflectivity to 1/e (∼37 %) of its initial value, a typical unit is μJ/cm^2,
- modulation depth (q_0), also known as saturable (bleachable) losses and
- non-saturable losses (q_{nonsat}), preferably as small as possible.

In addition to these parameters, properties like damage threshold and two-photon absorption (TPA) and the resulting roll-over (additional losses) can be important with ultrafast lasers. Typical SESAM behavior with increasing fluence is shown in Fig. 3.2.

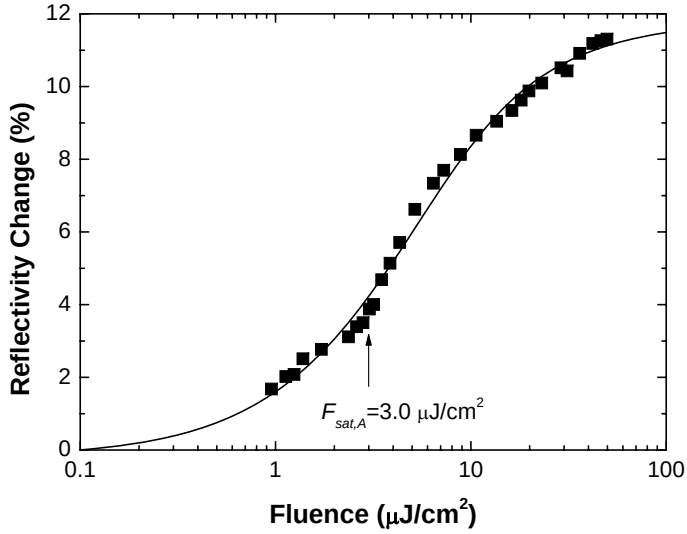

Fig. 3.2: *Nonlinear reflectivity of a GaInNAs-based SESAM [P1]*

3.2.2 Fiber components

Fiber lasers consist of different fiber components, and most of them contribute to the cavity dispersion. Typical components are fiber couplers, like output couplers and wavelength division multiplexers (WDMs), fiber isolators, fiber pigtailed pump diodes and gain fiber. All these components are based on commercial mature technology and are readily available.

Whereas laser mirrors have individual GDDs per reflection, for fiber the dispersion accumulates throughout the whole fiber. Moreover, the dispersion for fibers is a sum of material and waveguide dispersion and thus it is convenient to account for these

together using a mode-propagation constant [146], β, and expand it mathematically in a Taylor series about the spectrum center frequency, ω_0, as

$$\beta(\omega) = n(\omega)\frac{\omega}{c} = \beta_0 + \beta_1(\omega-\omega_0) + \frac{1}{2}\beta_2(\omega-\omega_0)^2 + \frac{1}{6}\beta_3(\omega-\omega_0)^3 + \cdots, \quad (3.5)$$

where

$$\beta_m = \left(\frac{d^m\beta}{d\omega^m}\right)_{\omega=\omega_0} \qquad (m = 0,1,2,\ldots). \quad (3.6)$$

The β_2 represents dispersion of the group velocity and is the main mechanism responsible for pulse broadening in fiber. The phenomenon is known as group velocity dispersion (GVD) and β_2 is the GVD parameter. However, in fiber optics literature, dispersion is often given by the dispersion parameter, D, which is related to β_2 by the relation

$$D = -\frac{2\pi c}{\lambda^2}\beta_2. \quad (3.7)$$

D is usually given per unit length in units ps/nm/km and for standard fiber it is zero around 1.31 μm. This wavelength is called the zero-dispersion wavelength, λ_D. Near λ_D third order dispersion (TOD) becomes dominant.

3.3 Dispersion compensation techniques for the 1 μm region

The fiber's normal dispersion is one of the major obstacles for ultrafast pulse generation in ytterbium fiber lasers even though mode locking with short pulses is also possible in positive net-cavity dispersion fiber lasers [153].

If a light pulse is propagated through a medium with normal dispersion, the result is that higher frequency components (blue) travel slower than lower frequency (red) components. The pulse therefore becomes chirped. Conversely, if a pulse travels through an anomalously dispersive medium, high frequency components travel faster than lower frequency ones. The result of GVD, whether negative or positive, is ultimately temporal spreading of the pulse.

However, there are various ways to compensate for the cavity dispersion and this thesis provides a few new ways to do it. A common dispersion compensation method uses a diffraction grating pair, where the pulse is spread spatially and different frequencies propagate for different distances. The basic concept of a diffraction grating

pair is shows in Fig. 3.3. Positive features include high damage threshold and large attainable dispersion. However, such a system easily has 25 % losses even with good alignment and it is somewhat bulky due to the required free space components. In addition to the gratings, the light has to be collimated from the fiber to the gratings with an extra lens and reflected back with a mirror. Gratings can also be positioned in a more complicated non-parallel configuration with two lenses to achieve normal dispersion for e.g. pulse stretching.

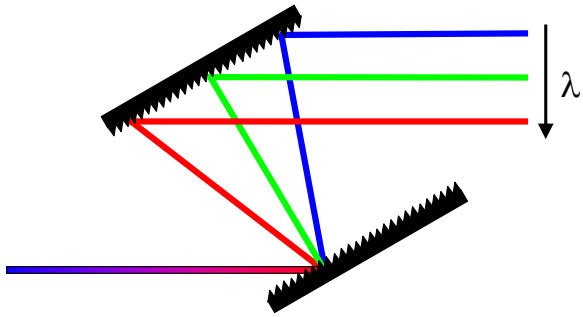

Fig. 3.3: *Grating pair configuration for anomalous dispersion i.e. the shorter wavelengths (in blue) travel a shorter path than the longer wavelengths (in red). The arrow points in the direction of increasing wavelength.*

Another common method for dispersion compensation is a prism pair, or four prisms to restore the original shape of the collimated beam. The prism sequence, shown in Fig. 3.4, is a classical solution for creating negative or positive dispersion in a laser cavity [154,155]. Prisms are generally used at the minimum deviation angle, i.e. with the incident angle equal to the exiting angle. The apex angle, ϕ, should be cut in such a way that the rays enter and leave each prism at Brewster's angle. This minimizes reflection losses from the prism surfaces. Anomalous dispersion at 1 μm occurs when the angular dispersion, which is anomalous, overcomes the prism's normal material dispersion. This requires the prism separation, L, to be large enough, making the con-

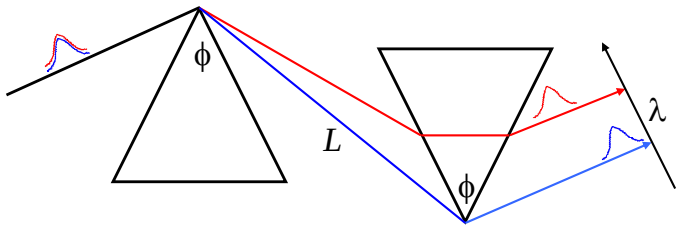

Fig. 3.4: *A prism pair inducing negative (anomalous) group delay dispersion.*

figuration space-consuming. Moreover, a prism pair configuration is difficult to align and doesn't produce high dispersion values at reasonable prism separations. This is why prism pair use with fiber lasers is typically limited to compensation of higher order terms with e.g. grating pairs. Detailed calculations of dispersive properties can be found for example in [155, 156].

In addition to grating pairs and prisms, there are also various other methods for dispersion compensation at the Yb-gain region; these include GTI's and FP etalons, which are discussed in this thesis, various semiconductor structures like dispersion-compensating saturable absorber mirrors (D-SAM), resonant saturable absorber mirrors (RSAM) and dispersive fibers like photonic band gap fibers (PBGF) [157, 158] (see Fig. 3.5), which are a form of photonic crystal fiber (PCF), fiber tapers and chirped fiber Bragg gratings (CFBGs). Typical properties of these components are summarized in Table 3.1. In this table we are particularly interested in the bandwidth-GDD-product ($\Delta\omega_{GDD}$ [THz] x β_2 [fs^2]), which gives a good figure of merit for the method. We also compare the third order dispersion (TOD) to the reveal methods' suitability to ultrashort pulse generation. From the table we can conclude that no single method is suitable for every application but when it comes to fiber lasers, DCMs, chirped mirrors, prism, D-SAMs and RSAMs are of little use around 1 μm due to their small dispersion. The CFBGs are also difficult to use because of their large dispersion, and they have mainly been used in CPA applications. However, quite recently, state-of-the-art CFBG with lower dispersion, on the order of 0.1 ps/nm, have been demonstrated with tens of nm bandwidth, and the laser could produce ps-pulses and down to 218 fs pulses with external compression [159].

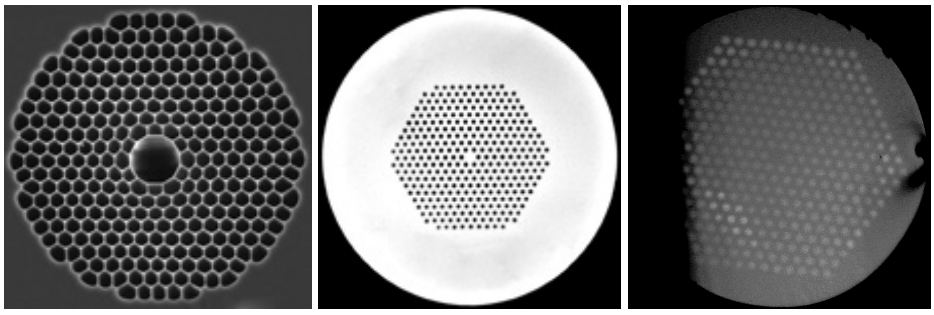

(a) (b) (c)

Fig. 3.5: *A Few examples of photonic bandgap fiber cross-sections: (a) hollow core [160], (b) high nonlinearity [161] and (c) dispersion compensating [162].*

Table 3.1: *Comparison between different dispersion compensation methods. Bandwidths for GDD are FWHM unless the device transmission or reflectivity sets a more strict limitation for laser operation. GDDs are average values over the usable band.*

Method	Bandwidth (nm) / (THz)	GDD (fs^2)	Bandwidth x GDD (THz x fs^2)	TOD (fs^3)	References
GTI	1.8 / 0.51	$-1.44 \cdot 10^5$	$-7.4 \cdot 10^4$	$\sim 5 \cdot 10^{7\diamondsuit}$	[P2]
GTIP	3.5 / 1.0	$-1.53 \cdot 10^5$	$-1.5 \cdot 10^5$	$\pm 3 \cdot 10^{7\diamondsuit}$	Fig. 3.10
FP etalon$^\sharp$	3.56 / 0.98*	$-2.0 \cdot 10^4$	$-1.95 \cdot 10^4$	$-6 \cdot 10^6$	[P4]
DCM	370 / 49	–100	$-4.9 \cdot 10^3$	very low	[163]
DCM pair*	600 / 250	$\sim$ –50	$-1.2 \cdot 10^4$	very low	[164]
Chirped mirror	300 / 128	–50	$-6.4 \cdot 10^3$	+75	[129]
Grating pair$^\diamond$	$\sim$ 80 / 22	$-8.2 \cdot 10^4$	$-1.8 \cdot 10^6$	$+1.8 \cdot 10^{5\dagger}$	[165]
Prism pair‡	500 / 180	–640	$-1.1 \cdot 10^5$	+1380	[155]
PBGF	22 / 6.1	$-5 \cdot 10^4$	$-3.1 \cdot 10^5$	$1.4 \cdot 10^6$	[162]
Fiber taper$^\bullet$	100 / 27.3	$-2.87 \cdot 10^4$	$-7.8 \cdot 10^5$	$3 \cdot 10^4$	[166]
CFBR	27 / 7.4	$-2.58 \cdot 10^{6\maltese}$	$-1.9 \cdot 10^7$	high	[149]
D-SAM	15 / 6.3	-400	$-2.5 \cdot 10^3$	low	[167]
RSAM	7 / 1.9	–3150	$-5.8 \cdot 10^3$	$2.0 \cdot 10^5$	[168]

Remarks
$\diamondsuit$ A typical value, TOD varies considerably in the usable range as seen in Fig. 3.11
$\sharp$ Values are for one round trip
$*$ Bandwidth is limited by the transmission
$\star$ Two-mirror system, bandwidth x GDD per mirror is $-6.2 \cdot 10^3$ THz fs^2
$\diamond$ Double pass, 1200 lines/mm, separation 1 cm, β=55°, bandwidth is a rough estimate
$\dagger$ The ratio of TOD and GDD increases with lines/mm, e.g. typical $\beta_3/\beta_2 = -4$ fs for 1200 lines/mm and $\beta_3/\beta_2 = -15$ fs for 1750 lines/mm
$\ddagger$ Double pass, $L = 50$ cm
$\bullet$ Taper waist diameter about 1.8 μm, waist length 20 cm, TOD estimated in [169]
$\maltese$ Far too great for Yb-fiber laser cavity compensation, used mainly in CPA configurations

3.4 GTI dispersion compensation

One of the major results of this thesis is the demonstration that a properly designed GTI can compensate for the Yb-doped fiber laser cavity dispersion [P1–P2]. This is possible due to the large anomalous dispersion in a GTI below the resonance wavelength (see Fig. 3.6). However, the large dispersion can be generated only over a relatively narrow bandwidth. The autocorrelation reveals that the spectrum is sufficient to support at least 1.5 ps pulses which are shown in Fig. 3.7. A certain error in the pulse width measurement is always present with autocorrelation due to the fact that the pulse shape is assumed. We used a Gaussian pulse shape in our fit and believe that it best resembled our situation. At the time, we were not able to perform dispersion measurements for our GTI in [P2] but later it was fully characterized using a phase-locked interferometer dispersion measurement system. As a result, the

calculated GDD values proved to be accurate within a few percent compared to the measured values, which is evident from the group delay results presented in Fig. 3.8.

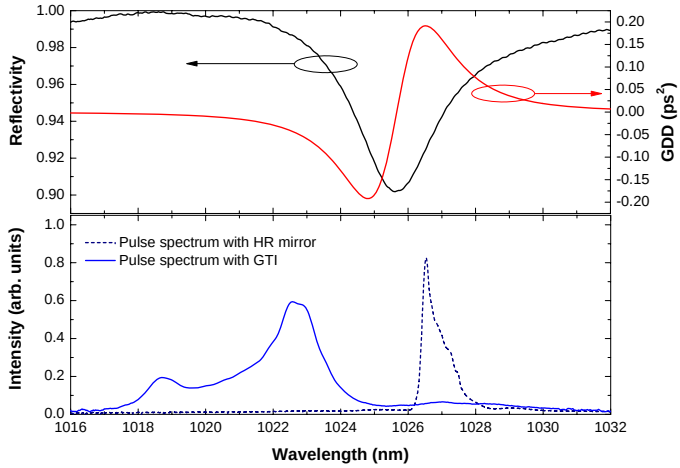

Fig. 3.6: *(top) The measured reflectivity and calculated GTI group delay dispersion in [P2]. (bottom) Laser spectra with and without GTI dispersion compensation.*

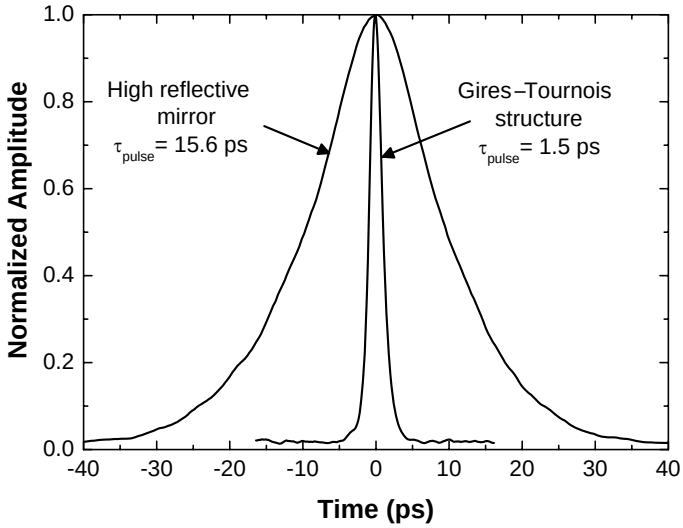

Fig. 3.7: *The autocorrelation trace in our Yb-doped fiber laser using a normal high reflective mirror and a GTI. The pulse widths were obtained from the Gaussian fits of autocorrelation with a conversion factor that is a function of the assumed pulse shape. For a Gaussian pulse the factor is 0.707. We can see that the pulse width is shortened to a tenth of the original using a GTI structure.*

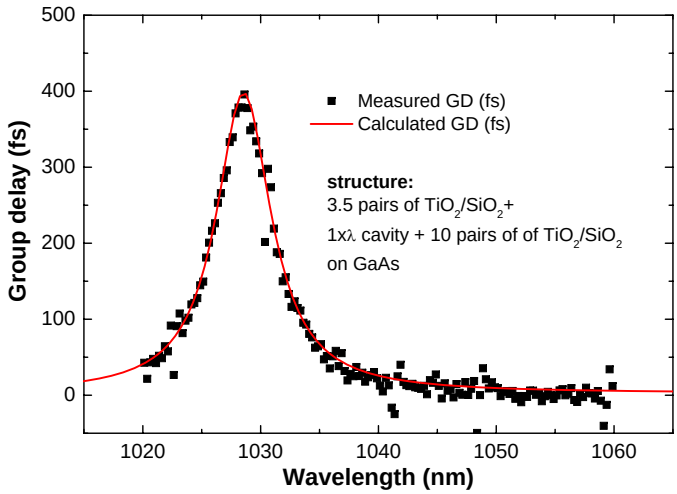

Fig. 3.8: *The measured GTI group delay and the calculated target shows remarkably good correlation. The measured sample is similar to the one shown in [P2] but with one pair less in the top DBR section.*

The GTI's FWHM bandwidth times its maximum dispersion is fairly constant but we can increase it by using a GTI prism (GTIP) which was invented during this thesis work and is to the best of my knowledge, the first time that this idea is presented. The prism is a cut and polished piece of glass or other transparent material with parallel, polished ends at a selected angle with respect to the sides. This structure is shown in Fig. 3.9. The sides of this structure are coated with a reduced finesse GTI and a high reflective mirror providing a multiple-bounce setup. The makes the usable bandwidth larger and reduces the amount of dispersion per reflection.

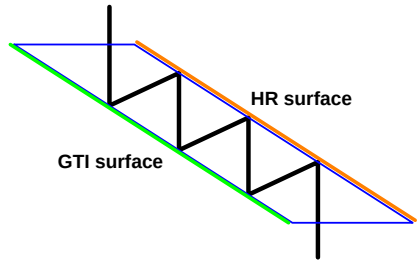

Fig. 3.9: *GTI prism structure and beam propagation with three reflections from the GTI surface i.e. a total of six reflections per laser cavity round trip.*

Since the bottom mirrors are evaporated last, we can evaporate a large number of DBR pairs to minimize losses and even finish the structure with a metallic material to

minimize optical leakage. The light propagates in the prism and experiences multiple (N) reflections from the GTI surface which increase the dispersion by a factor of N. The advantageous effect is that a broader dispersion compensation bandwidth with lower losses can be achieved. It is also worth noting that the reflection losses are distributed more evenly throughout the usable bandwidth. An example of this effect is shown in Fig. 3.10. Naturally, the finesse of the GTI cannot be reduced too much since each GTI bounce needs to compensate for the dispersion of the GTIP glass substrate. The alternative would be to build the GTIP as a free space component consisting of a parallel high reflective mirror and a GTI. This way the number of bounces and the GTIP aperture could be varied more easily even though the idea of a compact, integrated component would be lost.

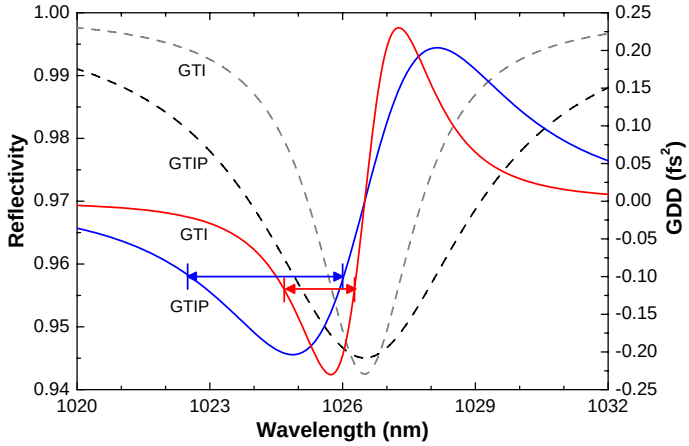

Fig. 3.10: *Reflectivity (dashed line) and group delay dispersion (solid line) comparison between a single reflection from a conventional GTI and 4 reflections inside a GTIP. The GTIP has 3.5 and the GTI 4.5 pairs in the top DBR, respectively, yielding roughly the same losses and dispersion but broader usable bandwidth for GTIP. The usable bandwidth is marked with bidirectional arrows.*

The GTIP also has other advantages over a conventional GTI: due to the GTIP's lower finesse in the GTI structure, the TOD is essentially smaller, as can be seen in Fig. 3.11. The GTI also sets a fixed wavelength for dispersion compensation when used at normal incidence reflection mode. That wavelength depends on the evaporated cavity thickness. Now, since the GTI surface in the GTIP is designed to operate at an angle, the resonance wavelength depends on the angle and the component can be tuned continuously over several tens of nm by rotating it about its center. At the same time, the laser cavity stays aligned since the GTIP ends are parallel and the GTIP geometry does not change the beam direction but merely shifts it spatially by

a small amount. The tuning is limited by the laser beam diameter and the GTIP aperture. Since the reflectivity of a DBR mirror is angle-dependent, the GTI finesse changes slightly over the tuning range, and eventually the losses grow faster as the angle deviates significantly from the designed angle of operation. Still, I believe that the tuning range can easily be tens of nanometers in the ytterbium gain bandwidth.

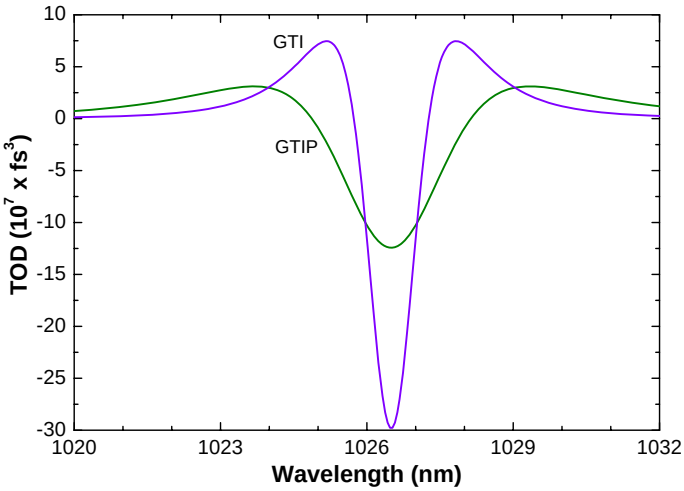

Fig. 3.11: *An example of the GTIP's and the GTI's third order dispersion. Both exhibit a large TOD but the GTIP's is still notably less.*

3.5 Fabry–Pérot etalons for dispersion compensation

Fabry–Pérot etalons have conventionally been used as spectral filters in many optical and laser applications. However, these have relied on high finesse FP etalons or interferometers and typically assumed that only the high transmission peaks of etalons are relevant to the system. Now, it has been shown in publications [P4] and [S3] that with low finesse FP etalons, the fiber laser tends to operate in the anomalous dispersion range of the etalon resulting in pulse shortening. Unlike that of an asymmetric GTI, the FP etalon's dispersion at wavelengths shorter than the resonance wavelength is normal in reflection but anomalous for transmission. The change in the sign of the dispersion occurs at a "critical point" when the top (R_{top}) and the bottom (R_{bottom}) mirror reflectivities change from roughly equal ($R_{top} \approx R_{bottom}$) to a situation where the bottom mirror has notably higher reflectivity than the top mirror, i.e. $R_{top} \ll R_{bottom}$. Also, if the cavity has losses (or gain) like in a semiconductor GTI device [170, 171], the critical point can change significantly.

Fig. 3.12 presents the FP etalon transmission with the corresponding mode-locked pulse spectrum and we can clearly see that the laser operates in the anomalous dispersion regime of the etalon. This is evident from Fig. 3.13 which shows a set of round-trip transmission curves as the etalon is tuned. The figure also shows the measured round-trip dispersions in transmission mode which are different from the dispersion characteristics observed in the reflection.

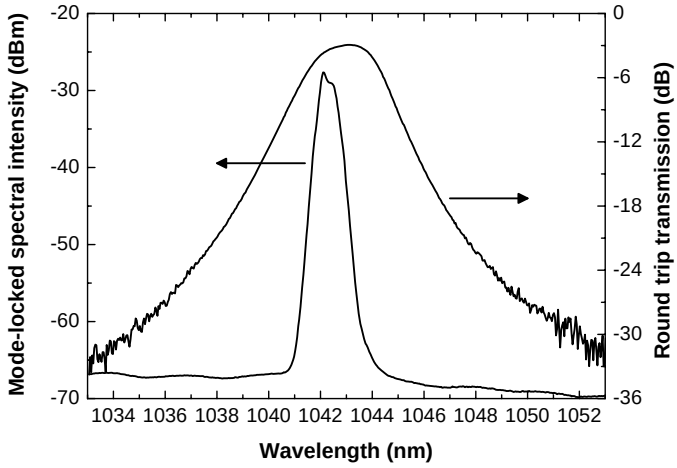

Fig. 3.12: *Fabry–Pérot etalon configuration's round trip transmission in a laser cavity with the resulting mode-locked spectrum.*

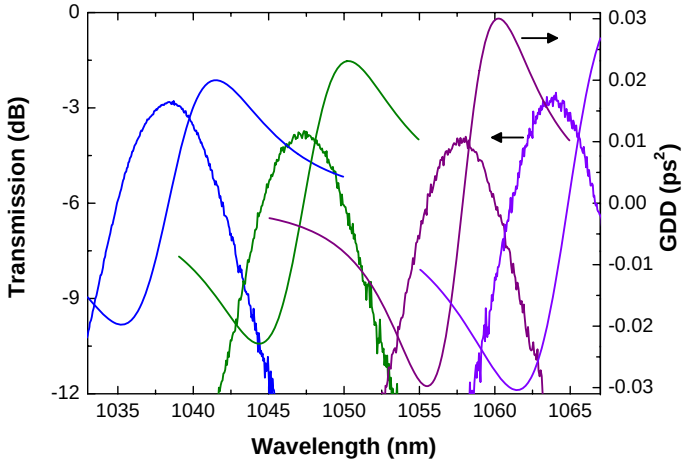

Fig. 3.13: *Example of Fabry–Pérot etalon tunability and transmission GDD measurements.*

The benefits of using a FP etalon in the laser cavity include easy, continuous tunabil-

ity and solitonic sideband suppression, shown in Fig. 3.14. The reason the sidebands should be suppressed is that in certain cases the spectral sidebands contribute to pulse broadening [137], and naturally in some applications the sidebands would cause inaccuracy to the system wavelength.

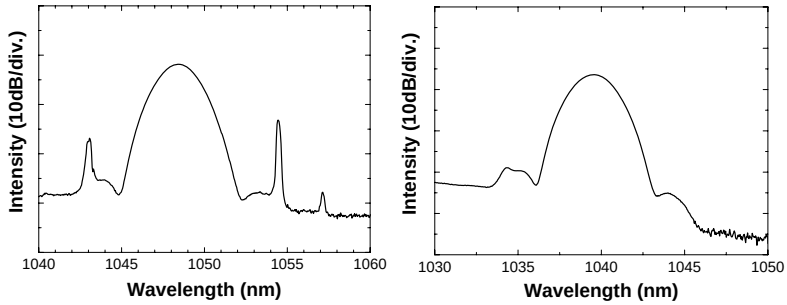

(a) Without etalon (b) With etalon

Fig. 3.14: *When a laser operates in the soliton regime, the cavity anomalous dispersion leads to the formation of solitonic sidebands visible in (a). The FP etalon helps to filter out these spectral impurities. The laser in the situation in (b) is the same as in (a) except for the etalon placed in the cavity to enable tuning and additional dispersion.*

3.6 Summary

Use of a Gires–Tournois interferometer dispersion compensator and a short length of highly doped ytterbium fiber providing net anomalous group-velocity dispersion allowed us to realize a compact fiber laser. By incorporation of a novel semiconductor saturable absorber mirror based on a GaInNAs structure, self-starting 1.5-ps-pulse mode-locked operation was obtained at 1023 nm with a repetition rate of 95 MHz. In addition, this chapter presents a novel GTI configuration where a GTI is integrated to a glass prism enabling wavelength tunability and improved dispersion characteristics.

This thesis also describes a dielectric thin film Fabry–Pérot etalon operated as a dispersion compensator in a mode-locked fiber laser cavity. The etalon generates anomalous dispersion near the low-loss spectral window and, consequently, the laser mode-locked by the semiconductor saturable absorber favors operation in the anomalous dispersion regime without a spectral filter. The etalon compensator is tunable, compact, easy to align, and suitable for picosecond and subpicosecond pulsed operation.

4. FIBER LASER DYNAMICS AND RELAXATION OSCILLATIONS

This chapter discusses fiber laser dynamics and provides insight into two gain materials, namely ytterbium (Yb) and thulium-holmium (Tm-Ho). We concentrate on discussing material properties with respect to laser energy levels and laser relaxation oscillations. The motivation for this comes from the laser tunability and starting mechanisms. When we tune the operation wavelength, the laser behavior can be changed if the type of energy level scheme alters. Also the start-up of mode locking can occur through low frequency instability and Q-switching, which can cause optical damage to the most fragile components in the system. These components include pump diodes and thin film structures like semiconductor saturable absorbers and evaporated thin films coatings. In addition to this, we also obtain valuable information about the laser material, such as its transition cross section.

4.1 Dynamics

Rare-earth-doped fibers exploiting the three- and four-level transitions in Er^{3+}, Nd^{3+}, Pr^{3+}, Yb^{3+} and Tm^{3+} are now commonly used in a number of applications, including fiber lasers and optical amplifiers. For these sources, especially those operated in the mode-locked or Q-switched regime, it is important to know the process that governs the transient emission buildup, including the population inversion dynamics, the effect of spontaneous emission and the nature of the laser transition.

Previously it has been shown that in glasses doped with erbium or neodymium, the mechanism of laser transition changes over the gain bandwidth [172–174]. This feature could influence the oscillation dynamics of the laser, which in turn may strongly affect the characteristics of pulsed operation. The laser stability, especially near the threshold, is also susceptible to chaotic behavior [175].

Mode-locked fiber laser dynamics is largely controlled by the saturable absorber used, as discussed in section 3.2.1. Their tunability properties typically govern the mode-locked laser tuning, since their properties can change rapidly when moving

away from the targeted central wavelength, and thus one needs several different absorbers to cover a broad tuning range [P1]. However, in some cases the absorber can have almost a hundred nanometer tuning range with little change in the pulse properties [176].

4.2 Relaxation oscillations

When a laser is turned on, the laser experiences spiking behavior. This is due to the fact that once the number of photons exceeds the steady-state level, the laser starts to burn up the exited states at a much faster rate than the pump can supply them. This appears as a spike in the output but the cavity photons are quickly depleted. The process is a consequence of the stimulated emission short life time compared to the pump process performance. However, the net gain recovers periodically and the cycle is repeated [177]. Once the large-amplitude initial spiking behavior in a laser oscillator has damped down to small-amplitude fluctuations about the steady-state level, we can see nearly sinusoidal oscillations called relaxation oscillations. An example of these is presented in Fig. 4.1.

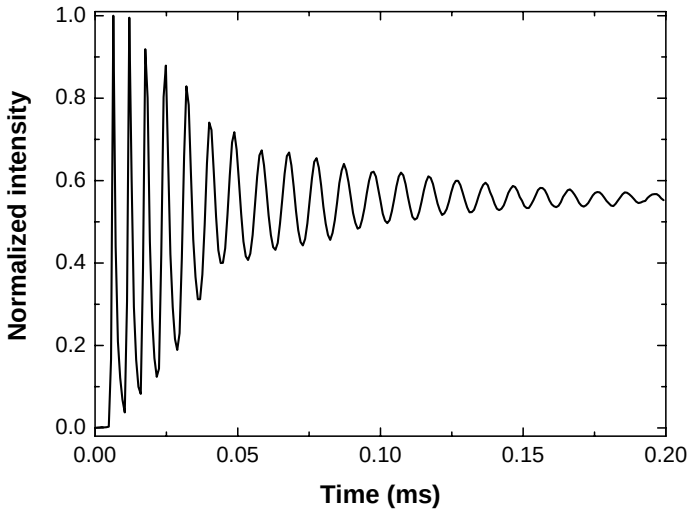

Fig. 4.1: *Example of relaxation oscillation in a thulium-holmium fiber laser. The first five peaks on the left represent typical spiky laser behavior and the oscillations in the middle and on the right are typical relaxation oscillations.*

The laser relaxation oscillation was shown to contain the information about the transition levels, in particular, from the wavelength dependence of the characteristic frequency, f_{relax}. General laser theory discloses that ω^2_{relax} varies linearly with $(r-1)$,

where r is a pumping rate normalized to the threshold value [173] and $r = \frac{P}{P_{th}}$, where P is the pump power and P_{th} is the pump power at laser threshold. The slope of this dependence varies with wavelength for the three-level transition and is essentially wavelength-insensitive for four-level laser systems. The origin of the wavelength dependence of ω^2_{relax} for three-level systems comes from the rate equations taking into account the thermal population of the levels [172]:

$$\omega^2_{relax} = \frac{1}{\tau_c \tau_s} \left(1 + c\,\tau_c\,\sigma\,\eta\,f^l N\right)(r-1), \tag{4.1}$$

where N is the total number of active ions per gain volume, c is the speed of light, σ is the laser transition cross section,

$$\eta = \frac{l}{L + l(n-1)}, \tag{4.2}$$

where L is the total cavity length and l the length of the gain medium, n is the refractive index, f^l is the fractional thermal occupation of the lower laser level and τ_c and τ_s are the cavity and laser transition lifetimes.

We can see from eq. (4.1) that the wavelength-dependent term in parentheses disappears if the population of the terminal level can be neglected, i.e. $f^l = 0$. An important consequence of this feature is that the relaxation oscillation frequency depends on the absorption at the signal wavelength as a result of the thermal population of the ground level, i.e. when $f^l \neq 0$. The relaxation oscillation wavelength dependence offers a method to distinguish between three- and four-level transitions. This knowledge can then be used in spectroscopic studies and in determining parameters like the laser transition cross-section [178, 179]. The preferable laser gain material is based on four-level system [180] because three-level introduces various additional constraints. For example, reabsorption in the gain fiber is higher for the three-level system than for four-level systems. The lower laser level has no appreciable population during laser operation for four-level gain media. In that way, reabsorption of the laser radiation is avoided if there is no absorption on other transitions at the lasing wavelength. This also means that there is no absorption in the gain medium in the unpumped state, and the gain should rise linearly with the absorbed pump power. In addition, the laser threshold is generally expected to be lower in four-level material than for a three-level system.

4.3 Ytterbium

First we studied the relaxation oscillations in an ytterbium fiber laser at room temperature in a wide spectral range [P3]. The measurements were performed with the setup shown in Fig. 4.2. A linear cavity containing a section of Yb^{3+}-doped fiber as the gain medium was pumped through a wavelength division multiplexer (WDM). The 980-nm pump diode was isolated from laser cavity backreflections by placing two additional WDMs in series to protect the diode and increase the system stability. A diffraction grating serving as a cavity mirror was placed in a Littrow configuration to provide wavelength tunability. The laser output was taken from a fiber loop mirror at the opposite end of the cavity. In addition, a 1-kHz chopper was placed in the free space section of the cavity to observe the transient evolution of the laser emission towards its stationary state.

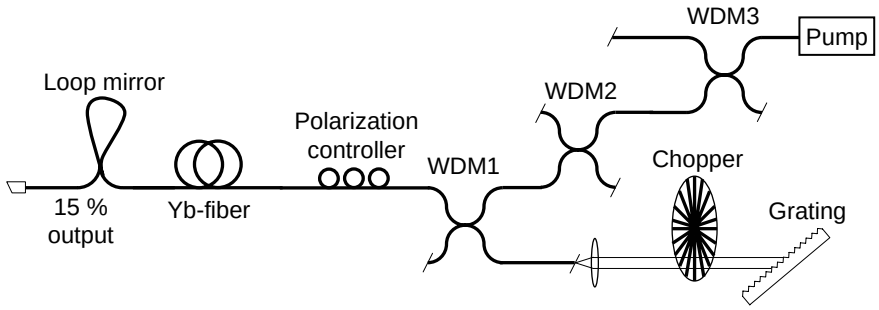

Fig. 4.2: *The experimental setup for measuring ytterbium fiber relaxation oscillations.*

The relaxation oscillation frequency can be measured in two different ways. The first method is to observe the oscillations with a digital oscilloscope that is triggered from the chopper. The data is then entered into a program that picks up the peaks from the small-signal oscillations and calculates the corresponding frequency. The second method is to look at the output signal radio frequency (RF) spectrum using an electrical spectrum analyzer (ESA). The relaxation oscillation frequency appears as a wide maximum in the range of tens or hundreds of kHz and can easily be identified as it increases with increasing pump power. However, one should not mistake the relaxation oscillation frequency with its higher order harmonics or the chopper frequency. A mistake would be most likely near the threshold level, as here they are on the same order of magnitude. Both methods give essentially the same results within the precision of these measurements. Error in these measurements is caused mainly by temperature changes in the system and slight changes in the laser cavity alignment

while tuning the wavelength. Another possible source of error is associated with determining the laser threshold which is done by plotting the laser output power versus pump power and extracting the threshold from the linear fit to data. Laser threshold can also be distinguished from the oscilloscope screen, as the first laser spikes appear around threshold pump power.

As we know from eq. (4.1), the square of relaxation oscillation frequency is proportional to the normalized pump power. We therefore performed a set of measurements of f_{relax}^2 versus pump power to determine the slope $\omega_{relax}^2/(r-1)$ for each wavelength, as shown in Fig. 4.3. We found out that the slope depends on the wavelength below 1060 nm, as shown in Fig. 4.4, indicating three-level operation. Whereas at longer wavelengths of the ytterbium fiber gain spectrum the laser transitions becomes closer to four-level. This tendency is of course expected, because three-level behavior is inevitable for gain media with a very small quantum defect. In 980-nm pumped Yb, the energy spacing between the lower laser level and the ground state is naturally small, so the thermal population of the lower laser level could be significant. In conclusion, in [P3] we identified four-level behavior at longer wavelengths and that a change in dynamics to a three-level mechanism occurs below 1060 nm wavelength.

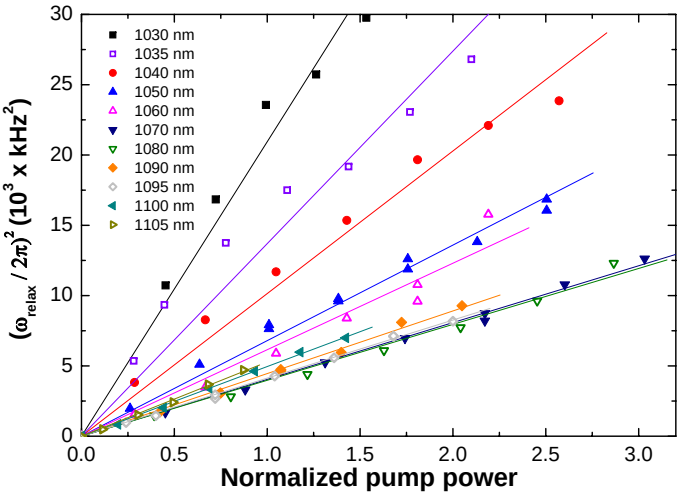

Fig. 4.3: *The ytterbium relaxation oscillation frequencies squared in the 1030–1105 nm range as a function of normalized pump power.*

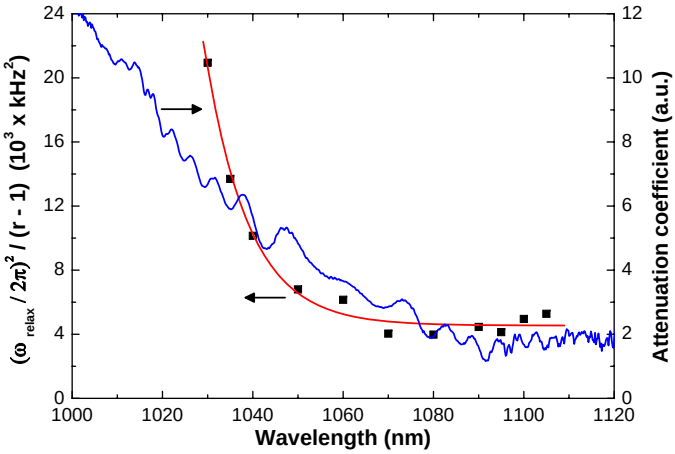

Fig. 4.4: *Characteristic ytterbium relaxation oscillation frequency slope, $\omega^2_{relax}/(r-1)$, in 1030–1105 nm wavelength range and the gain fiber attenuation. A notable change in dynamic behavior is observed around 1060 nm.*

4.4 Thulium-holmium

Another material studied during this work is thulium, usually co-doped with holmium. The results of Tm-Ho relaxation oscillations are presented in paper [P5]. Our results were later confirmed in [181] without holmium co-doping but the main tendency remains the same. Measurements were performed in a similar way as for ytterbium although we used optical components at the 2 μm wavelength region. The experimental setup is shown in Fig. 4.5. The main difference was related to the pumping, which was much more powerful than that used in the ytterbium experiments.

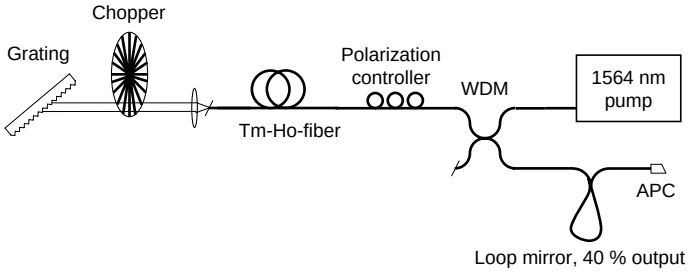

Fig. 4.5: *The thulium-holmium relaxation oscillation measurement setup.*

The high pump power, up to 6 W at 1564 nm, used here enabled us to perform measurements in a broad range of 1860–2020 nm. The relaxation oscillation curves at

different wavelengths as a function of normalized pump power are shown in Fig. 4.6. However, we believe that more pump power and less losses with improved fiber quality would have enabled us to examine the long-wavelength tail of the gain material in more detail, giving us a better understanding of the gain medium.

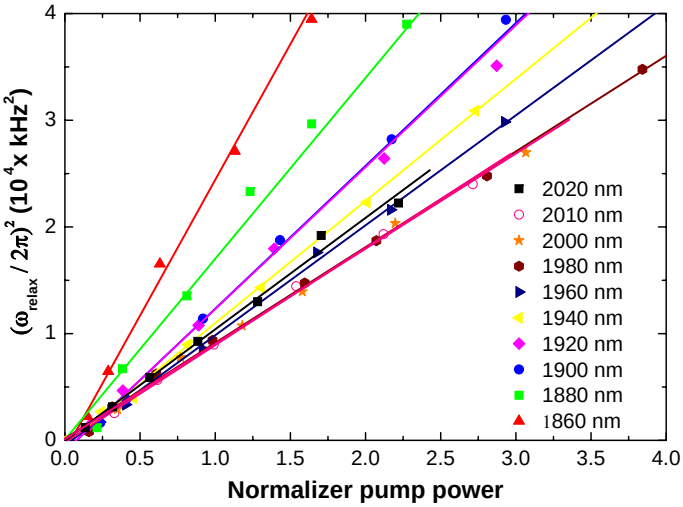

Fig. 4.6: *The thulium-holmium relaxation oscillation frequencies squared in the 1860–2020 nm range as a function of normalized pump power.*

Fig. 4.7 summarizes the results in the form of the relaxation oscillation frequency squared versus normalized pump power. The figure reveals that the Tm-Ho fiber laser operates as a three-level system at shorter wavelengths ($\lambda < 1960$ nm) and the slopes become fairly wavelength insensitive at longer wavelengths, suggesting that the laser operates as a four-level scheme. However, since the measurement range was limited to 2020 nm, we could not verify if the three-level nature would appear due to Ho-related transitions, but even then for further increases, perhaps in the region 2050–2100 nm, we expect that the four-level transition of Ho will dominate. Moreover, looking at recent measurements with thulium [181] using up to 17.5 W of absorbed pump power, we can argue that part of our long-wavelength tail is still in a quasi-three-level region, and it is obvious that the dynamics of thulium-holmium are fairly complicated. The situation could be further clarified by a systematic study of Ho-co-doped Tm-fibers with different Ho-concentrations, and having larger pump powers at our disposal would broaden our measurement range.

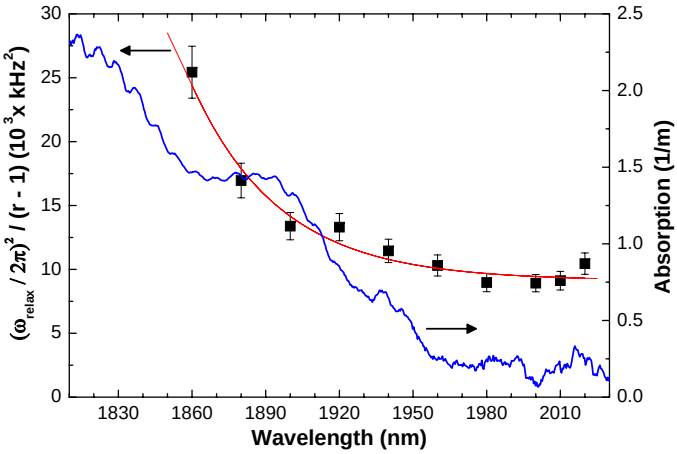

Fig. 4.7: *Characteristic thulium-holmium relaxation oscillation frequency slope,* $\omega^2_{relax}/(r-1)$*, in 1860–2020 nm wavelength range.*

4.5 Summary

In this chapter the relaxation dynamics of ytterbium and thulium-holmium gain materials were studied. It was observed that in both materials a dramatic change in laser dynamics occurs in the middle of the gain bandwidth. Both materials shift from three-level to four-level operation in the long-wavelength tail of the laser tuning range.

5. HIGH REPETITION RATE SHORT PULSE FIBER LASERS

In this chapter we discuss a novel method to shorten the length of an all-fiber laser cavity by moving the pump coupler outside the cavity and pumping the laser through a thin film dichroic output coupler. This output coupler is a mirror consisting of approximately 20–30 thin layers deposited on the fiber end. The dichroic structure acts as a laser output coupler and a wavelength division multiplexer. The short-length cavity enables a larger fundamental repetition rate, yet maintains the quality and short duration of the pulse. The laser is highly compact and free of bulk elements.

5.1 Why high repetition rate?

High repetition rate lasers are routinely used in telecom applications, where pulse width is typically on the order of tens to hundreds of ps. However, there are a number of other applications where high repetition rate is beneficial but the pulses need to be shorter, and the required wavelength is outside the range where fast telecom lasers are available.

Fiber lasers do not usually have a high repetition rate; typically it is on the order of tens of MHz. Shortening the laser cavity makes the laser more compact and increases the fundamental repetition rate, which is given by

$$f = \frac{c}{2nL}, \tag{5.1}$$

where c is the speed of light, n the effective refractive index of the cavity, in this case the fiber, and L the cavity length. The higher repetition rate enables new, interesting technological solutions in different applications. These include measurement systems that monitor fast moving processes, e.g. chemical reactions, which require a high repetition rate and simultaneously short pulses. J. Hult et al. [182] for instance, needed to build a four Nd:YAG laser cluster to reach a repetition rate of just 100 MHz and their system repetition rate was still inadequate: ”Three-dimensional imaging of OH radicals is another goal, which can be reached only when high-repetition-rate

pumping of the dye laser becomes possible."

High repetition rates are particularly important in, for example, generating quasi-cw UV light for illumination within semiconductor inspection. The use of short pulses is important in order to generate simple and efficient frequency conversion and at the same time the repetition rate needs to exceed about 400–500 MHz to give the appearance of cw-light. However, when powers in the UV approach the level of several Watts, it is important to have low pulse energy to avoid the potential for ablation of the material under inspection. With conventional diode pumped solid-state lasers, it is difficult to attain high repetition rates, but this can be enabled by fibre lasers such as the one described within this thesis.

There are also other applications where a high fundamental repetition rate is preferable. Applications at 1 μm include micromachining, where high repetition rates enable a high speed of material processing, e.g. the drilling process. High repetition rates and, therefore, high average powers in two-photon microscopy enable a strong signal and a good signal to noise ratio. This is why high repetition rate, short pulse lasers are key elements in nonlinear bioimaging techniques such as two-photon fluorescence excitation (TPE) microscopy. Typically, however, only a fraction of the laser power available can be delivered to the sample before photoinduced damage becomes excessive [183]. High repetition rate is also important to reduce photobleaching.

Harmonic mode locking, in contrast to high-fundamental repetition rate mode locking, requires electronic control of the repetition rate and additional elements such as amplitude modulators, which makes the setup more complex and more expensive. This is why we expect that dichroic fiber coatings will simplify a number of laser systems and that the increased repetition rate would be useful in a number of different applications.

5.2 Dichroic fiber end facet coatings

In contrast to the situation which existed a few years ago, coated fiber ends are now commercially available and simple anti-reflection coated fibers are already sold from stock. More complicated customized coatings are still rare, but demand for them is constantly growing. In [P6] we present a challenging dichroic mirror on a fiber connector end with transmission and reflection regions close to each other, 980 and 1040 nm. Such a mirror naturally raises several problems to solve. First, the required steep slope from high pump transmission to high reflectivity for the lasing wavelength automatically necessitates multiple, maybe 20–40 or even more layers, which leads

to adhesion problems. Second, it is not advisable to heat fiber connectors above a certain temperature because of the fiber-to-ferrule thermal expansion mismatch and possible fiber polymer coating damage. Third, not all materials have good adhesion to the fiber end facet at low temperatures, and fourth, a too thick coating may not necessarily work well in reflection for a single-mode fiber with a mode field diameter $\sim$6 μm, which is only twice the coating thickness. This means that we need to find a proper balance between laser requirements and coating thickness, and to do so with the materials that are available to us.

Most of the problems set by the targeted dichroic mirror are related to material properties to a greater or lesser degree. Therefore, we need to keep in mind that common electron beam evaporation materials have the most favorable general properties for thin film structure fabrication. Typical desired features in order of importance are

- no radioactivity,
- no toxicity,
- high or low refractive index,
- good adhesion,
- low absorption,
- low stress,
- homogeneity,
- good heat conductivity,
- suitable thermal expansion coefficient and
- low cost.

However, the order of importance can vary depending on the application. In the end, we need to make a compromise between the parameters. For example, even though TiO_2 has a high refractive index and is widely used in the thin film industry, it is prone to structural transformation, and multilayer coatings that consist of TiO_2 have shown failures such as tensile fracture and delamination [184, 185]. Tantalum pentoxide, Ta_2O_5, on the other hand, is susceptible to developing coating defects such as nodules [186] when it is deposited under higher oxygen partial pressure and substrate temperatures [187, 188]. In this research we found zirconium oxide, or zirconia, ZrO_2, to be the best material for our purposes even though it has a tendency to form inhomogeneous optical layers. This problem stems from the very high temperature required for evaporation and the tendency for multiple crystal phases to develop within the different temperature gradients in the e-beamed area [189]. However, by sacrificing some layer homogeneity we gain better adhesion to the optical fiber and

to the low index material, SiO_2. MgF_2 would also have been a possible low index material but we avoid it due to its known high tensile stress. Fluorides in general tend to be in tensile stress, a fact that limits the thickness to which MgF_2 layers can be deposited [98].

In [P6] we deposited dielectric thin films onto a single-mode fiber end, typically assembled with a FC/PC-connector. After testing different materials and temperature regimes to achieve good adhesion to an optical fiber end facet, we found that high temperature (150 °C and above) has a detrimental effect on the coatings and leads to poor adhesion and structural defects due to thermal stress. As a high index material, TiO_2 proved to have a weaker adhesion to fiber compared to ZrO_2. However, ZrO_2 tablets have a tendency to shoot out fragments of material during the evaporation unless they are heated carefully and a spiral electron beam shape is used. The best results were achieved when the sample was heated to 90 °C with ZrO_2 as a high index material (n=1.88 at 1 μm, evaporation rate 0.1–0.2 nm/s, $1.3 \cdot 10^{-4}$ mbar pressure) and SiO_2 as a low index material (n=1.44 at 1 μm, evaporation rate 0.35 nm/s, pressure around $5 \cdot 10^{-5}$ mbar). Oxygen was added to sustain the pressure. An example of a successful coating is shown in Fig. 5.1.

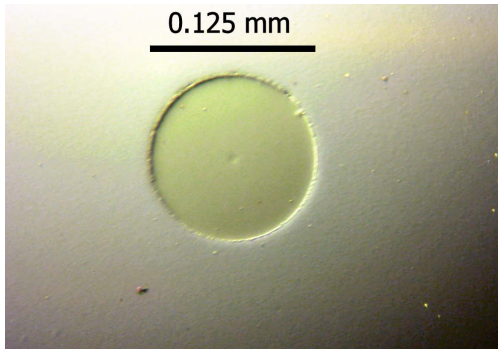

Fig. 5.1: *A successful coating with a smooth surface.*

Since the exact refractive index and actual evaporation rate depend on various factors such as chamber gas partial pressures, evaporation rate, substrate temperature and evaporation beam shape, careful calibration is needed and the mirror design should be tolerant to small perturbations in the evaporation process. It should be noted here that the dichroic mirror which was targeted for the current application should satisfy quite challenging requirements – a high throughput at the pump wavelength λ_p, and a given reflectivity at the signal wavelength λ_s which determines the output coupling of the laser cavity. An ideal spectral profile for this purpose would be a step-like shape. In practice, however, the mirror quality is largely determined by the spectral slope

$dR/d\lambda$ in the range between λ_p and λ_s, as shown in Fig. 5.2.

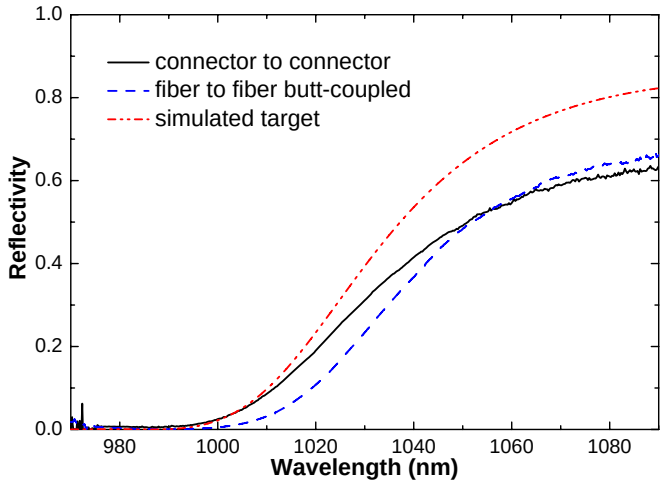

Fig. 5.2: *Reflectivity spectra of a typical dichroic coating on fiber connector. The design shown had 21 layers of ZrO_2 and SiO_2. The variation in the spectral response may originate from the small air gap between the coated fiber and the matched fiber end. The coating thickness (3 µm) is relatively large compared to the 6 µm mode field diameter, resulting in small leakage of light to the fiber cladding.*

However, it is increasingly difficult to design structures with higher slopes when the number of layers is limited. We solved this problem by a common mathematical optimization process: first we defined the criteria for the thin film reflectivities and transmissions at the pump and signal wavelength regions, and second, we started the optimization from multiple different randomized structures, keeping the total amount of layers constant. This process was then repeated iteratively by adjusting the number of layers, target weights and wavelength ranges to maximize the slope while keeping a reasonable margin for error in deposition and avoiding too thick a layer structure. After designing these layer structures, they were deposited on fiber ends and characterized for reflectivity, transmission, film quality and durability and tested in a fiber laser. Once feedback had been obtained from the measurements and performance of the mode-locked laser, the coating design was improved with multiple iterations until the fiber laser worked properly with a high repetition rate. Our dichroic layer structure provided low reflectivity at the pump wavelength ($R_p < 0.5$ % at 980 nm) and reflectivity of $R_s > 40$ % at 1040 nm to ensure acceptable output coupling. The results are presented in Fig. 5.2. The evaporation process was found to be well controlled and allowed for repeatable results. Since thicker structures would not improve the overall performance, the number of layers was limited to 21–27.

5.3 Compact fiber laser with photonic crystal fiber

Publication [P6] demonstrates a short cavity, high repetition rate laser with ultrashort pulses using dichroic fiber end coatings described in the previous section. The dichroic coating is essential here for shortening the cavity. In contrast to high repetition rate erbium [190] or erbium-ytterbium [191] lasers, we also need to manage the cavity dispersion at 1.04 μm. In our laser we chose to use solid-core photonic bandgap fiber (SC-PBGF) for dispersion compensation. PBGF's dispersion and transmission characteristics are presented in Fig. 5.3. We also considered other all-fiber dispersion compensation methods, such as CFBGs, but they would have resulted in a major overcompensation due to their large anomalous dispersion [192]. The experimental setup is shown in Fig. 5.4. The passive mode locking was self-started using a SESAM whose details are described in [193].

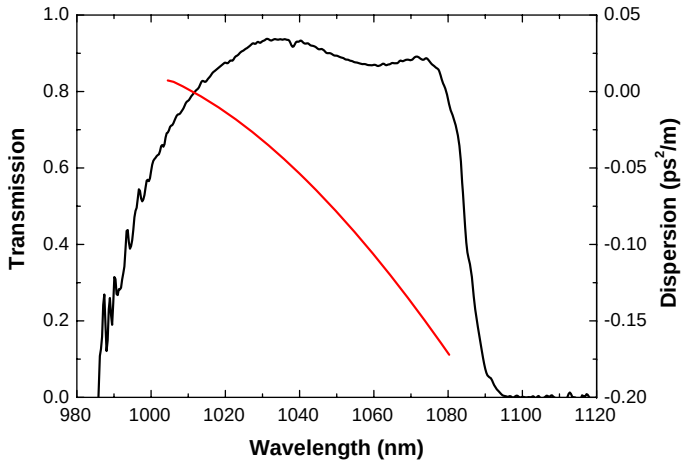

Fig. 5.3: *Solid-core photonic bandgap fiber transmission (black) and group delay dispersion per unit length (red).*

The cavity shortening down to 18 cm of fiber was achieved by placing the fiber coupler outside the cavity, resulting in a repetition rate of 571 MHz. We believe that further increase in the repetition rate would be possible using Yb-doped PBG fiber [194, 195]. The combination of doped dispersion managed fiber and dichroic fiber end coating could result in an even shorter cavity, and therefore an over 1 GHz repetition rate with ultrashort pulses seems viable. This would mean an approximately 10 cm long fiber cavity. A possible difficulty could be pumping efficiency and polarization sensitivity of the doped PBG fiber.

In our laser the output pulse duration was measured to be 572 fs which is evident from

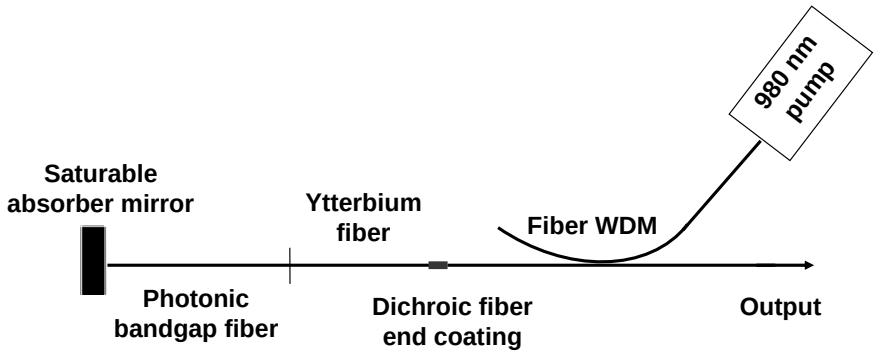

Fig. 5.4: *Fiber laser setup with a dichroic fiber end coating as a cavity end. The highly doped ytterbium fiber was 8 cm and the PBG fiber 10 cm long. The fiber WDM separated the up to 300 mW of 980-nm pump light and 1050-nm wavelength region for lasing.*

the interferometric autocorrelation measurements presented in Fig. 5.5. The figure also shows a nearly Gaussian spectrum that results in a time-bandwidth product by factor of ~ 2 over the transform limited time-bandwidth product. We believe that the pulses become positively chirped in the output fiber pigtail external to the laser cavity. The PBG fiber's third order dispersion is also likely to contribute to the pulse duration.

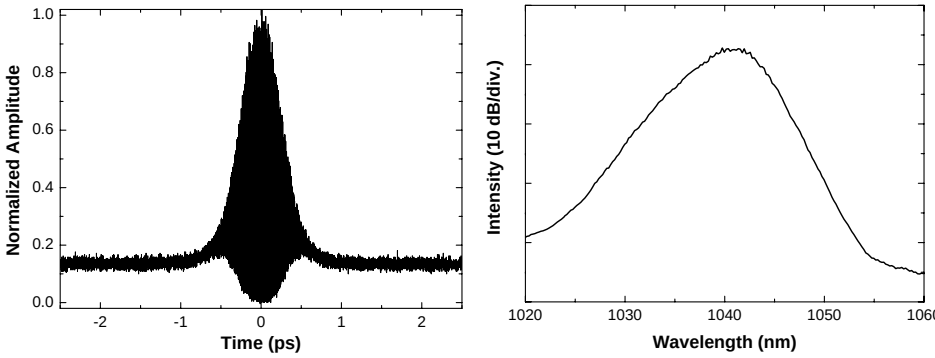

(a) (b)

Fig. 5.5: *(a) Interferometric autocorrelation shows 572 fs pulse width. (b) Nearly Gaussian pulse spectrum. Time-bandwidth product of 0.957 reveals that the pulses are slightly chirped in the output pigtail and could be compressed externally.*

5.4 Summary

To summarize, we have built a short all-fiber laser cavity and achieved a 571-MHz fundamental repetition rate, which is, to the best of our knowledge, the highest reported value for a 1 μm ytterbium fiber laser with ultrashort pulses. The pulse width of 572 fs is also a clear demonstration that our cavity dispersion is well balanced. It is anticipated that the dichroic fiber end coatings developed in this thesis will lend themselves to numerous future applications with high repetition rate fiber lasers, and enable novel laser configurations.

6. CONCLUSIONS

This thesis aimed at finding new ways to handle ultrashort pulse fiber laser dispersion issues and studying their dynamical properties. The emphasis was on dielectric thin films structures and their application to fiber laser cavities to improve system performance. The main achievements of this thesis are as follows:

A systematic investigation of ytterbium- and thulium-holmium-doped fiber laser relaxation oscillations revealed a dramatic change in laser dynamics in the middle of the gain bandwidth. Both materials shift from three-level to four-level operation in the long-wavelength tail of the laser tuning range.

Ytterbium fiber lasers were systematically studied in this thesis. A new dispersion compensation method for fiber lasers was successfully demonstrated. In our experiments we showed that a dielectric Gires–Tournois interferometer can compensate for Yb-fiber laser dispersion and enable 1.5-ps pulse duration.

This thesis reports optimized low finesse Fabry–Pérot etalons as dispersive elements in a fiber laser cavity. We have demonstrated that a FP etalon can provide anomalous dispersion for the fiber laser cavity and together with a semiconductor saturable absorber give rise to ultrashort pulses. The additional benefits of FP etalons in a fiber laser include convenient tuning over the whole gain bandwidth and solitonic sideband suppression.

In order to accommodate the increasing demand for more compact fiber lasers, we developed novel dichroic fiber end coatings. These coatings were deposited with an electron beam evaporator directly onto fiber end facets. The dichroic fiber end coating combined the properties of a laser output coupler and a pump coupler which enabled us to place the fiber pump combiner outside the cavity. The laser dispersion was managed with modern photonic crystal technology resulting in a pulse duration of 572 fs. These efforts allowed us to realize a compact all-fiber ytterbium fiber laser with a record high fundamental repetition rate of 571 MHz with ultrashort pulses.

In summary, we have studied mode-locked fiber lasers using optical thin film components. A number of thin film structures were designed, manufactured and applied in a new way to fiber lasers. The thesis demonstrates several cavities for which fiber laser performance is improved through the use of thin films. The most important contributions to the fiber laser field are the thorough study of different kinds of dispersive mirrors to compensate for fiber laser cavity dispersion and the investigation of dichroic coatings on fiber end facets.

BIBLIOGRAPHY

[1] J. Rautiainen, A. Härkönen, P. Tuomisto, J. Konttinen, L. Orsila, M. Guina, and O. G. Okhotnikov, "1-W at 617 nm generation by intracavity frequency conversion in semiconductor disk laser," *Electronics Letters*, vol. 43, no. 18, pp. 980–981, 2007.

[2] A. Härkönen, J. Rautiainen, T. Leinonen, Y. A. Morozov, L. Orsila, M. Guina, M. Pessa, and O. G. Okhotnikov, "Intracavity sum-frequency generation in dual-wavelength semiconductor disk laser," *IEEE Photonics Technology Letters*, vol. 19, no. 19, pp. 1550–1552, 2007.

[3] A. Härkönen, J. Rautiainen, M. Guina, J. Konttinen, P. Tuomisto, L. Orsila, M. Pessa, and O. G. Okhotnikov, "High power frequency doubled GaInNAs semiconductor disk laser emitting at 615 nm," *Optics Express*, vol. 15, no. 6, pp. 3224–3229, 2007. [Online]. Available: http://www.opticsexpress.org/abstract.cfm?URI=oe-15-6-3224

[4] E. J. Saarinen, A. Härkönen, R. Herda, S. Suomalainen, L. Orsila, T. Hakulinen, M. Guina, and O. G. Okhotnikov, "Harmonically mode-locked VECSELs for multi-GHz pulse train generation," *Optics Express*, vol. 15, no. 3, pp. 955–964, 2007. [Online]. Available: http://www.opticsexpress.org/abstract.cfm?URI=oe-15-3-955

[5] A. Härkönen, S. Suomalainen, E. Saarinen, L. Orsila, R. Koskinen, O. Okhotnikov, S. Calvez, and M. Dawson, "4-W single-transverse mode VECSEL utilising intra-cavity diamond heat spreader," *Electronics Letters*, vol. 42, no. 12, pp. 693–694, 2006.

[6] L. Orsila, R. Herda, and O. G. Okhotnikov, "High repetition rate mode-locked ytterbium fiber laser using dichroic fiber mirrors and photonic bandgap fiber technology," in *Proceedings of Fiber Lasers V: Technology, Systems, and Applications*, J. Broeng and C. H. III, Eds., vol. 6873,

no. 1. SPIE, 25 February 2008, p. 68731N. [Online]. Available: http://link.aip.org/link/?PSI/6873/68731N/1

[7] J. Rautiainen, A. Härkönen, P. Tuomisto, J. Konttinen, L. Orsila, M. Guina, and O. G. Okhotnikov, "1-W red light generation by intracavity doubling in a 1240 nm GaInNAs semiconductor disk laser," in *Proceedings of Solid State Lasers XVII: Technology and Devices*, W. A. Clarkson, N. Hodgson, and R. K. Shori, Eds., vol. 6871, no. 1. SPIE, 25 February 2008, p. 68711A. [Online]. Available: http://link.aip.org/link/?PSI/6871/68711A/1

[8] A. Härkönen, J. Rautiainen, J. Konttinen, T. Leinonen, P. Tuomisto, L. Orsila, M. Guina, M. Pessa, and O. Okhotnikov, "Optically-pumped semiconductor disk lasers for second-harmonic and sum-frequency generation," in *Proceedings of Nonlinear Optics: Materials, Fundamentals and Applications Topical Meeting and Tabletop Exhibit, Kona, Hawaii, USA*. OSA, 30 July–3 August 2007.

[9] E. J. Saarinen, A. Härkönen, R. Herda, S. Suomalainen, L. Orsila, T. Hakulinen, M. Guina, and O. G. Okhotnikov, "Harmonically mode-locked semiconductor disk lasers with multi-GHz repetition rate," in *Conference Digest of European Conference on Lasers and Electro-Optics, 2007 and the International Quantum Electronics Conference. CLEOE-IQEC 2007*. European Physical Society, 20–25 June 2007, pp. CB13–2–THU.

[10] A. Härkönen, J. Rautiainen, J. Konttinen, T. Leinonen, P. Tuomisto, L. Orsila, M. Guina, M. Saarinen, M. Pessa, and O. G. Okhotnikov, "Optically-pumped semiconductor disk lasers for second-harmonic and sum-frequency generation," in *Conference Proceedings of VIII Optics Days 2007, Lappeenranta, Finland*. Finnish Optical Society, 3–4 May 2007, p. 10.

[11] ——, "Optically-pumped semiconductor disk lasers for second-harmonic and sum-frequency generation," in *COST-288 Meeting, Metz, France*, 26–28 March 2007.

[12] A. Turtiainen, J. Viheriälä, L. Orsila, A. Tukiainen, A. Isomäki, and M. Pessa, "Spectroscopic ellipsometry in optoelectronics," in *Proceedings of the XL Annual Conference of the Finnish Physical Society, Tampere, Finland*. Institute of Physics, 9–11 March 2006, p. 132.

[13] A. Isomäki, M. Rusu, L. Orsila, M. Guina, and O. Okhotnikov, "Properties and applications of resonant nonlinear semiconductor reflectors," *Physica Scripta*, vol. 114, pp. 145–151, 2004.

[14] M. Guina, A. Vainionpää, A. Härkönen, L. Orsila, J. Lyytikäinen, and O. G. Okhotnikov, "Vertical-cavity saturable-absorber intensity modulator," *Optics Letters*, vol. 28, no. 1, pp. 43–45, 2003. [Online]. Available: http://ol.osa.org/abstract.cfm?URI=ol-28-1-43

[15] M. D. Guina, A. M. Vainionpää, L. Orsila, A. Härkönen, J. Lyytikäinen, L. A. Gomes, and O. G. Okhotnikov, "Saturable absorber intensity modulator," *IEEE Journal of Quantum Electronics*, vol. 39, no. 9, pp. 1143–1149, 2003.

[16] C. Porzi, L. Poti, A. Bogoni, L. Orsila, and M. Guina, "Double wavelength conversion with multi-resonant saturable absorber-based vertical-cavity semiconductor gate," in *Technical Digest of 12th Optoelectronics and Communications Conference (OECC) and 16th International Conference on Integrated Optics and Optical Fiber Communication (IOOC), Pacifico Yokohama, Kanagawa, Japan*. Institute of Electronics, Information and Communication Engineers, 9–13 July 2007, pp. 68–69.

[17] C. Porzi, M. Guina, L. Orsila, A. Bogoni, and L. Potì, "Simultaneous dual-wavelength conversion with multiresonant saturable absorption vertical-cavity semiconductor gate," *IEEE Photonics Technology Letters*, vol. 20, no. 7, pp. 499–501, April 1, 2008.

[18] C. Porzi, F. Fresi, L. Potì, A. Bogoni, M. Guina, L. Orsila, O. G. Okhotnikov, and N. Calabretta, "All-optical packet envelope detection using a slow semiconductor saturable absorber gate and a semiconductor optical amplifier," *IEEE Journal of Selected Topics in Quantum Electronics*, accepted for publication in 2008-01-28.

[19] C. Porzi, F. Fresi, L. Poti, A. Bogoni, M. Guina, L. Orsila, O. Okhotnikov, and N. Calabretta, "Contention resolution by means of packet envelope detection circuit with a slow saturable absorber-based vertical cavity semiconductor gate," in *Conference Proceeding of 19th Annual Meeting of the IEEE Lasers and Electro-Optics Society, Montreal, Quebec, Canada*. IEEE, 29 October–2 November 2006, pp. 559–560.

[20] A. Isomäki, M. Rusu, L. Orsila, M. Guina, and O. G. Okhotnikov, "Properties and applications of resonant nonlinear semiconductor reflectors," in *20th Nordic Semiconductor Meeting, Tampere, Finland*, 25–27 August 2003.

[21] L. A. Gomes, M. Guina, A. Vainionpää, A. Härkönen, L. Orsila, J. Lyytikäinen, M. B. Marques, and O. G. Okhotnikov, "Vertical-cavity saturable absorber intensity modulator," in *Proceedings of 4th Conference on Telecommunications (ConfTele) 2003, Aveiro, Portugal*. Telecommunications Institute, 18–20 June 2003.

[22] A. Vainionpää, M. Guina, A. Härkonen, L. Orsila, J. Lyytikäinen, M. Pessa, and O. G. Okhotnikov, "Surface-normal saturable absorber intensity modulator," in *Proceedings of IEEE International Conference on Indium Phosphide and Related Materials, 2003. Santa Barbara, USA*. IEEE, 12–16 May 2003, pp. 351–354.

[23] M. Guina, A. Härkönen, L. Orsila, A. Vainionpää, J. Lyytikäinen, and O. G. Okhotnikov, "Vertical-cavity saturable absorber intensity modulator," in *Optical Fiber Communication Conference, Atlanta, USA*, vol. Technical Digest OSA Trends in Optics and Photonics Vol. 86. OSA, 23–28 March 2003, pp. 79–80.

[24] M. Guina, N. Xiang, A. Vainionpää, S. Suomalainen, J. Lyytikäinen, L. Orsila, O. Okhotnikov, and T. Sajavaara, "Stretched-pulse fiber laser mode-locked with dispersive saturable absorber mirror," in *Technical Digest of Conference on Lasers and Electro-Optics (CLEO) 2002*. OSA, 2002, pp. 523–524.

[25] M. Rusu, S. Kivistö, L. Orsila, and O. G. Okhotnikov, "Practical Raman shifter based on a novel, highly nonlinear optical fiber," in *Proceeding of 2nd EPS-QEOD EuroPhoton Conference, Pisa, Italy*, vol. Europhysics Conference Abstracts: Volume 30J. European Physical Society, 10–15 September 2006, p. TuC5.

[26] L. Orsila, M. Rusu, S. Kivistö, A. Isomäki, R. Herda, A. Härkönen, T. Hakulinen, J. Kerttula, J. Rautiainen, E. Saarinen, M. Guina, and O. G. Okhotnikov, "Broadband light sources based on nonlinear fiber waveguides," in *Proceedings of the XL Annual Conference of the Finnish Physical Society, Tampere, Finland*. Institute of Physics, 9–11 March 2006, p. 305.

[27] A. Isomäki and L. Orsila, "Analyses of modulation bandwidth and coupling performance of plastic optical fibers," in *Conference Proceedings of 2nd Optics Days, Tampere, Finland*. Finnish Optical Society, 20–21 April 2001, p. P46.

[28] N. Kaiser and H. K. Pulker, *Optical Interference Coatings*, W. T. Rhodes, Ed. Springer-Verlag Berlin, 2003.

[29] B. Waggoner, "Robert Hooke, referenced 2007-11-15." [Online]. Available: http://www.ucmp.berkeley.edu/history/hooke.html

[30] J. J. MacIntosh and P. Anstey, *Stanford Encyclopedia of Philosophy*. Stanford University, 2007, ch. Robert Boyle, referenced 2007-11-15. [Online]. Available: http://plato.stanford.edu/entries/boyle/

[31] Wolfram Research, *Eric Weisstein's World of Science*, 2007, ch. Newton, Isaac (1642–1727), referenced 2007-11-15. [Online]. Available: http://scienceworld.wolfram.com/biography/Newton.html

[32] H. A. Macleod, *Thin-Film Optical Filters*, 3rd ed. Institute of Physics Publishing, 2001.

[33] E. Hecht, *Optics*, 3rd ed. Massachusetts: Addison-Wesley, 1998.

[34] Fraunhofer-Gesellschaft, "Joseph von Fraunhofer, referenced 2007-11-19," 2007. [Online]. Available: http://www.fraunhofer.de/EN/company/profile/joseph/index.jsp

[35] C. Fabry and A. Pérot, "Théorie et applications d'une nouvelle méthode de spectroscopie interférentielle," *Annales de Chimie et de Physique*, vol. 16, no. 7, pp. 115–144, 1899.

[36] J. F. Mulligan, "Who were Fabry and Pérot?" *American Journal of Physics*, vol. 66, no. 9, pp. 797–802, September 1998. [Online]. Available: http://www.physics.rutgers.edu/ugrad/387/Mulligan98.pdf

[37] Wikipedia, "Charles Fabry, version 13:28, 20 September 2007," 2007. [Online]. Available: http://en.wikipedia.org/wiki/Charles_Fabry

[38] ——, "Jean-Baptiste Alfred Perot, version 04:12, 3 October 2007," 2007. [Online]. Available: http://en.wikipedia.org/wiki/Alfred_Perot

[39] W. Steckelmacher, *Vacuum Science and Technology: Pioneers of the 20th Century*. AIP Press, 1994, ch. Cecil Reginald Burch (1901–1983), pp. 25–27.

[40] W. Steckelmacher and L. Holland, "Fifty years of advances in vacuum science and technology," *Journal of Physics E: Scientific Instruments*, vol. 6, pp. 948–951, 1973.

[41] B. E. A. Saleh and M. C. Teich, *Fundamentals of Photonics*, 2nd ed. John Wiley & Sons, 2007.

[42] Wikipedia, "Theodore Harold Maiman, version 13:43, 8 November 2007," 2007. [Online]. Available: http://en.wikipedia.org/wiki/Theodore_Harold_Maiman

[43] T. H. Maiman, "Stimulated optical radiation in ruby," *Nature*, vol. 187, pp. 493–494, 1960.

[44] E. Snitzer, "Optical maser action of Nd^{+3} in a barium crown glass," *Physical Review Letters*, vol. 7, no. 12, pp. 444–446, December 1961.

[45] ——, "Optical dielectric waveguides," *PGMTT National Symposium Digest*, vol. 61, no. 1, pp. 45–46, May 1961.

[46] C. J. Koester and E. Snitzer, "Amplification in a fiber laser," *Applied Optics*, vol. 3, no. 10, pp. 1182–1186, 1964.

[47] S. Poole, D. Payne, R. Mears, M. Fermann, and R. Laming, "Fabrication and characterization of low-loss optical fibers containing rare-earth ions," *Journal of Lightwave Technology*, vol. 4, no. 7, pp. 870–876, 1986.

[48] S. B. Poole, D. N. Payne, and M. E. Fermann, "Fabrication of low-loss optical fibres containing rare-earth ions," *Electronics Letters*, vol. 21, no. 17, pp. 737–738, 1985. [Online]. Available: http://link.aip.org/link/?ELL/21/737/1

[49] H. J. Shaw, M. Chodorow, and M. J. F. Digonnet, "Fiber optic amplifier," United States Patent 4,515,431, May 1985.

[50] P. Urquhart, "Review of rare earth doped fibre lasers and amplifiers," *IEE Proceedings Journal Optoelectronics*, vol. 135, no. 6, pp. 385–407, December 1988.

[51] I. P. Alcock, A. C. Tropper, A. I. Ferguson, and D. C. Hanna, "Q-switched operation of a neodymium-doped monomode fibre laser," *Electronics Letters*, vol. 22, no. 2, pp. 84–85, 1986. [Online]. Available: http://link.aip.org/link/?ELL/22/84/1

[52] I. P. Alcock, A. I. Ferguson, D. C. Hanna, and A. C. Tropper, "Mode-locking of a neodymium-doped monomode fibre laser," *Electronics Letters*, vol. 22, no. 5, pp. 268–269, 1986. [Online]. Available: http://link.aip.org/link/?ELL/22/268/1

[53] M. E. Fermann, "Ultrashort-pulse sources based on single-mode rare-earth-doped fibers," *Applied Physics B: Lasers and Optics*, vol. 58, no. 3, pp. 197–209, 1994.

[54] I. N. Duling, L. Goldberg, and J. F. Weller, "High-power, mode-locked Nd:fibre laser pumped by an injection-locked diode array," *Electronics Letters*, vol. 24, no. 21, pp. 1333–1335, 13 October 1988.

[55] G. Geister and R. Ulrich, "Neodymium-fibre laser with integrated-optic mode locker," *Optics Communications*, vol. 68, no. 3, pp. 187–189, 1 October 1988.

[56] M. W. Phillips, A. I. Ferguson, and D. C. Hanna, "Frequency-modulation mode locking of a Nd^{3+}-doped fiber laser," *Optics letters*, vol. 14, no. 4, pp. 219–221, 1989.

[57] J. D. Kafka, T. Baer, and D. W. Hall, "Mode-locked erbium-doped fiber laser with soliton pulse shaping," *Optics Letters*, vol. 14, no. 22, p. 1269, 1989. [Online]. Available: http://ol.osa.org/abstract.cfm?URI=ol-14-22-1269

[58] J. D. Kafka and T. M. Baer, "Subpicosecond fiber laser," United States Patent 4,835,778, May 1989.

[59] M. E. Fermann, M. Hofer, F. Haberl, and S. P. Craig-Ryan, "Femtosecond fibre laser," *Electronics Letters*, vol. 26, no. 20, pp. 1737–1738, 27 September 1990.

[60] M. E. Fermann, M. Hofer, F. Haberl, A. J. Schmidt, and L. Turi, "Additive-pulse-compression mode locking of a neodymium fiber laser," *Optics Letters*, vol. 16, no. 4, pp. 244–246, 1991.

[61] I. N. Duling, "All-fiber ring soliton laser mode locked with a nonlinear mirror," *Optics Letters*, vol. 16, no. 8, pp. 539–541, 1991.

[62] ——, "Subpicosecond all-fibre erbium laser," *Electronics Letters*, vol. 27, no. 6, pp. 544–545, 14 March 1991.

[63] J. Nilsson, J. K. Sahu, Y. Jeong, V. Philippov, D. B. Soh, C. A. Codemard, P. Dupriez, J. Kim, D. J. Richardson, A. Malinowski, A. N. Piper, J. H. Price, K. Furusawa, W. A. Clarkson, and D. N. Payne, "High power fiber lasers," in *Optical Fiber Communication Conference and Exposition and The National Fiber Optic Engineers Conference*. Optical Society of America, 2005, p. OTuF1. [Online]. Available: http://www.opticsinfobase.org/abstract.cfm?URI=URI=OFC-2005-OTuF1

[64] D. H. Sutter, G. Steinmeyer, L. Gallmann, N. Matuschek, F. Morier-Genoud, U. Keller, V. Scheuer, G. Angelow, and T. Tschudi, "Semiconductor saturable-absorber mirror assisted Kerr-lens mode-locked Ti:sapphire laser producing pulses in the two-cycle regime," *Optics Letters*, vol. 24, no. 9, pp. 631–633, 1999. [Online]. Available: http://ol.osa.org/abstract.cfm?URI=ol-24-9-631

[65] J. P. van der Ziel, W. T. Tsang, R. A. Logan, R. M. Mikulyak, and W. M. Augustyniak, "Subpicosecond pulses from passively mode-locked GaAs buried optical guide semiconductor lasers," *Applied Physics Letters*, vol. 39, no. 7, pp. 525–527, 1981. [Online]. Available: http://link.aip.org/link/?APL/39/525/1

[66] I. N. Duling, *Compact Sources of Ultrashort Pulses*. Cambridge University Press, 1995.

[67] U. Keller and A. C. Tropper, "Passively modelocked surface-emitting semiconductor lasers," *Physics Reports*, vol. 429, no. 2, pp. 67–120, 2006.

[68] K. Jasim, Q. Zhang, A. V. Nurmikko, A. Mooradian, G. Carey, W. Ha, and E. P. Ippen, "A passively mode-locked surface emitting diode laser," in *Proceedings of Conference on Lasers and Electro-Optics, 2003 (CLEO'03)*, 1–6 June 2003, p. CThPDC6.

[69] Q. Zhang, K. Jasim, A. V. Nurmikko, A. Mooradian, G. Carey, W. Ha, and E. Ippen, "Operation of a passively mode-locked extended-cavity surface-emitting diode laser in multi-GHz regime," *IEEE Photonics Technology Letters*, vol. 16, no. 3, pp. 885–887, March 2004.

[70] IPG Photonics, "Low-order-mode kilowatt fiber lasers operating at 1.07 microns, referenced 2007-12-29." [Online]. Available: http://www.ipgphotonics.com/apps_materials_multi.htm

[71] V. P. Gapontsev, "Penetration of fiber lasers into industrial market," in *Photonics West 2008, San Jose, CA, USA*, 19 January 2008, pp. 6873–01.

[72] J. Limpert, F. Roser, T. Schreiber, and A. Tünnermann, "High-power ultrafast fiber laser systems," *IEEE Journal of Selected Topics in Quantum Electronics*, vol. 12, no. 2, pp. 233–244, 2006.

[73] M. Rusu, "Frequency conversion using ultrafast fiber lasers," Ph.D. dissertation, Tampere University of Technology, Tampere, November 2006.

[74] T. Juhasz, F. H. Loesel, R. M. Kurtz, C. Horvath, J. F. Bille, and G. Mourou, "Corneal refractive surgery with femtosecond lasers," *IEEE Journal of Selected Topics in Quantum Electronics*, vol. 5, no. 4, pp. 902–910, July–August 1999.

[75] S. O. Konorov, V. P. Mitrokhin, A. B. Fedotov, D. A. Sidorov-Biryukov, V. I. Beloglazov, N. B. Skibina, A. V. Shcherbakov, E. Wintner, M. Scalora, and A. M. Zheltikov, "Laser ablation of dental tissues with picosecond pulses of 1.06-μm radiation transmitted through a hollow-core photonic-crystal fiber," *Applied Optics*, vol. 43, no. 11, pp. 2251–2256, 2004.

[76] K. Kim, Z. Guo, J. K.-J. Li, and S. Kumar, "Radiation heat transfer in tissue welding and soldering with ultrafast lasers," in *Proceedings of IEEE 29th Annual Bioengineering Conference, 2003*, 22–23 March 2003, pp. 185–186.

[77] X. Liu, D. Du, and G. Mourou, "Laser ablation and micromachining with ultrashort laser pulses," *IEEE Journal of Quantum Electronics*, vol. 33, no. 10, pp. 1706–1716, October 1997.

[78] D. Y. Shen, J. K. Sahu, and W. A. Clarkson, "High-power widely tunable Tm:fibre lasers pumped by an Er,Yb co-doped fibre laser at 1.6 μm," *Optics Express*, vol. 14, no. 13, pp. 6084–6090, 2006. [Online]. Available: http://www.opticsexpress.org/abstract.cfm?URI=oe-14-13-6084

[79] A. Hayward, W. A. Clarkson, P. W. Turner, J. Nilsson, A. B. Grudinin, and D. C. Hanna, "Efficient cladding-pumped Tm-doped silica fibre laser with high power singlemode output at 2 μm," *Electronics Letters*, vol. 36, no. 8, pp. 711–712, 13 April 2000.

[80] Cerac Inc., "Optical thin film technology: Mechanical properties," *Coating Material News*, vol. 17, no. 3, September 2007.

[81] B. Fan, M. Suzuki, and K. Tang, "Ion-assisted deposition of TiO_2/SiO_2 multilayers for mass production," *Applied Optics*, vol. 45, no. 7, pp. 1461–1464, 2006. [Online]. Available: http://ao.osa.org/abstract.cfm?URI=ao-45-7-1461

[82] J. T. Cox, H. Hass, and J. B. Ramsey, "Improved dielectric films for multilayer coatings and mirror protection," *Journal of Physics (Paris)*, vol. 25, pp. 250–254, 1964.

[83] E. T. Arakawa and M. W. Williams, "Optical properties of aluminum oxide in the vacuum ultraviolet," *Journal of Physics and Chemistry of Solids*, vol. 29, no. 5, pp. 735–744, May 1968.

[84] H. H. Li, "Refractive index of silicon and germanium and its wavelength and temperature derivatives," *Journal of Physical and Chemical Reference Data*, vol. 9, no. 3, pp. 561–658.

[85] H. W. Icenogle, B. C. Platt, and W. L. Wolfe, "Refractive indexes and temperature coefficients of germanium and silicon," *Applied Optics*, vol. 15, no. 10, pp. 2348–2351, 1976.

[86] C. M. Randall and R. D. Rawcliffe, "Refractive indices of germanium, silicon, and fused quartz in the far infrared," *Applied Optics*, vol. 6, no. 11, pp. 1889–1895, 1967.

[87] J. D. T. Kruschwitz and W. T. Pawlewicz, "Optical and durability properties of infrared transmitting thin films," *Applied Optics*, vol. 36, no. 10, 1997.

[88] D. Smith and P. Baumeister, "Refractive index of some oxide and fluoride coating materials," *Applied Optics*, vol. 18, no. 1, p. 111, 1979.

[89] J. P. Borgogno, B. Lazarrides, and E. Pelletier, "Automatic determination of the optical constants of inhomogeneous thin films," *Applied Optics*, vol. 21, no. 22, pp. 4020–4029, 15 November 1982.

[90] H. K. Pulker, "Characterization of optical thin films," *Applied Optics*, vol. 18, no. 12, pp. 1969–77, 1979.

[91] G. Hass and C. Salzberg, "Optical properties of silicon monoxide in the wavelength region from 0.24 to 14.0 microns," *Journal of Optical Society of America*, vol. 44, no. 3, pp. 181–187, March 1954.

[92] E. D. Palik, *Handbook of Optical Constants of Solids*. San Diego: Academic Press, 1985, vol. 1.

[93] H. K. Pulker, G. Paesold, and E. Ritter, "Refractive indices of TiO_2 films produced by reactive evaporation of various titanium-oxygen phases," *Applied Optics*, vol. 15, no. 12, p. 2986, 1976. [Online]. Available: http://ao.osa.org/abstract.cfm?URI=ao-15-12-2986

[94] H. Selhofer, E. Ritter, and R. Linsbod, "Properties of titanium dioxide films prepared by reactive electron-beam evaporation from various starting materials," *Applied Optics*, vol. 41, no. 4, pp. 756–762, 1 February 2002.

[95] G. Hass, "Preparation, properties and optical applications of thin films of titanium dioxide," *Vacuum*, vol. 11, pp. 331–345, 1952.

[96] K. Balasubramanian, X. F. Han, and K. H. Guenther, "Comparative study of titanium dioxide thin films produced by electron-beam evaporation and by reactive low-voltage ion plating," *Applied Optics*, vol. 32, no. 28, p. 5594, 1993. [Online]. Available: http://ao.osa.org/abstract.cfm?URI=ao-32-28-5594

[97] Cerac Inc., "Stress compensation techniques for oxide-compound coatings," *Coating Material News*, vol. 17, no. 3, September 2007.

[98] R. Thielsch, J. Heber, T. Feigl, and N. Kaiser, "Stress, microstructure and thermal-elastic properties of evaporated thin MgF_2-films," in *Proceedings of Optical Interference Coatings*. Optical Society of America, 2004, p. ThE6. [Online]. Available: http://www.opticsinfobase.org/abstract.cfm?URI=OIC-2004-ThE6

[99] R. Thielsch, A. Gatto, and N. Kaiser, "Mechanical stress and thermal-elastic properties of oxide coatings for use in the deep-ultraviolet spectral region," *Applied Optics*, vol. 41, no. 16, pp. 3211–3216, 2002.

[100] P. Leinonen, "Techniques for semiconductor laser processing," Ph.D. dissertation, Tampere University of Technology, Tampere, November 2007.

[101] FerroTec, "Electron beam evaporation, referenced 2007-12-06." [Online]. Available: http://www.ferrotec.com/technology/electronbeam.php

[102] P. Yeh, *Optical Waves in Layered Media*. New York: John Wiley & Sons, 1988.

[103] H. J. Cho, M. J. Shin, and J. C. Lee, "Effects of substrate and deposition method onto the mirror scattering," *Applied Optics*, vol. 45, no. 7, pp. 1440–1446, 2006.

[104] G. Rempe, R. J. Thompson, H. J. Kimble, and R. Lalezari, "Measurement of ultralow losses in an optical interferometer," *Optics Letters*, vol. 17, no. 5, pp. 363–366, 1992.

[105] Wikipedia, "Complex number, version 14:17, 4 November 2007." [Online]. Available: http://en.wikipedia.org/wiki/Complex_number

[106] D. N. Christodoulides, E. Bourkoff, R. I. Joseph, and T. Simos, "Reflection of femtosecond optical pulses from multiple-layer dielectric mirrors—analysis," *IEEE Journal of Quamtum Electronics*, vol. 22, no. 1, pp. 186–191, January 1986.

[107] J. A. Dobrowolski, D. Dalacu, L. Li, P. Ma, D. Poitras, and P. G. Verly, "50 years of optical interference coatings at the National Research Council of Canada," *Optical Engineering*, vol. 18, no. 6, pp. 24–30, June 2007.

[108] P. G. Verly, "Design of a robust thin-film interference filter for erbium-doped fiber amplifier gain equalization," *Applied Optics*, vol. 41, no. 16, pp. 3092–3096, 2002. [Online]. Available: http://ao.osa.org/abstract.cfm?URI=ao-41-16-3092

[109] D. A. B. Miller, "Fundamental limit for optical components," *Journal of Optical Society of America B*, vol. 24, no. 10, pp. A1–A18, 2007. [Online]. Available: http://josab.osa.org/abstract.cfm?URI=josab-24-10-A1

[110] W. Zhou, M. Tao, L. Chen, and H. Yang, "Microstructured surface design for omnidirectional antireflection coatings on solar cells," *Journal of Applied Physics*, vol. 102, no. 10, p. 103105, 2007. [Online]. Available: http://link.aip.org/link/?JAP/102/103105/1

[111] J. Lazar and P. Pokorny, "Deposition and measurements of antireflection coatings for semiconductor lasers," in *Proceedings of SPIE*, vol. 4356. SPIE, 2003, p. 297.

[112] J. T. Cox, G. Hass, and W. R. Hunter, "Rapid communications: Infrared reflectance of silicon oxide and magnesium fluoride protected aluminum mirrors at various angles of incidence from 8 micrometers to 12 micrometers," *Applied Optics*, vol. 14, no. 6, pp. 1247–1250, 1975. [Online]. Available: http://ao.osa.org/abstract.cfm?URI=ao-14-6-1247

[113] Perkin Elmer Corp., "Multilayer antireflection coating for low index materials," Great Britain Patent GB1221360, June 1968.

[114] Thin Film Center Inc., "The Essential Macleod." [Online]. Available: http://www.thinfilmcenter.com/EMacleod.asp

[115] J. Lee, T. Tanaka, S. Sasaki, S. Uchiyama, M. Tsuchiya, and T. Kamiya, "Novel design procedure of broad-band multilayer antireflection coatings for optical and optoelectronic devices," *Journal of Lightwave Technology*, vol. 16, no. 5, pp. 884–891, 1998.

[116] P. Savolainen, "Puolijohdelasereiden peilipäätyjen pinnoitus," Master's thesis, Tampere University of Technology, 1992.

[117] M. Saarinen, "Visible vertical-cavity light emitters," Ph.D. dissertation, Tampere University of Technology, Tampere, September 2002.

[118] D. I. Babic and S. W. Corzine, "Analytic expressions for the reflection delay, penetration depth, and absorptance of quarter-wave dielectric mirrors," *IEEE Journal of Quantum Electronics*, vol. 28, no. 2, pp. 514–524, February 1992.

[119] L. Orsila, "Interferometric dielectric reflectors for dispersion compensation in fibre lasers," Master's thesis, Tampere University of Technology, Tampere, May 2003.

[120] RP Photonics Consulting GmbH, "Finesse, referenced 2008-01-04." [Online]. Available: http://www.rp-photonics.com/finesse.html

[121] R. Menzel, *Photonics*. Springer-Verlag, 2001.

[122] F. Gires and P. Tournois, "Interféromètre utilisable pour la compression d'impulsions lumineuses modulées en fréquence," *Comptes rendus de l'Académie des sciences*, vol. 258, pp. 6112–6115, 1964.

[123] K. D. Li, W. H. Knox, and N. M. Pearson, "Broadband cubic-phase compensation with resonant Gires-Tournois interferometers," *Optics Letters*, vol. 14, no. 9, pp. 450–452, 1989.

[124] I. T. Sorokina, E. Sorokin, E. Wintner, A. Cassanho, H. P. Jenssen, and R. Szipőcs, "Prismless passively mode-locked femtosecond Cr:LiSGaF laser," *Optics Letters*, vol. 21, no. 15, pp. 1165–1167, 1996.

[125] ——, "14-fs pulse generation in Kerr-lens mode-locked prismless Cr:LiSGaF and Cr:LiSAF lasers: observation of pulse self-frequency shift," *Optics Letters*, vol. 22, no. 22, pp. 1716–1718, 1997. [Online]. Available: http://ol.osa.org/abstract.cfm?URI=ol-22-22-1716

[126] B. Golubovic, R. R. Austin, M. K. Steiner-Shepard, M. K. Reed, S. A. Diddams, D. J. Jones, and A. G. V. Engen, "Double Gires–Tournois

interferometer negative-dispersion mirrors for use in tunable mode-locked lasers," *Optics Letters*, vol. 25, no. 4, pp. 275–277, 2000. [Online]. Available: http://ol.osa.org/abstract.cfm?URI=ol-25-4-275

[127] R. Szipőcs, A. Köházi-Kis, S. Lakó, P. Apai, A. Kovács, G. DeBell, L. Mott, A. Louderback, A. Tikhonravov, and M. Trubetskov, "Negative dispersion mirrors for dispersion control in femtosecond lasers: chirped dielectric mirrors and multi-cavity Gires–Tournois interferometers," *Applied Physics B: Lasers and Optics*, vol. 70, no. 7, pp. 51–57, 2000.

[128] R. Szipőcs, K. Ferencz, C. Spielmann, and F. Krausz, "Chirped multilayer coatings for broadband dispersion control in femtosecond lasers," *Optics Letters*, vol. 19, no. 3, pp. 201–203, February 1994. [Online]. Available: http://ol.osa.org/abstract.cfm?URI=ol-19-3-201

[129] E. J. Mayer, J. Möbius, A. Euteneuer, W. W. Rühle, and R. Szipőcs, "Ultrabroadband chirped mirrors for femtosecond lasers," *Optics Letters*, vol. 22, no. 8, pp. 528–530, April 1997. [Online]. Available: http://ol.osa.org/abstract.cfm?URI=ol-22-8-528

[130] S. R. A. Dods, Z. Zhang, and M. Ogura, "Highly dispersive mirror in Ta_2O_5/SiO_2 for femtosecond lasers designed by inverse spectral theory," *Applied Optics*, vol. 38, no. 21, pp. 4711–4719, 1999. [Online]. Available: http://ao.osa.org/abstract.cfm?URI=ao-38-21-4711

[131] F. X. Kärtner, N. Matuschek, T. Schibili, U. Keller, H. A. Haus, C. Heine, R. Morf, V. Scheuer, M. Tilsch, and T. Tschudi, "Design and fabrication of double-chirped mirrors," *Optics Letters*, vol. 22, no. 11, June 1997.

[132] N. Matuschek, F. X. Kärtner, and U. Keller, "Theory of double-chirped mirrors," *IEEE Journal of Selected Topics in Quantum Electronics*, vol. 4, no. 2, 1998.

[133] ——, "Analytical design of double-chirped mirrors with custom-tailored dispersion characteristics," *IEEE Journal of Quantum Electronics*, vol. 35, no. 2, February 1999.

[134] N. Matuschek, L. Gallmann, D. Sutter, G. Steinmeyer, and U. Keller, "Back-side-coated chirped mirrors with ultra-smooth broadband dispersion characteristics," *Applied Physics B: Lasers and Optics*, vol. 71, no. 4, pp. 509–522, 2000.

[135] B. Braun, F. X. Kärtner, G. Zhang, M. Moser, and U. Keller, "56-ps passively Q-switched diode-pumped microchip laser," *Optics Letters*, vol. 22, no. 6, pp. 381–383, 1997. [Online]. Available: http://ol.osa.org/abstract.cfm?URI=ol-22-6-381

[136] S. Kivistö, R. Herda, and O. G. Okhotnikov, "Electronically tunable Yb-doped mode-locked fiber laser," *IEEE Photonics Technology Letters*, vol. 20, no. 1, pp. 51–53, 1 January 2008.

[137] L. E. Nelson, D. J. Jones, K. Tamura, H. A. Haus, and E. P. Ippen, "Ultrashort-pulse fiber ring lasers," *Applied Physics B: Lasers and Optics*, vol. 65, no. 2, pp. 277–294, 1997.

[138] R. Herda, "Semiconductor mirrors for ultrafast fiber technology," Ph.D. dissertation, Tampere University of Technology, Tampere, December 2006.

[139] E. P. Ippen, "Principles of passive mode locking," *Applied Physics B: Lasers and Optics*, vol. 58, no. 3, pp. 159–170, March 1994.

[140] A. J. DeMaria, D. A. Stetser, and H. Heynau, "Self mode-locking of lasers with saturable absorbers," *Applied Physics Letters*, vol. 8, no. 7, pp. 174–176, 1966. [Online]. Available: http://link.aip.org/link/?APL/8/174/1

[141] A. J. DeMaria, C. M. Ferrar, and G. E. Danielson, Jr., "Mode locking of a Nd^{3+}-doped glass laser," *Applied Physics Letters*, vol. 8, no. 1, pp. 22–24, 1966. [Online]. Available: http://link.aip.org/link/?APL/8/22/1

[142] T. Yu, E. A. Golovchenko, A. N. Pilipetskii, and C. R. Menyuk, "Dispersion-managed soliton interactions in optical fibers," *Optics Letters*, vol. 22, no. 11, pp. 793–795, 1997. [Online]. Available: http://ol.osa.org/abstract.cfm?URI=ol-22-11-793

[143] R. Paschotta, J. Nilsson, A. C. Tropper, and D. C. Hanna, "Ytterbium-doped fiber amplifiers," *IEEE Journal of Quantum Electronics*, vol. 33, no. 7, pp. 1049–1056, July 1997.

[144] S. Tammela, P. Kiiveri, S. Sarkilahti, M. Hotoleanu, H. Valkonen, M. Rajala, J. Kurki, and K. Janka, "Direct nanoparticle deposition process for manufacturing very short high gain Er-doped silica glass fibers," in *Proceedings of 28th European Conference on Optical Communication, 2002 (ECOC 2002), Copenhagen, Denmark*, vol. 4, 2002, p. 9.4.2.

[145] J. Swiderski, A. Zajac, M. Skorczakowski, Z. Jankiewicz, and P. Konieczny, "Rare-earth-doped high-power fiber lasers generating in near infrared range," *Opto-Electronics Review*, vol. 12, no. 2, pp. 169–173, 2004.

[146] G. Agrawal, *Nonlinear Fiber Optics*, 3rd ed. Academic Press, 2001.

[147] L. Quintino, A. Costa, R. Miranda, D. Yapp, V. Kumar, and C. J. Kong, "Welding with high power fiber lasers–A preliminary study," *Materials and Design*, vol. 28, no. 4, pp. 1231–1237, 2007.

[148] G. Genty, S. Coen, and J. M. Dudley, "Fiber supercontinuum sources (invited)," *Journal of Optical Society of America B*, vol. 24, no. 8, pp. 1771–1785, 2007. [Online]. Available: http://josab.osa.org/abstract.cfm?URI=josab-24-8-1771

[149] S. Kivistö, R. Herda, and O. G. Okhotnikov, "All-fiber supercontinuum source based on a mode-locked ytterbium laser with dispersion compensation by linearly chirped bragg grating," *Optics Express*, vol. 16, no. 1, pp. 265–270, 2008. [Online]. Available: http://www.opticsexpress.org/abstract.cfm?URI=oe-16-1-265

[150] M. Rusu, A. Grudinin, and O. Okhotnikov, "Slicing the supercontinuum radiation generated in photonic crystal fiber using an all-fiber chirped-pulse amplification system," *Optics Express*, vol. 13, no. 17, pp. 6390–6400, 2005. [Online]. Available: http://www.opticsexpress.org/abstract.cfm?URI=oe-13-17-6390

[151] E. R. Andresen, C. K. Nielsen, J. Thøgersen, and S. R. Keiding, "Fiber laser-based light source for coherent anti-Stokes Raman scattering microspectroscopy," *Optics Express*, vol. 15, no. 8, pp. 4848–4856, 2007. [Online]. Available: http://www.opticsexpress.org/abstract.cfm?URI=oe-15-8-4848

[152] RP Photonics Consulting GmbH, "Saturable absorbers, referenced 2008-01-08." [Online]. Available: http://www.rp-photonics.com/saturable_absorbers.html

[153] B. Ortaç, M. Plötner, T. Schreiber, J. Limpert, and A. Tünnermann, "Experimental and numerical study of pulse dynamics in positive net-cavity dispersion modelocked Yb-doped fiber lasers," *Optics Express*, vol. 15, no. 23, pp. 15 595–15 602, 2007. [Online]. Available: http://www.opticsexpress.org/abstract.cfm?URI=oe-15-23-15595

[154] O. Svelto, *Principles of Lasers*, 4th ed. New York: Plenum Press, 1998.

[155] R. L. Fork, O. E. Martinez, and J. P. Gordon, "Negative dispersion using pairs of prisms," *Optics Letters*, vol. 9, no. 5, pp. 150–152, February 1984.

[156] X. Zhang, "High-repetition-rate femtosecond optical parametric oscillators based on KTP and PPLN," Ph.D. dissertation, Phillipps-Univesität Marburg, Marburg/Lahn, Germany, October 2002.

[157] F. Gérôme, J. C. Knight, J. Clowes, and W. J. Wadsworth, "Soliton pulse delivery and compression using hollow-core photonic bandgap fibers," in *Proceedings of Nonlinear Photonics*. Optical Society of America, 2007, p. NThC1. [Online]. Available: http://www.opticsinfobase.org/abstract.cfm?URI=URI=NP-2007-NThC1

[158] F. Gèrôme, P. Dupriez, J. Clowes, J. C. Knight, and W. J. Wadsworth, "High power tunable femtosecond soliton source using hollow-core photonic bandgap fiber, and its use for frequency doubling," *Optics Express*, vol. 16, no. 4, pp. 2381–2386, 2008. [Online]. Available: http://www.opticsexpress.org/abstract.cfm?URI=oe-16-4-2381

[159] B. Ortaç, M. Plötner, T. Schreiber, J. Limpert, and A. Tünnermann, "Environmentally-stable wave-breaking-free mode-locked Yb-doped all-fiber laser," J. Broeng and C. H. III, Eds., vol. 6873, no. 1. SPIE, February 2008, p. 68731M. [Online]. Available: http://link.aip.org/link/?PSI/6873/68731M/1

[160] Crystal Fibre A/S, "Hollow-core photonic bandgap fibers, referenced 2008-02-03." [Online]. Available: http://www.crystal-fibre.com/products/airguide.shtm

[161] ——, "Nonlinear photonic crystal fibers, referenced 2008-02-03." [Online]. Available: http://www.crystal-fibre.com/products/nonlinear.shtm

[162] A. Isomäki and O. G. Okhotnikov, "All-fiber ytterbium soliton mode-locked laser with dispersion control by solid-core photonic bandgap fiber," *Optics Express*, vol. 14, no. 10, pp. 4368–4373, 2006. [Online]. Available: http://www.opticsexpress.org/abstract.cfm?URI=oe-14-10-4368

[163] E. Sorokin, S. Naumov, and I. T. Sorokina, "Ultrabroadband infrared solid-state lasers," *IEEE Journal of Selected Topics in Quantum Electronics*, vol. 11, no. 3, pp. 690–712, May–June 2005.

[164] F. X. Kärtner, U. Morgner, R. Ell, T. Schibli, J. G. Fujimoto, E. P. Ippen, V. Scheuer, G. Angelow, and T. Tschudi, "Ultrabroadband double-chirped mirror pairs for generation of octave spectra," *Journal of Optical Society of America B*, vol. 18, no. 6, pp. 882–885, 2001. [Online]. Available: http://josab.osa.org/abstract.cfm?URI=josab-18-6-882

[165] E. B. Treacy, "Optical pulse compression with diffraction gratings," *IEEE Journal of Quantum Electronics*, vol. 5, no. 5, pp. 454–458, 1969.

[166] M. Rusu, R. Herda, S. Kivistö, and O. G. Okhotnikov, "Fiber taper for dispersion management in a mode-locked ytterbium fiber laser," *Optics Letters*, vol. 31, no. 15, pp. 2257–2259, 2006. [Online]. Available: http://ol.osa.org/abstract.cfm?URI=ol-31-15-2257

[167] D. Kopf, G. Zhang, R. Fluck, M. Moser, and U. Keller, "All-in-one dispersion-compensating saturable absorber mirror for compact femtosecond laser sources," *Optics Letters*, vol. 21, no. 7, pp. 486–488, 1996.

[168] M. Moenster, U. Griebner, W. Richter, and G. Steinmeyer, "Resonant saturable absorber mirrors for dispersion control in ultrafast lasers," *IEEE Journal of Quantum Electron*, vol. 43, p. 174, 2007.

[169] A. Isomäki, "Ultrafast fiber lasers using novel semiconductor saturable absorbers and photonics-crystal dispersion compensation," Ph.D. dissertation, Tampere University of Technology, Tampere, October 2007.

[170] A. Isomäki, A. Vainionpää, J. Lyytikäinen, and O. G. Okhotnikov, "Semiconductor mirror for dynamic dispersion compensation," *Applied Physics Letters*, vol. 82, no. 17, p. 2773, 28 April 2003.

[171] A. Isomäki, A.-M. Vainionpää, J. Lyytikäinen, and O. G. Okhotnikov, "Semiconductor mirror for optical noise suppression and dynamic dispersion compensation," *IEEE Journal of Quantum Electronics*, vol. 39, no. 11, pp. 1481–1485, 2003.

[172] O. G. Okhotnikov and J. R. Salcedo, "Spectroscopy of the transient oscillations in a Nd^{3+}-doped fiber laser for the four-level $^4F_{3/2}$-$^4I_{11/2}$ (1060 nm) and three-level $^4F_{3/2}$-$^4I_{9/2}$ (900-nm) transitions," *Applied Physics Letters*, vol. 64, no. 20, pp. 2619–2621, 1994. [Online]. Available: http://link.aip.org/link/?APL/64/2619/1

[173] O. G. Okhotnikov, V. V. Kuzmin, and J. R. Salcedo, "General intracavity method for laser transition characterization by relaxation oscillations spectral analysis," *IEEE Photonics Technology Letters*, vol. 6, no. 3, pp. 362–364, 1994.

[174] O. G. Okhotnikov and J. R. Salcedo, "Laser transitions characterization by spectral and thermal dependences of the transient oscillation," *Optics Letters*, vol. 19, pp. 1445–1447, 1994.

[175] E. Lacot, F. Stoeckel, and M. Chenevier, "Dynamics of an erbium-doped fiber laser," *Physical Review A*, vol. 49, no. 5, pp. 3997–4008, May 1994.

[176] O. G. Okhotnikov, L. Gomes, N. Xiang, T. Jouhti, and A. B. Grudinin, "Mode-locked ytterbium fiber laser tunable in the 980–1070-nm spectral range," *Optics Letters*, vol. 28, no. 17, pp. 1522–1524, 2003.

[177] A. E. Siegman, *Lasers*. Sausalito: University Science Books, 1986.

[178] C. J. Kennedy, J. D. Barry, and R. R. Rice, "Measurement of parameters in a mode-locked and frequency-doubled Nd:YAG laser using relaxation oscillations," *Journal of Applied Physics*, vol. 47, no. 6, pp. 2447–2449, 1976. [Online]. Available: http://link.aip.org/link/?JAP/47/2447/1

[179] J. Harrison, G. A. Rines, and P. F. Moulton, "Long-pulse generation with a stable-relaxation-oscillation Nd:YLF laser," *Optics Letters*, vol. 13, no. 4, 1988.

[180] RP Photonics Consulting GmbH, "Gain media, referenced 2008-02-06." [Online]. Available: http://www.rp-photonics.com/gain_media.html

[181] M. Engelbrecht, F. Haxsen, D. Wandt, and D. Kracht, "Wavelength resolved intracavity measurement of the cross sections of a Tm-doped fiber," *Optics Express*, vol. 16, no. 3, pp. 1610–1615, 2008. [Online]. Available: http://www.opticsexpress.org/abstract.cfm?URI=oe-16-3-1610

[182] J. Hult, M. Richter, J. Nygren, M. Aldén, A. Hultqvist, M. Christensen, and B. Johansson, "Application of a high-repetition-rate laser diagnostic system for single-cycle-resolved imaging in internal combustion engines," *Applied Optics*, vol. 41, pp. 5002–5014, 2002.

[183] N. Ji, J. C. Magee, and E. Betzig, "High-speed, low-photodamage nonlinear imaging using passive pulse splitters," *Nature Methods*, vol. 5, no. 2, pp. 197–202, February 2008.

[184] K. H. Guenther, "Physical and chemical aspects in the application of thin films on optical elements," *Applied Optics*, vol. 23, no. 20, pp. 3612–3632, 15 October 1984. [Online]. Available: http://ao.osa.org/abstract.cfm?URI=ao-23-20-3612

[185] H. G. Shanbhogue, C. L. Nagendra, M. N. Annapurna, S. A. Kumar, and G. K. M. Thutupalli, "Multilayer antireflection coatings for the visible and near-infrared regions," *Applied Optics*, vol. 36, no. 25, pp. 6339–6351, 1997. [Online]. Available: http://ao.osa.org/abstract.cfm?URI=ao-36-25-6339

[186] K. H. Guenther, "Microstructure of vapor-deposited optical coatings," *Applied Optics*, vol. 23, no. 21, p. 3806, 1984. [Online]. Available: http://ao.osa.org/abstract.cfm?URI=ao-23-21-3806

[187] M. Cevro and G. Carter, "Ion beam and dual ion beam sputter deposition of tantalum oxide films," in *Proceedings of Optical Interference Coatings*, F. Abeles, Ed., vol. 2253, no. 1. SPIE, November 1994, pp. 1367–1380. [Online]. Available: http://link.aip.org/link/?PSI/2253/1367/1

[188] ——, "Ion-beam and dual-ion-beam sputter deposition of tantalum oxide films," *Optical Engineering*, vol. 34, no. 2, pp. 596–606, 1 February 1995.

[189] Cerac Inc., "Zirconia," *Coating Material News*, vol. 16, no. 1, pp. 2–3, March 2006.

[190] E. S. Boncristiano, L. A. M. Saito, and E. A. De Souza, "396 fs, 2.5–12 GHz asynchronous mode-locking erbium fiber laser," in *Proceedings of Conference on Lasers and Electro-Optics/Quantum Electronics and Laser Science Conference and Photonic Applications Systems Technologies*. Optical Society of America, 2007, p. CMC2. [Online]. Available: http://www.opticsinfobase.org/abstract.cfm?URI=URI=CLEO-2007-CMC2

[191] S. Yamashita, Y. Inoue, K. Hsu, T. Kotake, H. Yaguchi, D. Tanaka, M. Jablonski, and S. Set, "5-GHz pulsed fiber Fabry–Pérot laser mode-locked using carbon nanotubes," *IEEE Photonics Technology Letters*, vol. 17, no. 4, pp. 750–752, 2005.

[192] O. Katz, Y. Sintov, Y. Nafcha, and Y. Glick, "Passively mode-locked ytterbium fiber laser utilizing chirped-fiber-Bragg-gratings for dispersion control," *Optics Communications*, vol. 269, no. 1, pp. 156–165, 2007.

[193] R. Herda and O. G. Okhotnikov, "Dispersion compensation-free fiber laser mode-locked and stabilized by high-contrast saturable absorber mirror," *IEEE Journal of Quantum Electronics*, vol. 40, no. 7, pp. 893–899, July 2004.

[194] A. Isomäki and O. G. Okhotnikov, "Femtosecond soliton mode-locked laser based on ytterbium-doped photonic bandgap fiber," *Optics Express*, vol. 14, no. 20, pp. 9238–9243, 2006. [Online]. Available: http://www.opticsexpress.org/abstract.cfm?URI=oe-14-20-9238

[195] ——, "Femtosecond soliton mode-locked laser based on ytterbium-doped photonic bandgap fiber," in *Proceedings of 19th Annual Meeting of the IEEE Lasers and Electro-Optics Society, 2006. LEOS 2006*. IEEE, 29 October–2 November 2006, pp. 394–395.

Appendix 1

Publication 1

L. A. Gomes, L. Orsila, T. Jouhti, and O. G. Okhotnikov, ”Picosecond SESAM based ytterbium mode-locked fiber lasers,” *IEEE Journal of Selected Topics in Quantum Electronics*, vol. 10, no. 1, issue on Ultrafast Science and Technology, pp. 129–136, 2004.

Picosecond SESAM-Based Ytterbium Mode-Locked Fiber Lasers

Luís A. Gomes, Lasse Orsila, Tomi Jouhti, and Oleg G. Okhotnikov

***Abstract*—Using semiconductor saturable absorber mirrors and a grating-pair dispersion compensator, we obtain reliable self-starting mode locking of a ytterbium (Yb) fiber laser tunable over 125 nm. The 980–1105-nm tuning range is achieved by optimization of nonlinear reflection and bandgap characteristics of the multiple-quantum-well saturable absorber and by proper engineering of the laser cavity. A short-length Yb-doped double-clad amplifier seeded with mode-locked Yb-fiber laser produces picosecond pulses with energy of 30 nJ (700 mW of average power). A compact version of the fiber laser was built using a Gires–Tournois compensator and short length (1-cm long) of highly doped Yb fiber. Using a novel semiconductor saturable absorver mirror based on GaInNAs structure, self-started 1.5-ps pulse mode-locked operation was obtained at 1023 nm with a repetition rate of 95 MHz. A mode-locked Yb-doped fiber laser was also developed without using any dispersion compensation technique. Overall group-velocity dispersion was minimized by using highly doped Yb fiber in a compact amplifying loop cavity. Self-started mode-locked operation was obtained in 980–1030-nm wavelength range with a fundamental repetition rate of 140 MHz. Without using dispersion compensation, the lasers produced pulses in a range from 15 to 26 ps.**

***Index Terms*—Mode-locked lasers, optical fiber lasers, semiconductor devices, ytterbium (Yb).**

I. Introduction

In the past decades, diode pumped solid-state lasers have dominated the area of tunable ultrashort-pulse light sources, offering not only extremely short optical pulses comprising several optical cycles [1], but also broadband tunability [2]–[6]. Recent unprecedented growth of the telecom industry has resulted in the development of mature fiber technology, reliable and cost effective components that make suitably designed fiber lasers real contenders to conventional solid-state lasers. The broad fluorescence spectra of different fiber-gain media are attractive for tunable and ultrashort-pulse sources. Continuous wave (CW) operation of an Nd : glass fiber laser was reported over a tuning range of 900 to 945 nm and 1070 to 1135 nm [2] and, more recently, over 50-nm full width at half maximum (FWHM) [3]. For Er-doped fiber lasers, tuning over 35 nm was achieved in an actively mode-locked system [4] and over 50 nm in an additive-pulse mode-locked fiber soliton laser [5]. For fiber lasers doped with thulium, which exhibit a particularly wide fluorescence spectrum, a tuning range as wide as 100 nm was demonstrated [6].

Manuscript received June 13, 2003; revised October 15, 2003.

The authors are with the Optoelectronics Research Centre, Technical University of Tampere, FIN-333101 Tampere, Finland (e-mail: Oleg.Okhotnikov@orc.tut.fi).

Digital Object Identifier 10.1109/JSTQE.2003.822918

Ytterbium (Yb)-doped silica fiber having a broad-gain bandwidth, high optical conversion efficiency, and large saturation fluence offers an almost ideal gain medium for the generation and amplification of wavelength-tunable ultrashort optical pulses around 1 μm. An additional interesting feature of Yb-doped fiber lasers is that under certain conditions those lasers can operate at $\sim$977 nm. This makes them a promising alternative to mode-locked Ti : sapphire lasers and as a master source for frequency doubling to achieve 488 nm and thus substitute bulky and inefficient Ar-ion lasers. Despite significant attention to the development of practical user-friendly mode-locked sources operating in the region of 1 μm, there have been, so far, very few reports of successful demonstration of passively mode-locked fiber lasers [7], and there have been no reports on tunable fiber-based picosecond sources.

The main difficulty associated with short-pulse generation within Yb-doped fibers results from the high value of normal material dispersion for silica at wavelengths below 1.1 μm. Passively mode-locked fiber lasers that operate in the normal group-velocity dispersion (GVD) region of silica glass ($\lambda<1.3$ μm) may only be operated in the anomalous dispersion regime if dispersion compensators are introduced in the cavity [8], [9], since it does not appear feasible to achieve overall anomalous dispersion of the fiber by exploiting the waveguide dispersion of ordinary single-mode fibers. Using photonic crystal fibers (PCF) it is possible to obtain soliton pulse operation at shorter wavelengths [10]; however, the praticality of this technique is still to be studied.

Usually, to offset the material dispersion, intracavity dispersion compensation is preformed by using prisms or grating pairs within fiber laser systems. The negative dispersion generated by a Gires–Tournois interferometer (GTI) or by chirped mirrors is sufficient only to balance the dispersion of the laser rod of solid-state lasers. Nevertheless, because the GTI mirror is based on a multiple-beam concept, higher dispersion can, in principle, be generated with increasing the finesse of the interferometer. In practice, however, the resonance sharpness of GTI affects strongly the usable bandwidth of the compensator. For this reason, in a typical fiber laser with a length of active medium of $\sim$1 m or longer having large net normal dispersion of the cavity, short-pulse operation still requires dispersion compensators such as a grating pair [9]. Though bulk components add to the complexity and maintenance, they require alignment and increase the physical size of the system.

The advantage of the anomalous dispersion regime achieved by using dispersion compensators is that shorter pulses could be obtained due to pulse shaping assisted by soliton effects. Although soliton pulse shaping is a convenient method of

short-pulse generation from fiber lasers, soliton effects limit pulse duration and energy, resulting in multiple pulse operation for increased pump power [11]. Alternatively, the so-called stretched-pulse technique was introduced for erbium-doped systems, which minimizes soliton shaping. The principle of stretched-pulse mode locking uses cavity segments of large positive and large negative dispersion to introduce large changes of pulse width in the laser cavity and minimize nonlinear effects [12], [13]. Because silica fiber at $\sim$1 μm has a high value of normal dispersion, neodymium and Yb laser systems can be conveniently operated in the stretched-pulse regime [14], [15]. However, with large net normal dispersion, mode locking is difficult to initiate and operation suffers from instability. For this reason, typical stretched-pulse lasers operate with small net normal group-velocity dispersion exploiting an appropriate compensation technique [14]–[16].

To cope with the difficulty in obtaining self-starting mode locking within a laser with a Fabry–Pérot geometry, semiconductor saturable-absorber mirrors (SESAMs) have been conveniently used to ensure the self-starting character of the mode locking [17].

In this paper, we studied experimentally mode-locked Yb-doped fiber lasers with different geometries. The paper is organized as follows. In Section II, we present a picosecond mode-locked Yb fiber laser tunable over 125 nm from 980 to 1105 nm delivering pulses of 1–2-ps duration. The fiber laser is pumped by a single fiber-coupled diode laser operating at 915 nm and provides over 30 mW of average power in mode-locked regime across the entire tuning range. A mode-locked Yb-fiber laser using an intracavity Gires–Tournois interferometer that generates anomalous GVD is presented in Section III. The short-length highly doped Yb fiber provided a low value of net normal GVD that is compensated by a GTI mirror with a comparable amount of anomalous dispersion, while preserving an optical bandwidth sufficient for supporting picosecond pulses. In Section IV, we describe a compact dispersion compensator-free mode-locked Yb-fiber laser. The few-centimeter-long highly doped Yb-fiber and short segment of single-mode fiber are contained in the cavity providing a low value of net normal GVD.

II. Widely Tunable Short-Pulse Yb Fiber Laser

A schematic configuration of the tunable laser is shown in Fig. 1. The cavity contains a grating pair for intracavity dispersion compensation, a piece of Yb^{3+}-doped fiber with angle-cleaved end to suppress intracavity reflections, a wavelength-division multiplexer, and a loop mirror.

The large normal group-velocity dispersion introduced into the cavity by the fiber ($+0.16$ ps^2) is offset by the anomalous dispersion of the grating pair, resulting in net anomalous dispersion. A 35-, 50-, or 180-cm-long Yb-doped silica fiber (NA $=$ 0.13, cutoff wavelength $\sim$920 nm) is pumped by a pigtailed single-mode laser diode operating at 915 nm. The unsaturated fiber absorption at 915 nm was $\sim$140 dB/m. The signal/pump wavelength-selective coupler and the loop mirror were made of fiber with a cutoff wavelength of $\sim$910 nm. Depending on the operating spectral range, the fiber was pumped through a

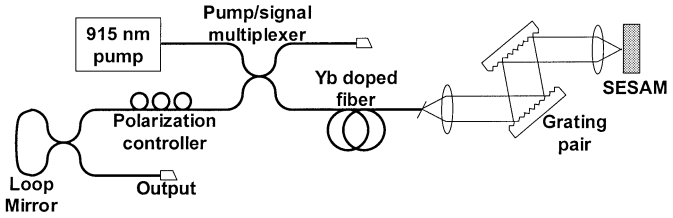

Fig. 1. Cavity configuration for a widely tunable Yb fiber laser.

915/990-, a 915/1050-, or a 915/1070-nm fiber multiplexer with a maximum launched pump power of 130 mW. The cavity was terminated by the 55% reflectivity loop-mirror from one end and by the SESAM structure from the other. Wavelength tunability was achieved by slight shifting of the objective in front of the SESAM in the transverse direction or by slight tilting of one of the gratings. Placing the objective on a micropositioner allowed us to perform tuning in a stable and repeatable way without need for realignment of the laser cavity. Gold-coated 1600- or 1200-line/mm diffraction grating pairs were used for dispersion compensation.

In order to achieve a broad tuning range, particular attention was paid to the design of the multiple-quantum-well saturable absorber mirror. Although the bandwidth (or stop band) of the distributed Bragg reflectors (DBRs) based on AlGaAs–GaAs composition are usually larger than 100 nm, the expected tuning range for a Yb-doped fiber laser could be as broad as 970–1150. Therefore, in order to avoid possible limitations arising from DBR bandwidth, two DBR mirrors with shifted central wavelengths were used in the SESAM samples covering the extended tuning range of the Yb-doped fiber laser. The central wavelength of one DBR mirror was centered around 1055 nm, whereas the other DBR had a center wavelength of the reflection bandwidth around 1000 nm.

The two SESAM samples were grown by all-solid-source molecular beam epitaxy. The first sample consists of a bottom mirror comprising 25 pairs of AlAs and GaAs quarterwave layers forming a DBR with a center wavelength of 1055 nm. The absorber was a double 8-nm-thick InGaAs quantum well structure placed into a $\lambda/4$ cavity. These layers were implanted with doses of 10^{12} cm^{-2} of 10 MeV Ni ions to decrease the SESAM recovery time to below 10 ps [18]. Another broadband SESAM structure operating in the 940–1050-nm wavelength range is based on GaInNAs material known as a dilute nitride system. It was monolithically grown on an n-type GaAs (001) substrate similar to the long-wavelength SESAM described in [19]. An antiresonant Fabry–Pérot structure of SESAMs is formed by the uncoated front surface and the highly reflecting AlAs–GaAs mirror stack [11]. An important feature of this GaInNAs-based SESAM is the high contrast in nonlinear reflectivity variation. The nonlinear reflectivity of the GaInNAs SESAM is shown in Fig. 2. The SESAM has a saturation fluence of 3 μJ/cm^2 and a modulation depth of 12%.

It is well known that the dilute nitride material, when used for light-emitting devices, requires a rapid thermal annealing (RTA) treatment to enhance the photoluminescence efficiency [20], [21]. This indicates that as-grown dilute nitride has a high level of crystal defects (imperfections). This property of dilute

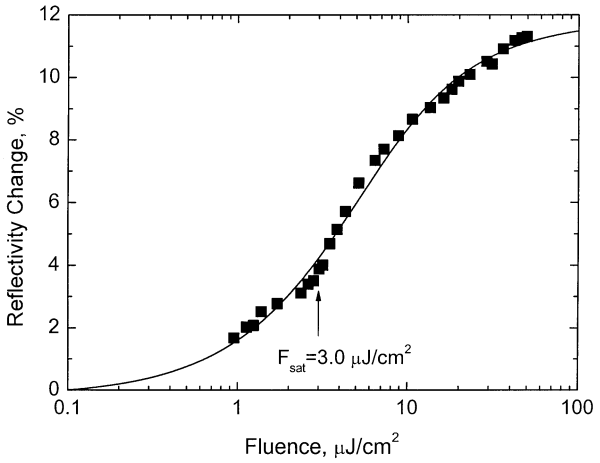

Fig. 2. Nonlinear reflectivity of the GaInNAs-based SESAM.

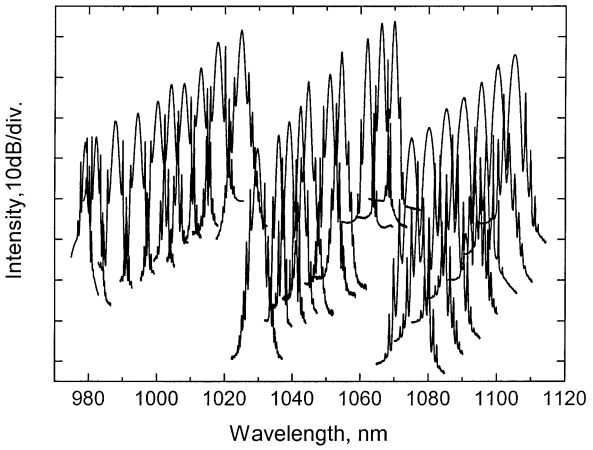

Fig. 3. Output spectra from the laser as a function of wavelength. Tuning over 980–1020-, 1020–1070-, and 1070–1105-nm bands was obtained with different pump/signal multiplexers, different lengths of Yb-doped fiber, and SESAMs, as shown in the text. Spectra shifted vertically for clarity.

nitride can be exploited, in particular, in SESAM based devices, since neither ion implementation nor low temperature growth are needed to decrease the recovery time.

The laser threshold for CW operation was about 20 mW. When the doped fiber length was short enough (∼35 cm) to ensure at least 50% population inversion along all fiber, the laser was operating at 980 nm without any wavelength selective elements. Pumpthrough power in this case was around 10 mW for 100 mW of launched pump power. When the doped fiber length was increased to 50 cm, so that 980-nm radiation was reabsorbed inside the fiber, the central lasing wavelength was shifted toward 1040 nm. With further increase in the fiber length up to 180 cm, the central lasing wavelength shifts gradually toward 1080 nm.

Without focusing optics and, therefore, with a collimated beam hitting the absorber mirror, CW operation was observed due to low nonlinearity of the SESAM response for low fluence. With a focusing objective in place, the mode-locked operation could be initiated without sign of Q-switching instability, thus preventing optical damage of the absorber mirror. Mode-locked operation was obtained for pump power above 40 mW, and it was self-starting over the whole tuning range for pump powers above 50 mW. By shifting the objective, we were able to continuously tune the mode-locked laser from 980 to 1020 nm (with a 915/990 WDM coupler and 35 cm of Yb fiber), from 1020 to 1070 nm (with a 915/1050 WDM coupler and 50 cm of Yb fiber), and from 1070 to 1105 nm (with a 915/1070 WDM coupler and 180 cm of Yb-doped fiber), as shown in Fig. 3. For the 980–1020-nm tuning range, we used a GaInNAs-based absorber; for the two other wavelength ranges we used the InGaAs absorber descrived previously. It should be noted that the use of three different pump launching elements was dictated by the spectral properties of fused biconical WDM couplers. Replacement of those with a combiner based on micro-optical technology will allow covering all the spectral range without the need for different intracavity elements. Another wavelength selective element, the SESAM, can also be adjusted for operation in a wide spectral range. Therefore, using optimized components it could be feasible to achieve continuous tuning over the entire spectral gain bandwidth in a compact laser configuration.

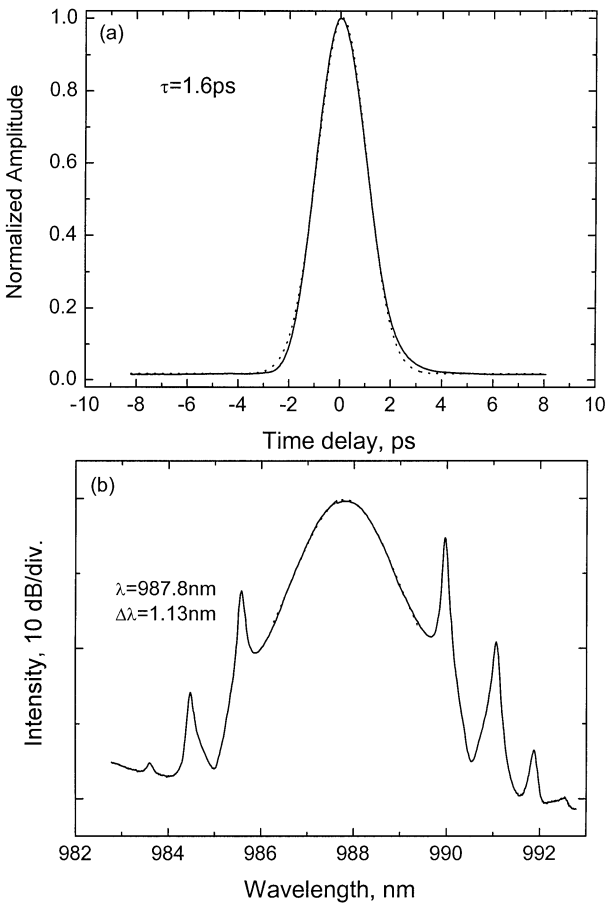

Fig. 4. (a) Autocorrelation trace and (b) optical spectrum of the Gaussian pulse when the distance between gratings is 2.9 cm. Dotted curve shows a Gaussian fit.

Since the pulse duration and shape in a stretched-pulse laser depend on the position inside the laser cavity, we have also measured the pulse width at a location closer to the grating pair compressor by adding an optional 7% output coupler near the WDM pump coupler. For 1600-lines/mm gratings with a separation of 2.9 cm, pulsewidths varied between 1.6 and 2 ps. Fig. 4 illustrates the autocorrelation and corresponding spec-

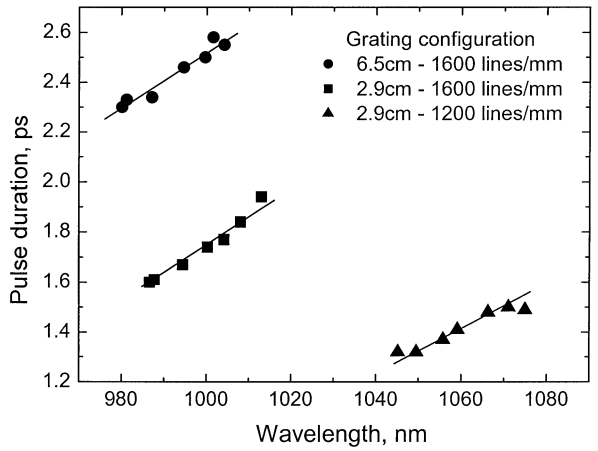

Fig. 5. Obtained pulse widths as a function of wavelength for different grating configurations.

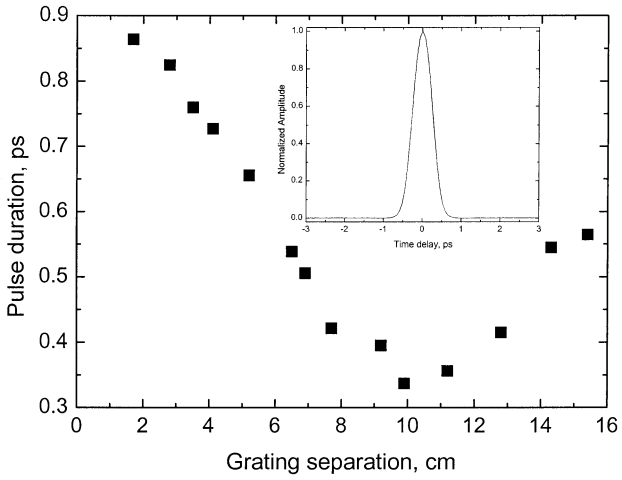

Fig. 6. Measured pulsewidth after external compression with 600-line/mm grating pair. Inset shows the autocorrelation of the shortest compressed pulse.

trum for the mode-locked pulse train at ∼987 nm, with a repetition rate of 33 MHz. It should be noted the excellent stability of the 1.6-ps pedestal-free pulses. The measured autocorrelation traces were best fitted, assuming a Gaussian temporal intensity profile with a time-bandwidth product equal to 0.47, which indicates nearly bandwidth-limited pulses with Gaussian temporal and spectral profiles. The pulse spectrum shows soliton sidebands confirming that the laser operates in the net anomalous dispersion regime.

The measurements plotted in Fig. 5 show the change in pulse duration versus the wavelength for different grating pair configurations. The average values of the cavity dispersion near 1 μm estimated from spectral sidebands in the pulse spectra were -1.75 ps^2 and -0.71 ps^2 for a compensator based on a 1600-lines/mm grating pair with separations of 6.5 and 2.9 cm, respectively. With a compensator using 1200-lines/mm gratings separated by 2.9 cm, the shortest pulse duration was ∼1 ps and had a time-bandwidth product of 1.52. Corresponding cavity dispersion was estimated to be -0.05 ps^2.

We then removed the output coupler and measured the output from the loop mirror, as shown in Fig. 1, where the pulses have

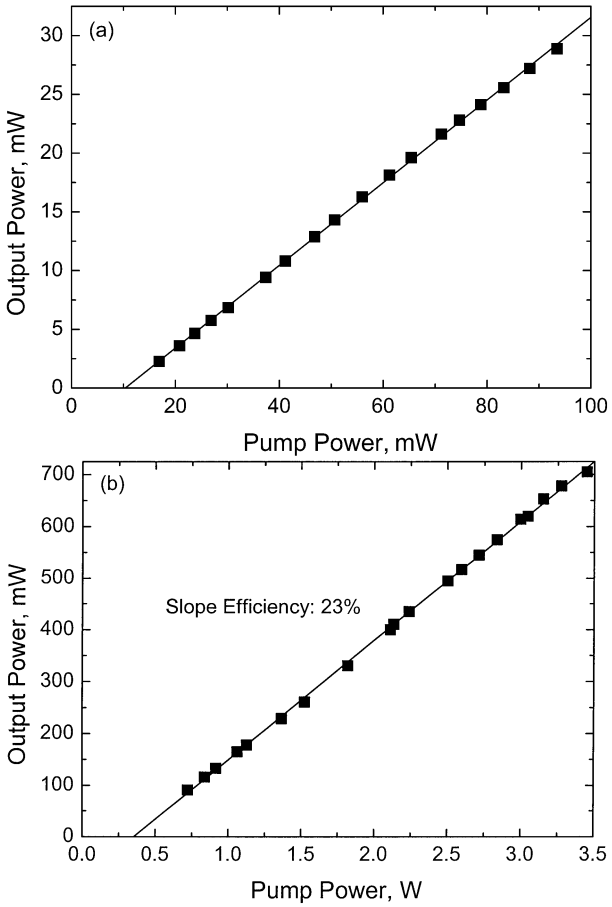

Fig. 7. (a) Output power from our mode-locked Yb laser and (b) average output power from the Yb amplifier for 15 mW of input power.

a strong chirp [7], and the time-bandwidth product usually exceeds the time-bandwidth product for transform-limited pulses by a factor of 3–4. To prove that the chirp is near linear, we have used an external dispersive delay line composed of 600-line/mm gratings. Fig. 6 plots the pulsewidth when the net dispersion was varied by changing the grating separation. The results confirm that the pulses are essentially linearly chirped. The shortest pulse thus obtained was only 340 fs long, with a time-bandwidth product of 0.57, as can be seen on the inset of Fig. 6.

Polarization dependence of the grating reflectivity results in the necessity to adjust the polarization state in order to optimize the mode-locked operation. Although the mode-locking could be started at virtually any position of the polarization controllers, most stable operation with the shortest pulses was achieved at only one orientation of the polarization controllers. This fact suggests that nonlinear polarization has probably played some role in pulse formation; this phenomenon requires, however, further investigation.

Average output power up to 30 mW was obtained, as shown in Fig. 7(a). Adding an isolator to the output of the laser reduced the maximum output power down to 15 mW but allowed us to use this laser in a master-oscillator power amplifier setup. In order to increase pulse peak power and energy we have employed a cladding pumped fiber amplifier supplied by New Optics, Ltd., U.K. To avoid temporal pulse broadening due to dispersion and spectral enrichment due

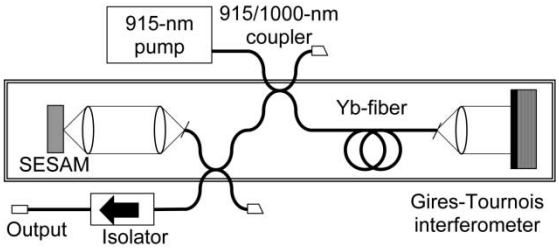

Fig. 8. Cavity configuration for a mode-locked Yb fiber laser using a GTI compensator.

to self-phase modulation, we have used an all glass double clad fiber with 50-μm pump cladding. Due to relatively small pump cladding, a 10-dB pump absorption was achieved with a doped fiber length of just 50 cm and thus allows us to avoid unwanted dispersive and nonlinear effects. The amplifier is counterpropagatingly pumped by a high brightness pump source delivering up to 4 W in a 50-μm, 0.22 NA fiber. We have achieved $>$700 mW of optical power throughout the entire gain band without noticeable distortion of the amplified pulses [see Fig. 7(b)] with output energies of 30 nJ.

III. Mode-Locked Fiber Laser Using a Gires–Tournois Interferometer Compensator

Dispersion compensation based on a GTI was studied using the laser setup shown in Fig. 8. The linear cavity is defined by the SESAM and the GTI reflector. The broadband GaInNAs-based SESAM structure described in Section II was used. The total length of the fiber within the cavity was 74 cm including a WDM and a 10% output coupler.

The highly doped Yb silica fiber (NA$=0.22$, cutoff wavelength $\sim$910 nm) had an unsaturated fiber absorption at 977 nm of $\sim$1900 dB/m. This Yb fiber was manufactured by Liekki Oy using direct nanoparticle deposition technology (DND) [22].

The Gires–Tournois interferometer we used was made using an electron beam evaporator. The GTI consists of bottom and top DBRs with 10 and 4.5 pairs of SiO_2/TiO_2, respectively, spaced by a 0.7-μm-thick layer of SiO_2. Calculated mirror reflectivities at 1023 nm are $R=0.936$ for the top DBR and $R=0.999$ for the bottom DBR. The GTI structure resonance was positioned near $\lambda=1022.8$ nm, as seen from the reflectivity spectrum shown in Fig. 9. Although an ideal Gires–Tournois interferometer is expected to have a flat power reflectance spectrum, there is a dip at resonance in the reflectance of the high-finesse GTI due to reduced reflectivity of the bottom mirror. The corresponding losses at the resonance would push the lasing spectrum away from the anomalous GVD regime toward the GTI reflection maximum [23]. To lock the pulse spectrum to the region of anomalous GVD, we have used a SESAM with a large change in nonlinear reflectivity (up to 12%), as shown in Fig. 2. With this absorber mirror, the decrease in cavity loss for short-pulse operation is higher than the loss penalty due to the dip in the GTI reflectivity at the lasing wavelength ($\leq$1%). As a result, the mode-locked operation starts spontaneously at the wavelength range with anomalous GVD and remains reliably trapped at this region.

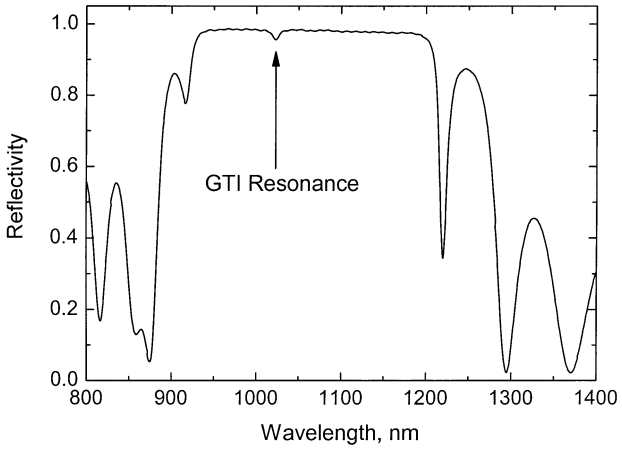

Fig. 9. Measured reflectivity of the Gires–Tournois structure. Reflectivity dip at resonance is shown.

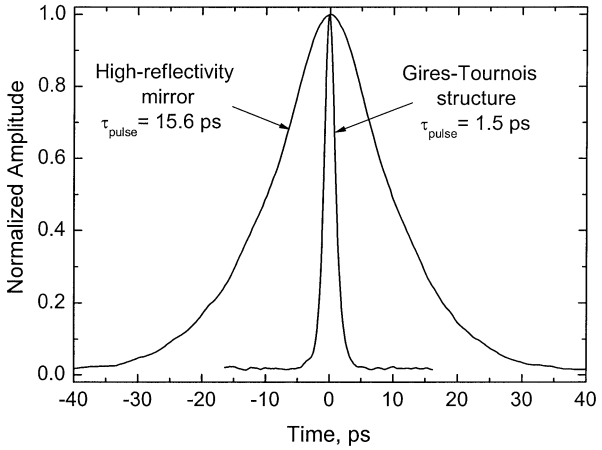

Fig. 10. Autocorrelation traces for pulsed operation with and without GTI.

The laser threshold for CW operation was about 15 mW. When the Yb-doped fiber length was $\sim$2.5 cm, the central lasing wavelength was within the range of 1020–1030 nm. With shorter lengths of Yb fiber, the laser was operating at 980 nm. Self-started mode-locked operation at spectral range around $\lambda=1023$ nm with anomalous GVD was obtained for pump power above 40 mW with an output power up to $\sim$1 mW. Fig. 10 illustrates autocorrelations traces for the laser operating with a GTI reflector and with the GTI replaced by an ordinary highly reflective mirror. The pulse durations were 1.5 and 15.6 ps, respectively, assuming a Gaussian pulse shape. Comparison of the autocorrelations shows that the GTI provides significant compensation of the fiber dispersion. Implementing the GTI resulted in a pulse shortening factor of the order of 10. The fundamental cavity frequency was 95 MHz.

Fig. 11 shows the GTI reflectivity and the resultant GVD around the resonance and pulse spectra with the GTI and with a highly reflective mirror used instead of the GTI. The negative GVD generated by GTI is approximately -0.05 ps^2 at the laser wavelength. The total dispersion in the cavity, including a double pass of the fiber segment and the GTI, were estimated to be -0.01 ± 0.005 ps^2. This estimation shows that the total cavity dispersion corresponds to a small net anomalous group-velocity dispersion. The uncertainty in the cavity dispersion relates to the

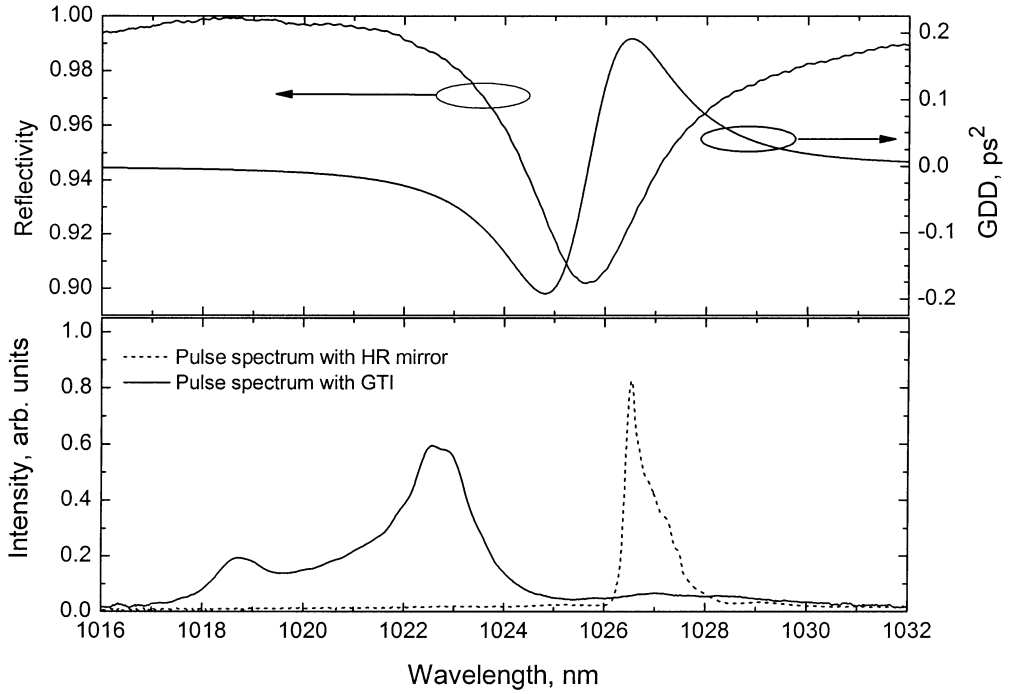

Fig. 11. GTI reflectivity near the resonant wavelength with calculated (upper graph) group-velocity dispersion and (lower graph) pulse spectra with and without dispersion compensation.

problem of estimating the dispersion of the highly doped Yb fiber.

It is important to note that using a SESAM with high contrast of nonlinear reflectivity, operation in the negative GVD regime near $\lambda = 1022.8$ nm was possible without any wavelength-selective elements, despite the reflectivity dip around the GTI resonant wavelength. Mode-locked operation occurs at this wavelength spontaneously for sufficient pumping power.

IV. Short Length Mode-Locked Fiber Laser

To further minimize dispersion induced by the fiber and avoid the need for any intracavity dispersion compensators, we built a short-length fiber laser, using highly doped Yb fiber, as shown in Fig. 12. The linear cavity is defined by the amplifying fiber loop mirror and the semiconductor saturable absorber mirror. Due to the short length of the fiber employed, the nonlinear effects in an amplifying loop mirror were not observed, thus mode-locked operation was initiated and stabilized exclusively by the SESAM.

Placing the Yb fiber in the loop mirror allows us to keep the signal/pump wavelength-selective coupler and the output coupler external to the laser cavity, thus to reduce further the fiber segment of the laser cavity. The fiber loop mirror was designed to couple $\sim$20% of the power to the output. It should also be mentioned that the fiber coupler forming the loop mirror acts as nearly symmetrical splitter at the pump wavelength of 915 nm; therefore, the Yb fiber was pumped from both ends providing near uniform inversion. A GaInNAs broadband SESAM structure similar to the one described in Section II, operating in the 940–1050-nm wavelength range, was used.

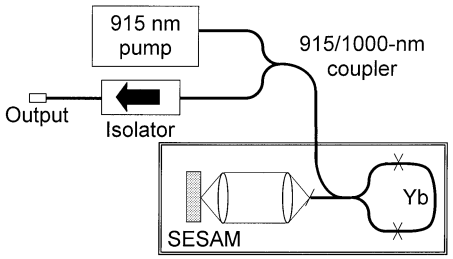

Fig. 12. Amplifying-loop cavity configuration for a short-length Yb fiber laser.

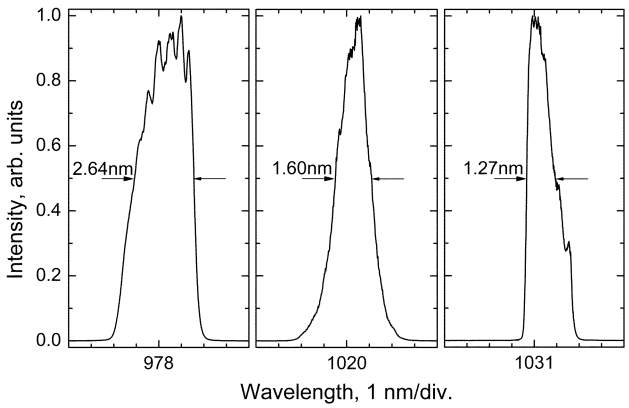

Fig. 13. Output spectra from the mode-locked laser in the 980–1030-nm wavelength range, obtained with Yb fiber with lengths ranged from 2.1 to 4.1 cm.

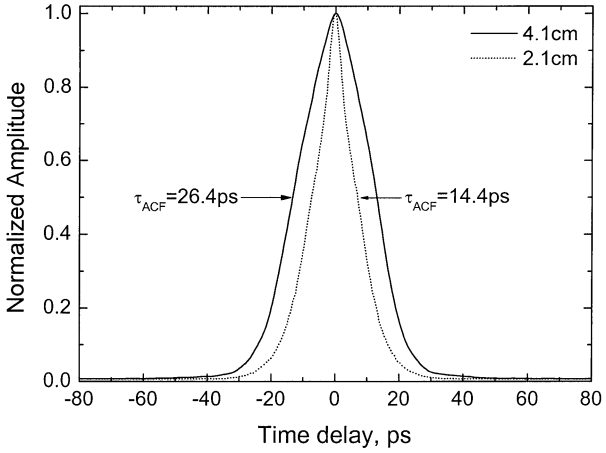

Fig. 14. Autocorrelation traces for pulsed operation with a length of Yb fiber of 2.1 and 4.1 cm.

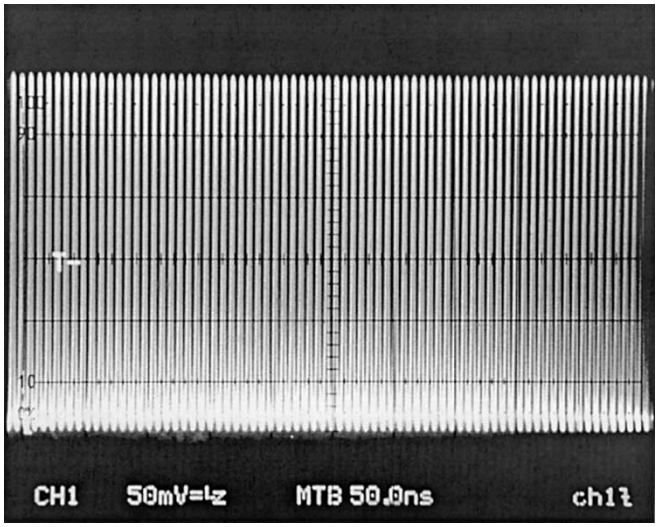

Fig. 15. Stable pulse train at the fundamental cavity frequency of 140 MHz.

The highly doped Yb fiber presented in Section III was used as a gain medium. This fiber allowed us to keep the total length of the fiber within the cavity to be below 12 cm.

The laser threshold for CW operation was about 15 mW. Self-started mode-locked operation was obtained for pump power above 40 mW with the output power up to $\sim$1 mW. When the Yb-doped fiber length was short enough ($\sim$2 cm), the laser was operating at 980 nm. With the length of doped fiber increased to 3–4 cm, the central lasing wavelength was shifted towards 1020–1030 nm due to reabsorption of 980 nm emission, as shown in Fig. 13. Fig. 14 illustrates autocorrelations traces for the lengths of Yb fiber of 2.1 and 4.1 cm. It can be seen that a longer Yb fiber, i.e., higher value of normal GVD, results in stronger pulse stretching. It is important to note that the pulse does not exhibit pedestal, though the autocorrelations cannot be fitted neither with a sech^2 nor a Gaussian profile. To compress the output pulses by removal of the positive temporal chirp, an anomalous dispersive delay line can be used [12], similar to the dechirping experiments using an external grating pair assembly described in Section II. The fundamental cavity frequency corresponds to the pulse repetition rate of 140 MHz, as seen from the scope trace in Fig. 15.

It should also be noted that stability of the short-cavity mode-locked lasers was further increased by using fiber butt coupling of the SESAM instead of lens coupling. This was achieved by applying a dielectric coating to the SESAM to reach an optimal fluence on the absorber mirror.

V. Conclusion

We have demonstrated a Yb-fiber laser generating mode-locked picosecond pulses over a wavelength range from 980 to 1105 nm. Optimal matching of the reflection characteristics and the band gap energy of a semiconductor absorber, spectral characteristics of pump wavelength-division multiplexer, and length of Yb fiber for a given pump power permit broad tuning of the mode-locked fiber laser. The pulsewidths achieved are 1–2 ps over the whole tuning range. A further reduction in the pulsewidth was achieved by pulse compression in an external dispersive delay line, resulting in 340-fs pulses.

To boost the average power, the pulses from tunable mode-locked laser were amplified in a short-length single stage amplifier with double-clad fiber. The pulse energy of 30 nJ with an average power of $>$700 mW obtained at the output of the amplifier is not only the highest reported in picosecond fiber systems but also sufficient enough for applications traditionally dominated by femtosecond Ti : Sapphire lasers.

We have also demonstrated a mode-locked Yb-fiber laser that is compact and easy to align. Overall anomalous group-velocity dispersion was obtained by using a short length cavity with 2.5 cm of highly doped Yb fiber and a Gires–Tournois compensator. Using a broadband semiconductor saturable absorber mirror, based on the GaInNAs material system, with a large change in nonlinear reflectivity, self-started 1.5-ps pulse mode-locked operation was obtained at 1023 nm with a repetion rate of 95 MHz. We have thus demonstrated that specially designed high-reflectivity Gires–Tournois mirrors can be attractive candidates for controlling intracavity dispersion in fiber lasers.

Finally, we also demonstrated a Yb-fiber laser without applying any dispersion compensation technique. Stable and self-starting pulse operation was obtained in the 980–1030-nm wavelength range with a repetition rate of 140 MHz. Overall, normal group-velocity dispersion was minimized by using a short length of highly doped Yb fiber in a compact amplifying loop-mirror cavity.

Acknowledgment

The authors would like to thank their colleague A. B. Grudinin from New Optics Ltd., U.K., for his help with the Yb-fiber power amplifier. The authors would also like to thank Liekki Oy, Finland, for providing Yb-doped fiber.

References

[1] G. Steinmeyer, D. H. Sutter, L. Gallmann, N. Matuschek, and U. Keller, "Frontiers in ultrashort-pulse generation: Pushing the limits in linear and nonlinear optics," *Science*, vol. 286, pp. 1507–1512, 1999.

[2] I. P. Alcock, A. I. Fergunson, D. C. Hanna, and A. C. Tropper, "Tunable, continuous-wave neodymium-doped monomode-fiber laser operating at 0.900–0.945 and 1.070–1.135μm," *Opt. Lett.*, vol. 11, pp. 709–711, 1986.
[3] O. G. Okhotnikov and J. R. Salcedo, "Spectroscopy of the transient oscillations in a Nd^{3+}-doped fiber laser for the four-level ${}^4\mathrm{F}_{3/2}$–${}^4\mathrm{I}_{11/2}$ (1060 nm) and three-level ${}^4\mathrm{F}_{3/2}$–${}^4\mathrm{I}_{9/2}$ (900-nm) transitions," *Appl. Phys. Lett.*, vol. 64, pp. 2619–2621, 1994.
[4] C. R. Ó. Cochláin, R. J. Mears, and G. Sherlock, "Low threshold tunable soliton source," *IEEE Photon. Technol. Lett.*, vol. 5, pp. 25–28, Jan. 1993.
[5] K. Tamura, E. P. Ippen, and H. A. Haus, "Optimization of filtering in soliton fiber lasers," *IEEE Photon. Technol. Lett.*, vol. 6, pp. 1433–1435, Dec. 1994.
[6] L. E. Nelson, E. P. Ippen, and H. A. Haus, "Broadly tunable sub-500 fs pulses from an additive-pulse mode-locked thulium-doped fiber ring laser," *Appl. Phys. Lett.*, vol. 67, pp. 19–21, 1995.
[7] L. Lefort, J. H. V. Price, D. J. Richardson, G. J. Spühler, R. Paschotta, U. Keller, A. R. Fry, and J. Weston, "Practical low-noise stretched-pulse Yb^{3+}-doped fiber laser," *Opt. Lett.*, vol. 27, pp. 291–293, 2002.
[8] M. E. Fermann, M. J. Andrejco, Y. Silberberg, and A. M. Weiner, "Generation of pulses shorter than 200 fs from a passively mode-locked Er fiber laser," *Opt. Lett.*, vol. 18, pp. 48–50, 1993.
[9] H. Lim, F. Ö. Ilday, and F. W. Wise, "Generation of 2-nJ pulses from a femtosecond ytterbium fiber laser," *Opt. Lett.*, vol. 28, pp. 660–662, 2003.
[10] H. Lim, F. O. Ilday, and F. W. Wise, "Femtosecond ytterbium fiber laser with photonic crystal fiber for dispersion control," *Opt. Express*, vol. 10, pp. 1497–1502, 2002.
[11] L. E. Nelson, D. J. Jones, K. Tamura, H. A. Haus, and E. P. Ippen, "Ultrashort-pulse fiber ring lasers," *Appl. Phys. B.*, vol. 65, pp. 277–294, 1997.
[12] K. Tamura, E. P. Ippen, H. A. Haus, and L. E. Nelson, "77-fs pulse generation from a stretched-pulse mode-locked all-fiber ring laser," *Opt. Lett.*, vol. 18, pp. 1080–1082, 1993.
[13] K. Tamura, C. R. Doerr, L. E. Nelson, H. A. Haus, and E. P. Ippen, "Technique for obtaining high-energy ultrashort-pulses from an additive-pulse mode-locked erbium-doped fiber ring laser," *Opt. Lett.*, vol. 19, pp. 46–48, 1994.
[14] V. Cautaerts, D. J. Richardson, R. Paschotta, and D. C. Hanna, "Stretched pulse Yb^{3+} silica fiber laser," *Opt. Lett.*, vol. 22, pp. 316–318, 1997.
[15] M. Hofer, M. E. Fermann, F. Haberl, and J. E. Townsend, "Active mode locking of a neodymium-doped fiber laser using intracavity pulse compression," *Opt. Lett.*, vol. 15, pp. 1467–1469, 1990.
[16] L. Lefort, J. H. V. Price, D. J. Richardson, G. J. Spühler, R. Paschotta, U. Keller, A. R. Fry, and J. Weston, "Practical low-noise stretched-pulse Yb^{3+}-doped fiber laser," *Opt. Lett.*, vol. 27, pp. 291–293, 2002.
[17] F. X. Kärtner, J. Aus der Au, and U. Keller, "Mode-locking with slow and fast saturable absorbers-what's the difference?," *IEEE J. Select. Topics Quantum Electron.*, vol. 4, pp. 159–168, 1998.
[18] E. L. Delpon, J. L. Oudar, N. Bouché, R. Raj, A. Shen, N. Stelmakh, and J. M. Lourtioz, "Ultrafast excitonic saturable absorption in ion-implanted InGaAs/InAlAs multiple quantum wells," *App. Phys. Lett.*, vol. 72, pp. 759–561, 1998.
[19] O. G. Okhotnikov, T. Jouhti, J. Konttinen, S. Karirinne, and M. Pessa, "1.5-μm monolithic GaInNA's semiconductor saturable-absorber mode locking of an erbium fiber laser," *Opt. Lett.*, vol. 28, pp. 364–366, 2003.
[20] W. Ha, V. Gambin, M. Wistey, S. Bank, K. Seongsin, and J. S. Harris Jr., "Multiple-quantum-well GaInNAs–GaNAs ridge-waveguide laser diodes operating out to 1.4 μm," *IEEE Photon. Technol. Lett.*, vol. 14, pp. 591–593, May 2002.
[21] T. Jouhti, C. S. Peng, E.-M. Pavelescu, J. Konttinen, L. A. Gomes, O. G. Okhotnikov, and M. Pessa, "Strain-compensated GaInNA's structures for 1.3-μm lasers," *IEEE J. Select. Topics Quantum Electron.*, vol. 8, pp. 787–794, July/Aug. 2002.
[22] S. Tammela, P. Kiiveri, S. Sarkilathi, M. Hotoleanu, H. Valkonen, M. Rajala, J. Kurki, and K. Janka, *Proc. ECOC*, 2002, paper 9.4.2.
[23] D. Korf, G. Zhang, R. Fluck, M. Moser, and U. Keller, "All-in-one dispersion-compensating saturable absorber mirror for compact femtosecond laser sources," *Opt. Lett.*, vol. 21, pp. 486–488, 1996.

Luís A. Gomes was born in Vale de Cambra, Portugal, in 1976. He received the M.Sc. degree in optoelectronics and lasers from the University of Porto, Portugal, in 2001. He is now working toward the Ph.D. degree in the field of optical fiber sources at the same university.

Since 1999, he has been a Researcher in the Optoelectronics and Electronic Systems Unit, INESC, Porto. He is currently on leave, working at the QRC, Tampere University of Technology, Tampere, Finland.

Lasse Orsila was born in Tampere, Finland, in 1979. He received the M.Sc. degree from Tampere University of Technology (TUT), Tampere, Finland, in 2003. He is currently working toward the Ph.D. degree at the Optoelectronics Research Centre, TUT.

His research interests include thin film mirrors and their applications on fiber lasers.

Tomi Jouhti was born in Espoo, Finland, in 1972. He received the M.Sc. degree from Helsinki University of Technology, Helsinki, Finland, in 1999.

Before joining the Optoelectronics Research Centre (ORC), Tampere, Finland, in 2001 he worked for the Nokia Research Center, Helsinki, Finland, where his research interests included optical data communications. Now at ORC, his research is focused on the crystal growth of novel III–V-semiconductor heterostructures by molecular beam epitaxy.

Oleg G. Okhotnikov received the Ph.D. degree in laser physics from P.N. Lebedev Physical Institute and the D.Sc. degree in laser physics from General Physics Institute, Russian Academy of Sciences, Moscow, in 1981 and 1992, respectively.

Since 1999, he has been a Full Professor at the Optoelectronics Research Centre (ORC), Tampere, Finland. He has published over 100 journal papers and holds six patents.

Appendix 2

Publication 2

L. Orsila, L. A. Gomes, N. Xiang, T. Jouhti, and O. G. Okhotnikov, ”Mode-locked ytterbium fiber lasers,” *Applied Optics*, vol. 43, no. 9, pp. 1902–1906, 2004.

Mode-locked ytterbium fiber lasers

Lasse Orsila, Luís A. Gomes, Ning Xiang, Tomi Jouhti, and Oleg G. Okhotnikov

A compact fiber laser is demonstrated with use of a Gires–Tournois compensator and a short length (2–4 cm-long) of highly doped ytterbium (Yb) fiber providing net anomalous group-velocity dispersion. With use of a novel semiconductor saturable absorber mirror based on GaInNAs structure, self-started 1.5-ps-pulse mode-locked operation was obtained at 1023 nm with a repetition rate of 95 MHz. A mode-locked Yb-doped fiber laser was developed without the use of any dispersion compensation technique. Overall group-velocity dispersion was minimized by using a short length of highly doped Yb fiber in a compact amplifying loop cavity. Self-started mode-locked operation was obtained in 980–1030-nm wavelength range with a fundamental repetition rate of 140 MHz.

OCIS codes: 140.4050, 190.5970.

1. Introduction

In past decades, diode-pumped solid-state lasers have dominated the area of tunable ultrashort-pulse light sources, offering not only extremely short optical pulses comprising several optical cycles[1] but also broadband tunability. The recent, unprecedented growth of the telecommunications industry has resulted in the development of mature fiber technology and reliable and cost-effective components, which make suitably designed fiber lasers better contenders than conventional solid-state lasers. The broad fluorescence spectra make different fiber gain media attractive for tunable and ultrashort pulse sources. Cw operation of a Nd:glass fiber laser was reported[2] over a tuning range of 30-nm FWHM and more recently[3] over 50-nm FWHM. For erbium-doped fiber lasers, tuning over 35 nm was achieved in an actively mode-locked system[4] and over 50 nm in an additive-pulse mode-locked fiber soliton laser.[5] For fiber lasers doped with thulium, which exhibits a particularly wide fluorescence spectrum, a tuning range as wide as 100 nm was demonstrated.[6]

Ytterbium (Yb)-doped silica fiber having a broad-gain bandwidth, high optical conversion efficiency, and large saturation fluence offers an almost ideal gain medium for the generation and amplification of wavelength-tunable ultrashort optical pulses around 1 μm. An additional interesting feature of Yb-doped fiber lasers is that under certain conditions those lasers can operate in the 977-nm spectral band. This makes them a very attractive alternative to mode-locked Ti:sapphire lasers and as a master source for frequency doubling to achieve 488 nm and thus substitute bulky and inefficient argon-ion lasers. Despite significant attention to the development of practical user-friendly mode-locked sources operating in the region of 1 μm, there have been so far very few reports of successful demonstration of passively mode-locked fiber lasers, and there have been no reports on tunable fiber-based picosecond sources.

The main difficulty associated with short-pulse generation within Yb-doped fibers results from the high value of normal material dispersion for silica at wavelengths below 1.1 μm. Passively mode-locked fiber lasers that operate in the normal group-velocity dispersion (GVD) region of silica glass ($\lambda < 1.3$ μm) may be operated only in the anomalous dispersion regime if dispersion compensators are introduced in the cavity,[7,8] since it does not appear to be feasible to achieve overall anomalous dispersion of the fiber by exploiting the waveguide dispersion of ordinary single-mode fibers. With use of photonic crystal fibers it is possible to obtain soliton pulse operation at shorter wavelengths.[9]

Usually, when it is necessary to offset the material dispersion, intracavity dispersion compensation can be preformed by use of prisms or grating pairs within all-fiber laser systems. The negative dispersion generated by a Gires–Tournois interferometer (GTI) or by chirped mirrors is sufficient for solid-state la-

The authors are with the Optoelectronics Research Centre, Tampere University of Technology, P. O. Box 692, FIN-33101, Tampere, Finland. L. Orsila's e-mail address is lasse.orsila@orc.tut.fi.

Received 2 June 2003; revised manuscript received 14 November 2003; accepted 7 January 2004.

0003-6935/04/091902-05$15.00/0

sers to balance the dispersion of the laser rod. Nevertheless, because the GTI mirror is based on a multiple-beam concept, higher dispersion can, in principle, be generated through an increasing of the finesse of the interferometer. In practice, however, the resonance sharpness of the GTI affects strongly the usable bandwidth of the compensator. For this reason, in a typical fiber laser with a length of active medium of 1 m or longer and therefore a large net normal dispersion of the cavity, short pulse operation still requires dispersion compensators such as a grating pair,[8] although bulk components add to the complexity and maintenance, require alignment, and increase the physical size of the system.

The advantage of the anomalous dispersion regime is that shorter pulses could be obtained when pulse shaping is assisted by soliton effects. Although soliton pulse shaping is a convenient method of short-pulse generation from fiber lasers, the soliton effects eventually limit pulse duration and energy.[10] Alternatively, the so-called stretched-pulse technique was introduced for erbium-doped systems, minimizing soliton shaping. The principle of stretched-pulse mode locking uses cavity segments of large positive and large negative dispersion to introduce large changes of pulse width in the laser cavity and minimize nonlinear effects.[11,12] Because silica fiber at ~1 μm has a high value of normal dispersion, the neodymium and Yb laser systems can be conveniently operated in the stretched-pulse regime.[13,14] However, with large net normal dispersion mode-locking is difficult to initiate, and operation suffers from instability. For this reason, typical stretched-pulse lasers operate with small net normal group-velocity dispersion[13–15] exploiting an appropriate compensation technique.

For coping with the difficulty in obtaining self-starting mode locking within a laser with a Fabry–Pérot geometry, semiconductor saturable-absorber mirrors (SESAM) have been conveniently used to ensure the self-starting character of the mode locking.[16]

In this paper we experimentally investigate mode-locked Yb-doped fiber lasers. This paper is organized as follows. In Section 2 we present a mode-locked Yb fiber laser using an intracavity GTI for the generation of net anomalous GVD. The short-length highly doped Yb fiber provided a low value of net normal GVD that is compensated by a GTI mirror with a comparable amount of anomalous dispersion, while preserving an optical bandwidth sufficient for supporting picosecond pulses. In Section 3 a compact dispersion compensator-free mode-locked Yb-fiber laser is presented. To avoid the need for dispersion compensators, we built a short-length Yb-fiber laser. The few-centimeters-long highly doped Yb fiber and the short segment of the single-mode fiber are contained in the cavity, providing a low value of net normal GVD.

2. Mode-locked Ytterbium Fiber Laser with Use of a GTI Compensator

Dispersion compensation based on a GTI was studied with use of the laser setup shown in Fig. 1. The

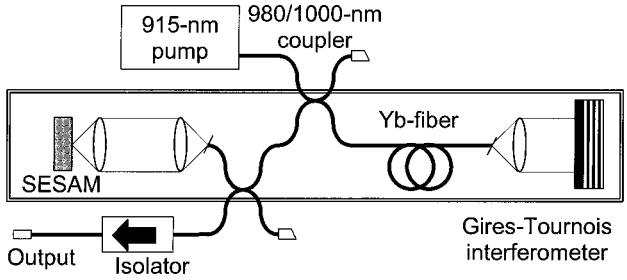

Fig. 1. Cavity configuration for a mode-locked Yb fiber laser with use of a GTI compensator.

linear cavity is defined by the SESAM and the GTI reflector. The total length of the fiber within the cavity was 74 cm, including a 10% output coupler. The Yb-doped silica fiber (NA = 0.22; cutoff wavelength, ~910 nm) had an unsaturated fiber absorption at 977 nm of ~1900 dB/m. This Yb fiber was manufactured by Liekki Oy (Lohjo, Finland) with use of direct nanoparticle deposition technology.[17]

The SESAM used, operating in the 940–1050-nm wavelength range, is based on a GaInNAs material known as a dilute nitride system. It was monolithically grown on an *n*-type GaAs (001) substrate and is similar to the long-wavelength SESAM described in Ref. 18. An antiresonant Fabry–Pérot structure of SESAMs is formed by the uncoated front surface and the highly reflecting AlAs/GaAs mirror stack.[10] This absorber allowed us to reliably trap the pulse spectrum at the regime with anomalous GVD of the GTI.

The GTI we used was made with use of an electron beam evaporator. The GTI consists of bottom and top distributed Bragg reflectors (DBRs) with 10 and 4.5 pairs of SiO_2/TiO_2, respectively, spaced by a 0.7-μm-thick of SiO_2. Calculated mirror reflectivities at 1023 nm are $R = 0.9356$ for the top DBR and $R = 0.9989$ for the bottom DBR. The GTI structure resonance was positioned near $\lambda = 1022.8$ nm, as seen from the reflectivity spectrum shown in Fig. 2. Al-

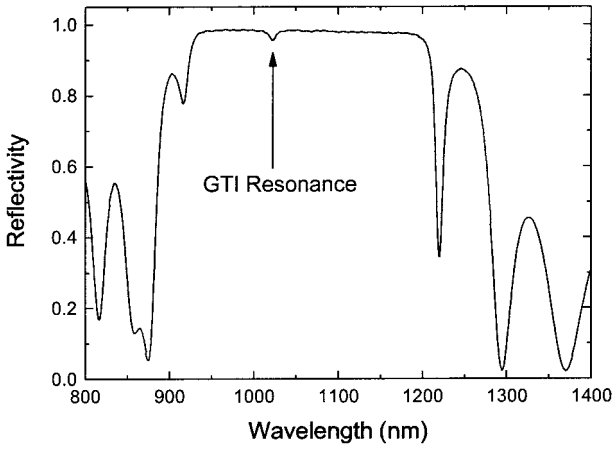

Fig. 2. Measured reflectivity of the Gires–Tournois structure. A reflectivity dip at resonance is shown.

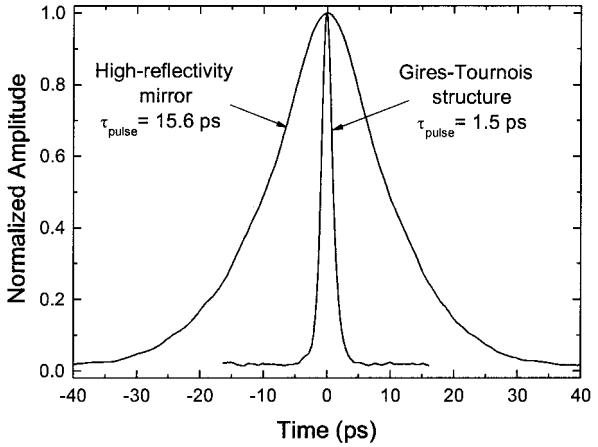

Fig. 3. Autocorrelation traces for pulsed operation with and without GTI.

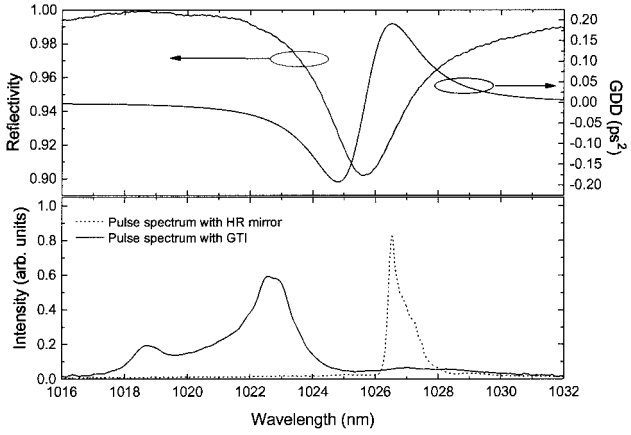

Fig. 4. Upper graph, GTI reflectivity near the resonant wavelength with calculated group-velocity dispersion; lower graph, pulse spectra with and without dispersion compensation.

though an ideal GTI is expected to have a flat power reflectance spectrum, there is a dip at resonance in the reflectance of the high-finesse GTI, owing to a reduced reflectivity of the bottom mirror. The resonant extra loss would push the lasing spectrum away from the anomalous GVD regime toward the GTI reflection maximum.[19] To lock the pulse spectrum to the region of the anomalous GVD, we have used a SESAM with a large change in nonlinear reflectivity (up to 8%).[18] With this absorber mirror, the decrease in cavity loss for short-pulse operation is higher than the loss penalty, owing to the dip in the GTI reflectivity at this wavelength ($\leq$1%). As a result, the mode-locked operation starts spontaneously at the wavelength range with the anomalous GVD and remains reliably trapped at this region.

The laser threshold for cw operation was ~15 mW. When the Yb-doped fiber length was ~2.5 cm, the central lasing wavelength was within the range of 1020–1030 nm. With shorter lengths of Yb fiber, the laser was operating at 980 nm. Self-started mode-locked operation at spectral range around λ = 1023 nm with an anomalous GVD was obtained for pump power above 40 mW with an output power up to ~1 mW. Figure 3 illustrates autocorrelations traces for the laser operating with a GTI reflector and with the GTI replaced with an ordinary highly reflective mirror. The pulse durations were 1.5 and 15.6 ps, respectively, assuming a Gaussian pulse shape. Comparison of the autocorrelations shows that the GTI provides significant compensation of the fiber dispersion. Implementing the GTI resulted in the pulse shortening factor of the order of 10. The time-bandwidth products without and with dispersion compensation by use of the GTI are 0.98 and 0.43, respectively, showing that the compensation results in the generation of transform-limited Gaussian pulses. The fundamental cavity frequency was 95 MHz.

Figure 4 shows the GTI reflectivity and the resultant GVD around the resonance and pulse spectra with the GTI and with a highly reflective mirror used instead of the GTI. The negative GVD generated by the GTI is approximately -0.05 ps^2 at the laser wavelength. The total dispersion in the cavity, including a double pass of the fiber segment and the GTI, was estimated to be -0.01 ± 0.005 ps^2. This estimation shows that the total cavity dispersion corresponds to a small, net anomalous group-velocity dispersion. The uncertainty in the cavity dispersion relates to the problem of estimating the dispersion of the highly doped Yb fiber.

It is important to note that, using a SESAM with high contrast of nonlinear reflectivity, the operation in the negative GVD regime near λ = 1022.8 nm was possible without any wavelength-selective elements despite the reflectivity dip around the GTI resonant wavelength. Mode-locked operation occurs spontaneously at this wavelength for sufficient pumping power.

3. Short Length Mode-Locked Ytterbium Fiber Laser

To minimize dispersion induced by the fiber and thus avoid the need for any intracavity dispersion compensators, we built a short-length fiber laser using highly doped Yb fiber, as shown in Fig. 5. The laser could be operated with an even smaller cavity dispersion by

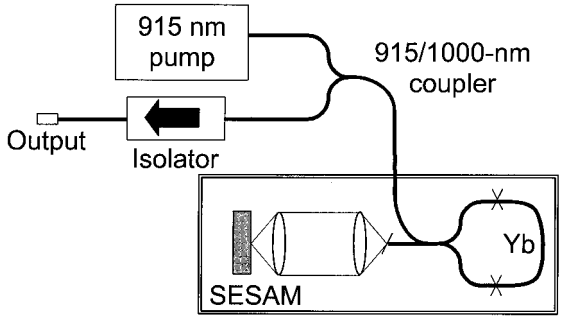

Fig. 5. Amplifying-loop cavity configuration for a short-length stretched-pulse Yb-fiber laser.

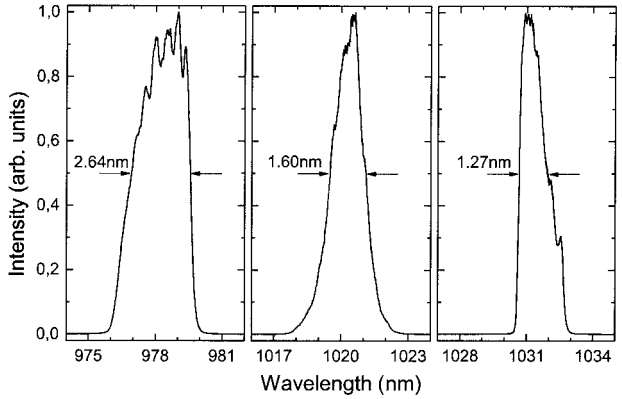

Fig. 6. Output spectra from the mode-locked laser in the 980–1030-nm wavelength range, obtained with Yb fiber with lengths ranging from 2.1 to 4.1 cm.

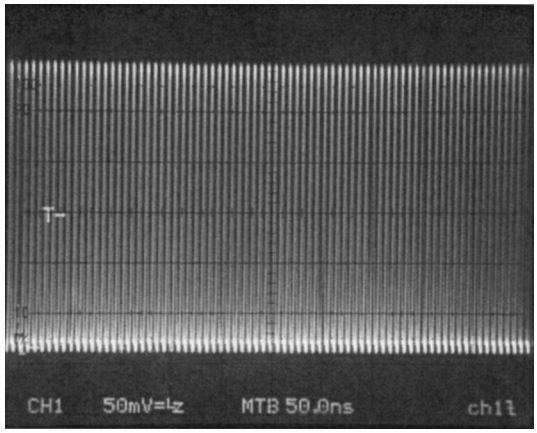

Fig. 8. Stable pulse train at the fundamental cavity frequency of 140 MHz.

simple use of the fiber section of the cavity consisting of a gain fiber. However, in such a setup we would need to use bulk optics to pump the Yb fiber, to take the output using mirror splitter, etc. Therefore the laser loses its main advantage: compactness and robustness of the all-fiber configuration.

The linear cavity is defined by the amplifying fiber loop mirror and the semiconductor saturable absorber mirror. Placing the Yb fiber in the loop mirror allows us to keep the signal/pump wavelength-selective coupler and the output coupler external to the laser cavity and thus to reduce further the fiber segment of the laser cavity. The signal/pump wavelength-selective coupler and the loop mirror were made of fiber with a cutoff wavelength of ~910 nm. The fiber loop mirror was designed to couple ~20% of the power to the output. It should also be mentioned that the fiber coupler forming the loop mirror acts as a nearly symmetrical splitter at the pump wavelength of 915 nm; therefore the Yb fiber was pumped from both ends, providing near-uniform inversion.

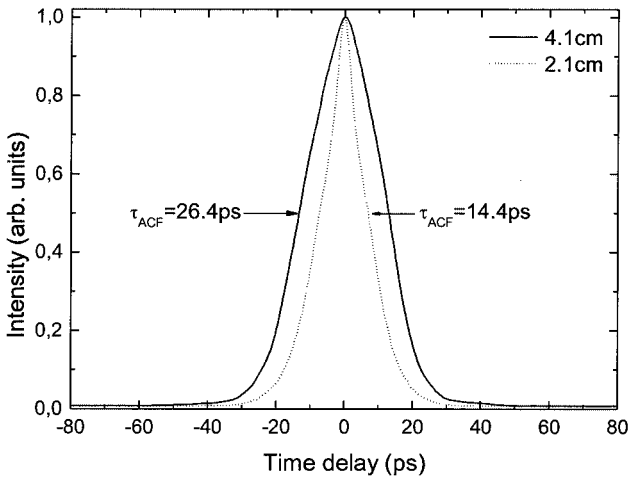

Fig. 7. Autocorrelation traces for stretched pulse operation with lengths of Yb fiber of 2.1 and 4.1 cm.

The SESAM and the Yb-doped fiber used were the same as described in the previous section.

The laser threshold for cw operation was ~15 mW. Self-started mode-locked operation was obtained for pump power above 40 mW, with the output power up to ~1 mW. When the Yb-doped fiber length was short enough (~2 cm), the laser was operating at 980 nm. When the length of doped fiber was increased to 3–4 cm, the central lasing wavelength was shifted toward 1020–1030 nm, owing to the reabsorption of 980-nm emission, as shown in Fig. 6. Figure 7 illustrates autocorrelation traces for the lengths of the Yb fiber of 2.1 and 4.1 cm. It can be seen that a longer Yb fiber, i.e., a higher value of a normal GVD, results in a stronger pulse stretching. It is important to note that the pulse does not exhibit the pedestal, though the autocorrelations can not be fitted neither with a sech^2 nor a Gaussian profile. To compress the output pulses by removal of the positive temporal chirp, we have used an anomalous dispersive delay line.[11] The experiments have shown that the chirp of the pulses is highly linear, resulting in an efficient pulse compression. These results will be presented in a future paper. The fundamental cavity frequency corresponds to the pulse repetition rate of 140 MHz, as seen from the scope trace in Fig. 8.

4. Conclusions

In conclusion, we have demonstrated mode-locked Yb-fiber laser operation in the normal and anomalous dispersion regime. To achieve the anomalous dispersion regime, we used a Gires–Tournois compensator in a short length cavity with a 2.5-cm highly doped Yb fiber. With use of a broadband semiconductor saturable absorber mirror based on GaInNAs, which has a large change in nonlinear reflectivity, self-started 1.5-ps pulse mode-locked operation was obtained at 1023 nm with a repetition rate of 95 MHz. Implementation of the GTI resulted in a pulse-shortening factor of the order of 10. Specially designed high-reflectivity Gires–Tournois mirrors have been proved to be attractive candidates for control-

ling intracavity dispersion in fiber lasers. We believe that if we use a GTI with smaller resonant losses, we would be able to avoid the bandwidth limitation provided by the present device. With improved design, currently under preparation, we expect to generate broader pulse spectrum corresponding to sub-500-fs pulses.

In the normal dispersion regime, stable and self-starting pulse operation was obtained without applying any dispersion compensation technique. Overall normal group-velocity dispersion was minimized by use of a short length of highly doped Yb fiber in a compact amplifying loop cavity. With use of the same broadband semiconductor saturable absorber mirror based on the GaInNAs material system, self-started mode-locked operation was obtained in the 980–1030-nm wavelength range with a repetition rate of 140 MHz.

In the cavity using the loop mirror, the self-phase modulation was negligible owing to low average power and relatively broad pulses (order of 10 ps). The small length of fiber further minimizes the influence of any nonlinear phase shift. In the setup using the GTI, we have estimated round-trip nonlinear phase shift to be ~0.2 rad. Therefore, although self-phase modulation may contribute to the pulse-shaping mechanism, our observations confirm the dominant role of the SESAM on pulse formation.

The authors would like to thank Liekki Oy for providing the Yb-doped fiber.

References

1. G. Steinmeyer, D. H. Sutter, L. Gallmann, N. Matuschek, and U. Keller, "Frontiers in ultrashort pulse generation: pushing the limits in linear and nonlinear optics," Science **286,** 1507–1512 (1999).
2. L. Reekie, R. J. Mears, S. B. Poole, and D. N. Payne, "Tunable single-mode fiber lasers," J. Lightwave Technol. **4,** 956–960 (1986).
3. O. G. Okhotnikov and J. R. Salcedo, "Spectroscopy of the transient oscillations in a Nd^{3+}-doped fiber laser for the four-level $^4F_{3/2}$-$^4I_{11/2}$ (1060-nm) and three-level $^4F_{3/2}$-$^4I_{9/2}$ (900-nm) transitions," Appl. Phys. Lett. **64,** 2619–2621 (1994).
4. C. R. O Cochláin, R. J. Mears, and G. Sherlock, "Low threshold tunable soliton source," IEEE Photon. Technol. Lett. **5,** 25–28 (1993).
5. K. Tamura, E. P. Ippen, and H. A. Haus, "Optimization of filtering in soliton fiber lasers," IEEE Photon. Technol. Lett. **6,** 1433–1435 (1994).
6. L. E. Nelson, E. P. Ippen, and H. A. Haus, "Broadly tunable sub-500-fs pulses from an additive-pulse mode-locked thulium-doped fiber ring laser," Appl. Phys. Lett. **67,** 19–21 (1995).
7. M. E. Fermann, M. J. Andrejco, Y. Silberberg, and A. M. Weiner, "Generation of pulses shorter than 200 fs from a passively mode-locked Er fiber laser," Opt. Lett. **18,** 48–50 (1993).
8. H. Lim, F. Ö. Ilday, and F. W. Wise, "Generation of 2-nJ pulses from a femtosecond ytterbium fiber laser," Opt. Lett. **28,** 660–662 (2003).
9. H. Lim, F. Ö. Ilday, and F. W. Wise, "Femtosecond ytterbium fiber laser with photonic crystal fiber for dispersion control," Opt. Express **10,** 1497–1502 (2002), http://www.opticsexpress.org.
10. L. E. Nelson, D. J. Jones, K. Tamura, H. A. Haus, and E. P. Ippen, "Ultrashort-pulse fiber ring lasers," Appl. Phys. B. **65,** 277–294 (1997).
11. K. Tamura, E. P. Ippen, H. A. Haus, and L. E. Nelson, "77-fs pulse generation from a stretched-pulse mode-locked all-fiber ring laser," Opt. Lett. **18,** 1080–1082 (1993).
12. K. Tamura, C. R. Doerr, L. E. Nelson, H. A. Haus, and E. P. Ippen, "Technique for obtaining high-energy ultrashort pulses from an additive-pulse mode-locked erbium-doped fiber ring laser," Opt. Lett. **19,** 46–48 (1994).
13. V. Cautaerts, D. J. Richardson, R. Paschotta, and D. C. Hanna, "Stretched pulse Yb^{3+} silica fiber laser," Opt. Lett. **22,** 316–318 (1997).
14. M. Hofer, M. E. Fermann, F. Haberl, and J. E. Townsend, "Active mode locking of a neodymium-doped fiber laser using intracavity pulse compression," Opt. Lett. **15,** 1467–1469 (1990).
15. L. Lefort, J. H. V. Price, D. J. Richardson, G. J. Spühler, R. Paschotta, U. Keller, A. R. Fry, and J. Weston, "Practical low-noise stretched-pulse Yb^{3+}-doped fiber laser," Opt. Lett. **27,** 291–293 (2002).
16. F. X. Kärtner, J. Aus der Au, and U. Keller, "Mode-locking with slow and fast saturable absorbers–what's the difference?," IEEE J. Sel. Top. Quantum Electron. **4,** 159–168 (1998).
17. S. Tammela, P. Kiiveri, S. Sarkilahti, M. Hotoleanu, H. Valkonen, M. Rajala, J. Kurki, and K. Janka, "Direct nanoparticle deposition process for manufacturing very short high gain Er-doped silica glass fibers," in *Proceedings of the 28th European Conference on Optical Communication*, P. Danielsen, ed. (European Conference on Optical Communication, Lyngby, Denmark, 2002), Vol. 4, paper 9.4.2.
18. O. G. Okhotnikov, T. Jouhti, J. Konttinen, S. Karirinne, and M. Pessa, "1.5-μm monolithic GaInNAs semiconductor saturable-absorber mode locking of an erbium fiber laser," Opt. Lett. **28,** 364–366 (2003).
19. D. Korf, G. Zhang, R. Fluck, M. Moser, and U. Keller, "All-in-one dispersion-compensating saturable absorber mirror for compact femtosecond laser sources," Opt. Lett. **21,** 486–488 (1996).

Appendix 3

Publication 3

L. Orsila and O. G. Okhotnikov, "Three- and four-level transition dynamics in Yb-fiber laser," *Optics Express*, vol. 13, no. 9, pp. 3218–3223, 2005.

Three- and four-level transition dynamics in Yb-fiber laser

Lasse Orsila and Oleg G. Okhotnikov

Optoelectronics Research Centre, Tampere University of Technology
P.O. Box 692, FIN-33101, Tampere, Finland
lasse.orsila@orc.tut.fi, oleg.okhotnikov@orc.tut.fi

Abstract: The behavior of transient oscillations has been studied experimentally for the first time in a broadly tunable ytterbium fiber laser. Spectroscopic study of the relaxation frequency allows one to distinguish three- and four-level transitions and provides a useful tool for controlling the dynamics of pulsed lasers. Particularly, the relaxation oscillation frequency depends on the occupation of the terminal level of the laser transition and clearly shows that the laser transition becomes four-level at the long-wavelength tail of the gain spectrum of ytterbium fiber ($\lambda > 1060$ nm). The wavelength dependence of relaxation oscillations can be used to determine the parameters of the gain material such as transition cross-section.

OCIS codes: (160.3380) Laser materials; (160.5690) Rare earth doped materials; (160.2290) Fiber materials; (140.3510) Lasers, fiber; (060.2270) Fiber characterization

References and links

1. L. Reekie, R. J. Mears, S. B. Poole, and D. N. Payne, "Tunable Single-Mode Fiber Lasers," J. Lightwave Technol. **LT-4**, 956–960 (1986).
2. O. G. Okhotnikov and J. R. Salcedo, "Spectroscopy of the transient oscillations in a Nd3+-doped fiber laser for the four-level $^4F_{3/2}$-$^4I_{11/2}$ (1060 nm) and three-level $^4F_{3/2}$-$^4I_{9/2}$ (900-nm) transitions," Appl. Phys. Lett. **64**, 2619–2621 (1994).
3. C. R. Ó. Cochláin, R. J. Mears, and G. Sherlock, "Low threshold tunable soliton source," IEEE Photon. Technol. Lett. **5**, 25–28 (1993).
4. K. Tamura, E. P. Ippen, and H. A. Haus, "Optimization of filtering in soliton fiber lasers," IEEE Photon. Technol. Lett. **6**, 1433–1435 (1994).
5. H. M. Pask, R. J. Carman, D. C. Hanna, A. C. Tropper, C. J. Mackechnie, P. R. Barber, and J. M. Dawes, "Ytterbium-Doped Silica Fiber Lasers: Versatile Sources for the 1–1.2 μm Region," IEEE J. Sel. Top. Quantum Electron. **1**, 2–13 (1995).
6. O.G. Okhotnikov, L. Gomes, N. Xiang, T. Jouhti, and A. B. Grudinin, "Mode-locked ytterbium fiber laser tunable in the 980–1070 nm spectral range," Opt. Lett. **28**, 1522–1524 (2003).
7. O.G. Okhotnikov, L. Gomes, N. Xiang, T. Jouhti, A. K. Chin, R. Singh and A.B. Grudinin, "980 nm picosecond fiber laser," IEEE Photon. Technol. Lett. **15**, 1519–1521 (2003).
8. O.G. Okhotnikov, V.V. Kuzmin and J.R. Salcedo, "General intracavity method for laser transition characterization by relaxation oscillation spectral analysis," IEEE Photon. Technol. Lett. **6**, 362–364 (1994).
9. O.G. Okhotnikov and J.R. Salcedo, "Laser transitions characterization by spectral and thermal dependences of the transient oscillation," Opt. Lett. **19**, 1445–1447 (1994).
10. C. J. Kennedy, J. D. Barry and R. R. Rice, "Measurement of parameters in a mode-locked and frequency-doubled Nd:YAG laser using relaxation oscillations," J. Appl. Phys. **47**, 2447–2449 (1976).
11. J. Harrison, G. A. Rines and P. F. Moulton, "Long-pulse generation with a stable-relaxation-oscillation Nd:YLF laser," Opt. Lett. **13**, 309–311 (1988).

1. Introduction

Telecom industry had resulted in development of mature fiber technology and reliable and cost effective components, which makes suitably designed fiber lasers real contenders to

#6906 - $15.00 US Received 18 March 2005; revised 12 April 2005; accepted 13 April 2005

conventional solid-state lasers. Rare-earth doped fibers exploiting the three-level and four-level transitions in Er^{3+}, Nd^{3+}, Pr^{3+} and Yb^{3+} are now used in many applications, including fiber lasers and optical amplifiers. For these sources, especially those operated in mode-locked or Q-switched regime, it is important to know the process that governs the transient emission buildup, including the population inversion dynamics, the effect of spontaneous emission and the nature of the laser transition. The broad fluorescence spectrum makes different fiber gain media particularly attractive for tunable and ultra short pulse sources. Cw operation for a Nd:glass fiber laser was reported over a tuning range of 30 nm [1] and more recently over 50 nm [2]. For Er-doped fiber lasers, tuning over 35 nm was achieved in an actively mode-locked system [3] and over 50 nm in a passively mode-locked fiber soliton laser [4].

Ytterbium-doped silica fiber having broad gain bandwidth, high optical conversion efficiency, and large saturation optical flux offers an almost ideal gain medium for the generation and the amplification of wavelength-tunable ultra short optical pulses. The broad gain spectrum of Yb fiber attracted many researchers; particularly emission and cross section were measured in [5]. For fiber lasers doped with ytterbium, which exhibits a particularly wide fluorescence spectrum, a tuning range of ~100 nm was demonstrated [6]. An additional interesting feature of Yb-doped fiber lasers is that under certain conditions those lasers can operate in the 977 nm spectral band, which make them very attractive as a master source for frequency doubling to achieve 488 nm and thus to substitute the bulky and inefficient Ar-ion lasers [7]. Therefore, the vast wavelength range of 980 to 1100 nm can be achieved with Yb-fiber lasers. Such broad wavelength tunability, however, requires knowledge of the mechanisms of the laser transition and dynamics. Earlier it was shown that in glasses doped with erbium and neodymium as active ions, the laser transition changes its property over the gain bandwidth [2, 8, 9]. This feature alters the oscillation dynamics of the lasers that in turn may strongly affect the characteristics of the pulsed operation. In particular, it was shown that notable transient effects in lasers that take the form of well-known relaxation oscillations have a characteristic period and damping decay time strongly dependent on the operation wavelength. Experiments performed with the rare-earth-doped fiber lasers clearly demonstrate the different wavelength dependence behavior of the transient oscillations depending on the nature of the laser transition. A close inspection of the frequency of relaxation oscillations ω_{relax} across the gain bandwidth resulted in some interesting features being observed [2, 8, 9]. The slopes of the linear dependencies of ω^2_{relax} vs. (r–1) were found to change noticeably with wavelength for the three-level transition relaxation oscillations; here r is a normalized pumping rate. In contrast, the linear dependence was wavelength independent for the four-level transition relaxation oscillations, as expected. The origin of the wavelength dependence of ω^2_{relax} for three-level systems was understood from the small-signal analytic solution of the rate equations, taking into account the thermal level population [2]:

$$\omega_{relax}^2 = \frac{1}{\tau_c \tau_s}\left(1 + c\tau_c \sigma \eta f^l N\right)(r-1). \qquad (1)$$

The symbols used in this equation are defined as follows: N is total number of active ions, c, σ are the speed of light and laser transition cross section, $\eta = l/[L + l\,(n-1)]$, where L, l are the total cavity length and the length of the gain medium, respectively, n is the refractive index, f^l is the fractional thermal occupation of the lower laser level and τ_c, τ_s are the cavity and laser transition lifetimes.

From this equation it is clear that the wavelength-dependent term in parentheses disappears for lasers operating on transitions with a negligible population on the terminal level ($f^l = 0$). An important consequence of this feature (not observed in four-level systems) is that the relaxation oscillation frequency depends directly on the absorption at the signal wavelength ($\sigma f^l \neq 0$) as a result of the finite thermal population of the ground level. Therefore the wavelength dependence of the relaxation oscillations provides a method to

#6906 - $15.00 US Received 18 March 2005; revised 12 April 2005; accepted 13 April 2005

distinguish three- and four-level transitions, and this can be useful in spectroscopic studies as well as in determining the parameters of the laser transition [9–11].

2. Experimental results

In this article we use this method to identify the mechanism of the laser transitions in ytterbium fiber laser. The measurements show that the transient buildup of the emission in the long-wavelength tail of the Yb-fiber gain spectrum (λ>1060 nm) reveals the 4-level nature of the laser transition contrary to the operation at shorter wavelengths. This feature modifies strongly the properties of the Yb-fiber laser, affects laser operation in a pulsed mode, e.g. Q-switching, and should be accounted for when constructing a pulse laser.

The linear cavity (see Fig. 1) containing a piece of Yb^{3+}-doped fiber as the gain medium was defined by a fiber loop mirror acting also as a 15% output coupler and a 1/1200 mm^{-1} reflection grating in a Littrow configuration. An intracavity antireflection coated lens was used to collimate the beam from the single-mode fiber onto the diffraction grating. Optical pumping for 980 nm region lasing was provided by a 915 nm diode laser through dichroic fiber combiner supplying up to 100 mW in the gain fiber. The tunable operation in the 1030–1105 nm wavelength range exploits a 980 nm pump diode with an appropriate fiber combiner. 1-kHz chopper placed in the open section of the cavity was used to observe the transient evolution of the laser emission towards its stationary state.

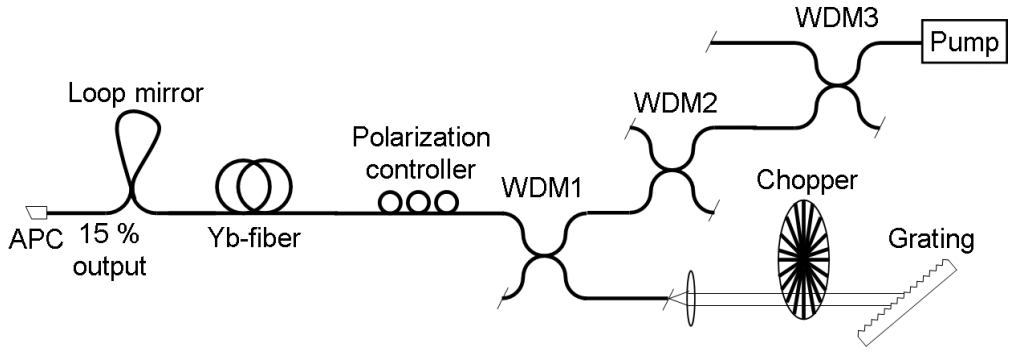

Fig. 1. Experimental setup. For 980 nm spectral range, a 915 nm pump was used with 30 cm Yb-fiber and three wavelength-division multiplexers (WDM) 1: 915/980, 2: 910/1024, 3: 920/1050. For 1030–1100 nm range, 142 cm-long Yb-fiber was pumped with 980 nm single-mode pigtailed diode laser through the cascade of three fiber WDMs 1: 980/1100, 2: 980/1030, 3: 980/1050.

A signal/pump wavelength-selective coupler and output coupler were made of fiber with a cutoff wavelength of 920 nm. Depending on the operating spectral range, the fiber was pumped through a different kind of fiber multiplexers (see Fig. 1) to achieve high extinction in a broad wavelength range. We have observed that external reflections may severely affect the dynamics of ytterbium fiber laser. Few pump multiplexers were then used in series to exclude any optical coupling between pump laser diode and fiber laser cavity.

When the doped fiber length was short enough (~30 cm) to ensure at least 50% population inversion along all fiber, the laser was operating straight at 980 nm even without any wavelength selective elements. Pump through power in this instance was around 10 mW (for 100 mW of launched power at 915 nm). When the doped fiber length was increased to 142 cm, so that 980 nm radiation was re-absorbed inside the fiber, the central lasing wavelength was shifted towards 1040 nm. It should be noted that the cavity length, L, and the total number of active ions in the cavity, N, affect the absolute value of the relaxation oscillation frequency, as seen from Eq. (1). However, although ω_{relax} changes with the length of the ytterbium fiber placed as an active medium, the nature of the laser transition (3- or 4-level transition) depends only on population of the terminal level (f^l) and obviously not on the amount of the gain fiber.

#6906 - $15.00 US Received 18 March 2005; revised 12 April 2005; accepted 13 April 2005

Yb^{3+}-doped fiber had a core diameter of 3.0 μm and showed absorption of 3.1 dB/m at 810 nm. The relaxation oscillation frequency ω_{relax} was determined from the repetition period of the small-amplitude strongly damped nearly sinusoidal oscillations (see Fig. 2).

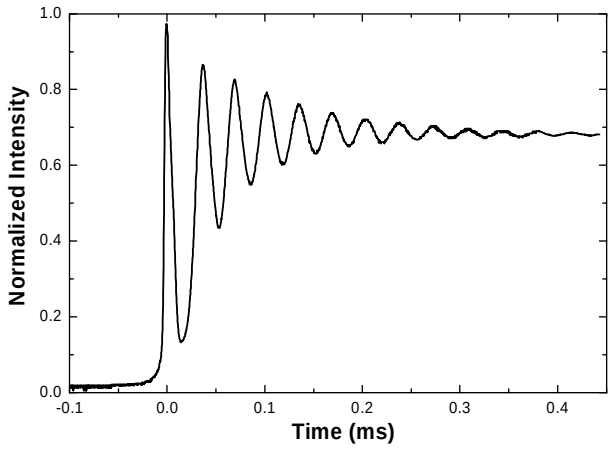

Fig. 2. Typical transient oscillations from an Yb^{3+}-doped fiber laser. Pumping rate normalized to the threshold pumping rate is r–1=0.12 and lasing wavelength is λ=1053 nm.

The wavelength-resolved relaxation oscillations measured at room temperature were analyzed over the whole gain spectrum of ytterbium fiber. Figures 3 and 4 show a plot of $(\omega_{relax}/2\pi)^2$ vs. (r–1), where r is the pumping rate normalized to the threshold pumping rate, around 980 and 1030–1105 nm, respectively, taking the lasing wavelength as a parameter. Although, we always observed linear dependencies for $(\omega_{relax}/2\pi)^2$ vs. (r–1), as it is expected from analysis based on rate equations; the relaxation oscillations originating at the four-level (λ>1060 nm) and three-level (λ<1060 nm) transitions exhibited different wavelength dependencies.

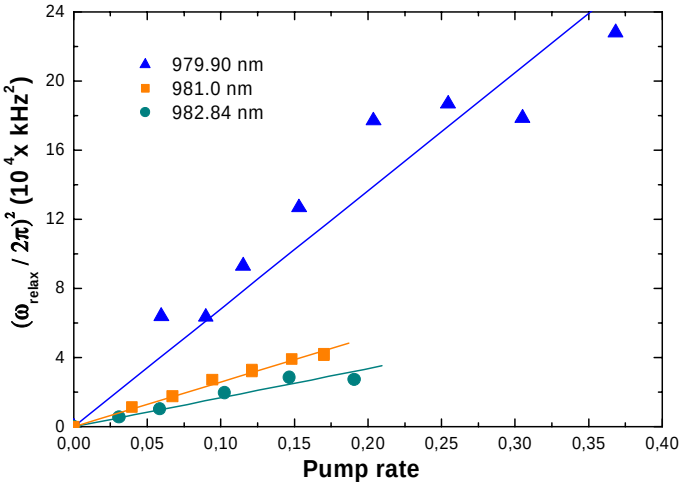

Fig. 3. $(\omega_{relax}/2\pi)^2$ versus normalized pumping rate (r–l) around 980 nm with the lasing wavelength as a parameter.

#6906 - $15.00 US
Received 18 March 2005; revised 12 April 2005; accepted 13 April 2005

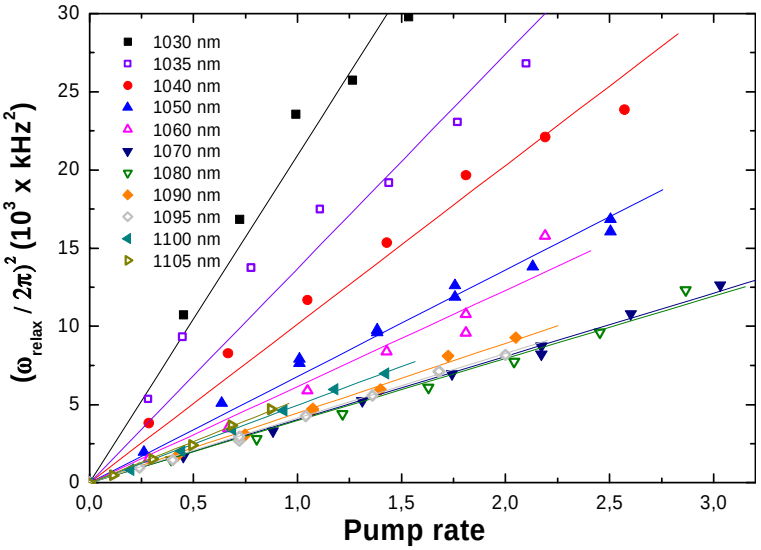

Fig. 4. $(\omega_{relax} / 2\pi)^2$ against normalized pumping rate (r–l) for 1030–1105 nm spectral range.

Figure 5 presents spectral dependence of the relaxation oscillation parameter $(\omega_{relax} /2\pi)^2/(r–1)$, i.e., the slope of the linear dependencies of $(\omega_{relax} /2\pi)^2$ vs. (r–1). As seen from the Fig., this slope changes noticeably with wavelength for the three-level transition. It, however, was fairly wavelength independent for λ>1060 nm demonstrating the four-level nature of laser transition at the long-wavelength tail of the ytterbium gain spectrum [8, 9]. Particularly, the strong decrease in the frequency of the relaxation oscillations was observed at long wavelength resulting in a slow laser dynamics. It is also evident from the Fig. 5 that the individual absorption transitions originated from Stark sublevels with different equilibrium populations have pronounced correlation with transient dynamics. We can deduce from the absorption spectrum that the lasing transitions for λ>1060 nm becomes four-level owing to negligible population of the ground level at room temperature.

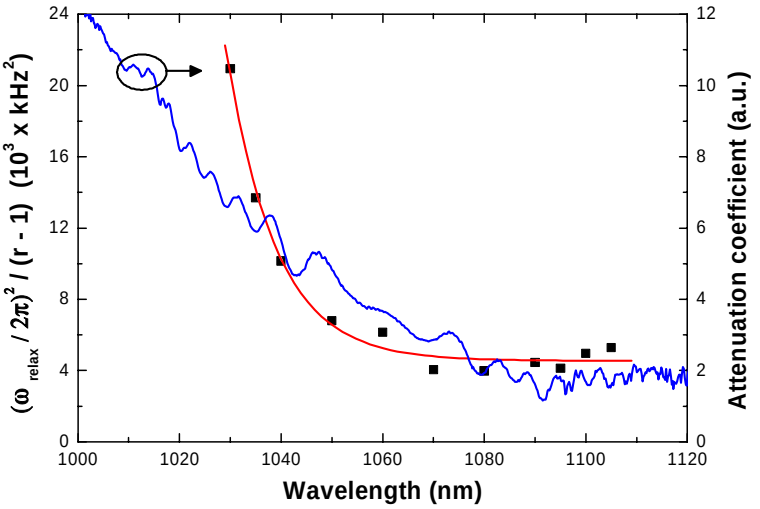

Fig. 5. Wavelength dependence of the relaxation oscillation parameter $(\omega_{relax} / 2\pi)^2$ / (r–l) derived from the plots presented in Fig. 4 and of the Yb^{3+}–φιβερ αττενυατιον.

#6906 - $15.00 US
Received 18 March 2005; revised 12 April 2005; accepted 13 April 2005

3. Summary

In summary, the relaxation oscillations in the tunable ytterbium fiber laser were studied at room temperature in a wide spectral range. The measurements revealed remarkable wavelength dependence of the oscillator dynamics that reflects the change in the character of the laser transition. Particularly, the laser transition at the long-wavelength edge of the gain spectrum (λ>1060 nm) functions as a four-level system contrary to the short-wavelength operation, where transition corresponds to three-level behavior. This phenomenon significantly alters the transient dynamics and should be accounted in pulsed lasers especially in broad gain spectrum tunable lasers.

Acknowledgments

The authors acknowledge the support from the Finnish Academy of Science and Letters.

#6906 - $15.00 US Received 18 March 2005; revised 12 April 2005; accepted 13 April 2005

Appendix 4

Publication 4

L. Orsila, R. Herda, T. Hakulinen and O. G. Okhotnikov, ”Thin-film Fabry–Pérot dispersion compensator for mode-locked fiber lasers,” *IEEE Photonics Technology Letters* vol. 19, no. 1, pp. 6–8, 2007.

Thin-Film Fabry–Pérot Dispersion Compensator for Mode-Locked Fiber Lasers

Lasse Orsila, Robert Herda, Tommi Hakulinen, and Oleg G. Okhotnikov

***Abstract*—We demonstrate a dielectric thin-film Fabry–Pérot etalon operated as a dispersion compensator in a mode-locked fiber-laser cavity. The etalon generates anomalous dispersion near the low-loss spectral window and, consequently, the laser mode-locked by the semiconductor saturable absorber favors operation at anomalous dispersion regime without spectral filter. The etalon compensator is tunable, compact, easy to align, and suitable for picosecond and subpicosecond pulse operation.**

***Index Terms*—Optical fiber dispersion, optical fiber lasers, optical films, thin films, ultrafast optics.**

I. Introduction

FABRY–PÉROT etalons may generate large dispersion near the resonant wavelength [1]. It has been recently shown that the amount of the dispersion induced by the optimized etalon could be sufficient to balance the dispersion of a fiber laser cavity [2], [3]. Gires–Tournois interferometer representing strongly asymmetric etalon operating in reflection exhibits, however, increased losses near the resonant wavelength. For this reason, the use of the etalon in reflection near the resonant wavelength would make the mode-locking difficult to achieve and should employ additional wavelength-selective elements to enforce the laser operation at high-loss state [4]. This feature can be avoided by using the Fabry–Pérot etalon in transmission. With this geometry, cavity-enhanced anomalous dispersion regime of the etalon is near the spectral range of high transmission.

This study demonstrates an attractive potential of a transmission thin-film etalon (TFE) for dispersion compensation in mode-locked fiber lasers. Particularly, we show that TFE is able to introduce an amount of anomalous dispersion with an optical bandwidth sufficient to support subpicosecond pulses in a fiber laser with a cavity length below 1 m. The etalon acts as an intracavity spectral filter and sets the operation wavelength spontaneously close to the low-loss resonance of the etalon. By tilting the etalon relative to the laser beam, the resonant wavelength of the etalon can be adjusted to the desired operation wavelength.

II. TFE Structure and Characteristics

Since the dispersion of the etalon is largely determined by the free-spectral range and mirror reflectivities [5], these parameters were set to ensure the amount of anomalous dispersion that can compensate the dispersion of single-mode fiber with a length of $\sim$1 m at 1 μm, which is a typical length of the fiber laser cavity. Another important objective of the compensator design is a width of the spectral band, where etalon generates significant amount of anomalous dispersion. The target value for the bandwidth pursued in the simulation was $\sim$2 nm that allows for subpicosecond pulse generation.

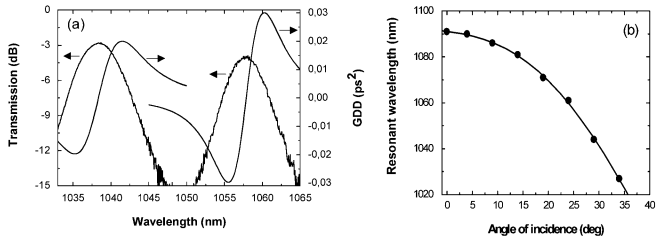

Fig. 1. (a) Measured round-trip transmission and GDD of the etalon operation in transmission mode for two angles, left 31.2° and right 26.8°. (b) Tuning of the resonant wavelength obtained by tilting the etalon.

Symmetrical TFE was made using electron beam evaporator. The etalon consists of bottom and top distributed Bragg reflectors with 4.5 pairs made of Al_2O_3, SiO_2, and TiO_2 spaced by a SiO_2 cavity with an optical length of 2λ. It is relevant to notice here, that an ideal symmetrical etalon has no losses at the resonant wavelength. The rear side of the etalon substrate was antireflection-coated with eight layers of TiO_2 and SiO_2 to prevent unwanted Fabry–Pérot effects between the TFE mirror and the substrate–air interface. The TFE resonance was positioned near $\lambda = 1060$ nm for an angle between an optical axis and normal to etalon surface of $\alpha \sim 25°$.

Fig. 1(a) shows transmission spectrum and group delay dispersion (GDD) of the etalon. Dispersion measurements were performed with a phase-locked interferometer. Both measurements and numerical simulations indicate the transmission window picked at the resonant wavelength of 1040 nm for $\alpha = 30°$.

The simulations agree well with the measured data. The anomalous GDD of approximately -0.02 ps^2 is generated by TFE near the resonant wavelength. The tilting of the etalon relative to the laser beam allows for tuning of the operation wavelength. Fig. 1(b) shows the tuning range of the etalon that covers the whole gain bandwidth of an ytterbium fiber.

III. Experimental Results

Fig. 2 shows the setup of the mode-locked fiber laser employing a symmetrical Fabry–Pérot etalon compensator operating in transmission mode. The short-length cavity was made

Manuscript received May 30, 2006; revised October 27, 2006. This work was supported in part by the Academy of Finland and in part by EU FP6.

The authors are with the Optoelectronics Research Centre, Tampere University of Technology, FIN-33101 Tampere, Finland (e-mail: lasse.orsila@tut.fi).

Digital Object Identifier 10.1109/LPT.2006.888041

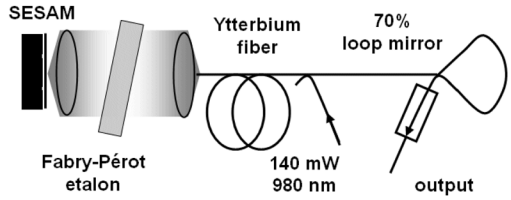

Fig. 2. Passively mode-locked ytterbium fiber laser with dispersion compensation using Fabry–Pérot etalon.

using a 70-cm-long highly doped ytterbium fiber with specified unpumped absorption of 414 dB/m at 976 nm. The ytterbium-doped fiber is pumped with a 980-nm laser diode delivering up to 140 mW in a single-mode fiber. The laser cavity contains a 980/1050-nm pumping fiber coupler and a short-length loop mirror as a cavity reflector and a 30% output coupler. The TFE was inserted in a collimated beam within the laser cavity, as shown in Fig. 2. Throughout this study, the cavity dispersion determined mainly by the fiber segment was varied to explore etalon characteristics at different regimes.

Self-starting mode-locked operation was ensured by the semiconductor saturable absorber mirror (SESAM) [6]. A high modulation depth absorber mirror grown by all-solid-source molecular beam epitaxy was similar to that described in [3]. The important property of this SESAM is that it could start mode-locking in a wide range of cavity dispersion [7]. The pump power threshold for self-starting mode-locking was 100 mW. The overall cavity length including the air-gap section corresponds to a fundamental pulse repetition rate of $\sim$50 MHz. Typical laser output power was $\sim$1 mW. Excess loss of etalon was below 20% mainly due to some asymmetry in the mirrors reflectivities. Optimal performance of mode-locked operation was achieved at moderate pump powers slightly above the threshold avoiding an excessive spectral broadening resulted in additional cavity loss due to the limited etalon bandwidth.

The performance of the etalon compensator was studied by varying the cavity dispersion of the mode-locked laser. Without a TFE compensator, a very broad square-shaped spectrum with the bandwidth of 4 nm was observed indicating a stretched pulse regime, as shown in Fig. 3(a). With an etalon inserted into the cavity, the pulsewidth experiences significant narrowing from 26 down to 2.1 ps, as seen from the autocorrelation trace presented in Fig. 3(b). Thus, using a TFE compensator provides pulse shortening by a factor of $\sim$12. The time-bandwidth product reduces from 28 to 2.32 remaining still quite high. This was attributed to the large dispersion of a long fiber segment that could not be fully compensated by the TFE resulting in overall normal cavity dispersion estimated as $+0.001$ ps^2.

Since the maximum of the etalon transmission occurs at the resonance, it is generally expected that laser spectrum would be picked at this wavelength. The experimental observations confirmed by the numerical simulation show, however, that the mode-locked fiber laser tends to operate with central wavelength blue-shifted from the resonance to the spectral point, where the etalon generates essential amount of anomalous dispersion, as seen from Fig. 4. This feature results from SESAM that gains more complete saturation of the absorption at anomalous dispersion regime, where shorter pulses and, consequently, higher

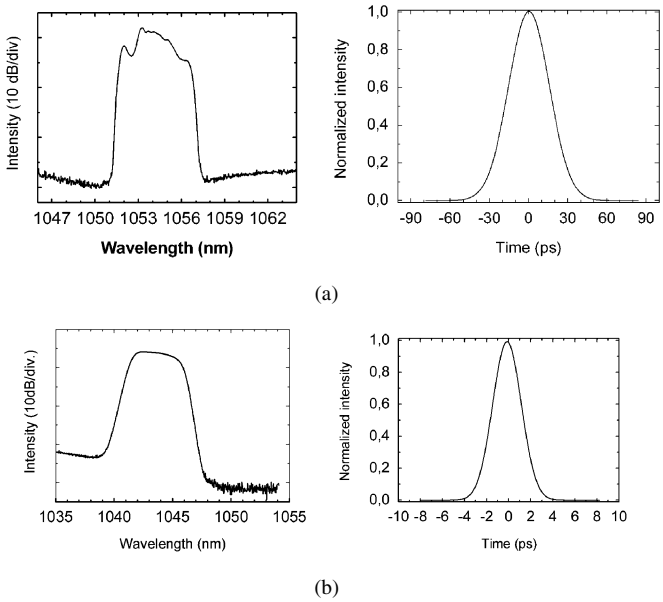

Fig. 3. (a) Optical spectrum and autocorrelation of 26-ps pulses obtained without dispersion compensation. The time-bandwidth product is 28. Estimated cavity dispersion is $\beta_2 = +0.021$ ps^2. (b) Optical spectrum and autocorrelation of 2.1-ps pulses obtained with dispersion compensated by the etalon; the time-bandwidth product is 2.32. Estimated cavity dispersion is $\beta_2 = +0.001$ ps^2. Except for the etalon, the cavity is the same as in (a).

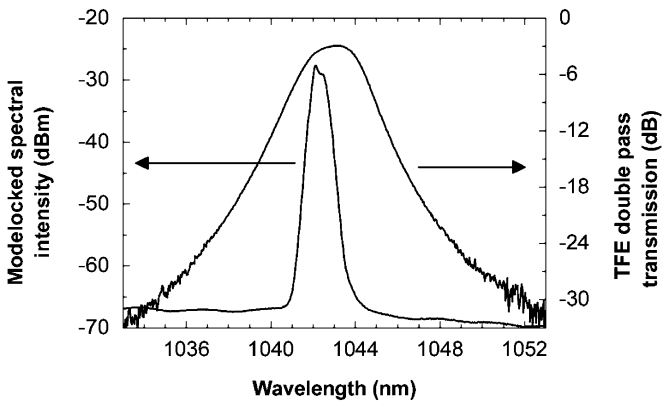

Fig. 4. Mode-locked pulse and TFE double-pass transmission spectra. Pulse spectrum is blue-shifted relative to TFE transmission peak towards the regime with anomalous dispersion.

peak powers could be achieved. The decrease in SESAM absorption, therefore, compensates the etalon loss due to detuning from the resonant wavelength. By tilting the etalon, its transmission maximum shifts to shorter wavelengths providing the tunable pulse operation between 1032 and 1060 nm.

The cavity dispersion was then slightly decreased. Fig. 5 illustrates spectra and autocorrelations for this configuration operating with and without TFE. The measurements revealed that implementing the etalon compensator resulted in a pulsewidth shortening from 3.9 to 1.3 ps, while the time-bandwidth product reduces from 10 to 0.5, respectively, demonstrating an essential improvement in pulse quality. The total cavity dispersion was estimated to be -0.015 ps^2 in anomalous regime. Although, the laser is expected to operate in soliton regime, the optical spectrum displayed in Fig. 5(b) shows no evidence of distinctive

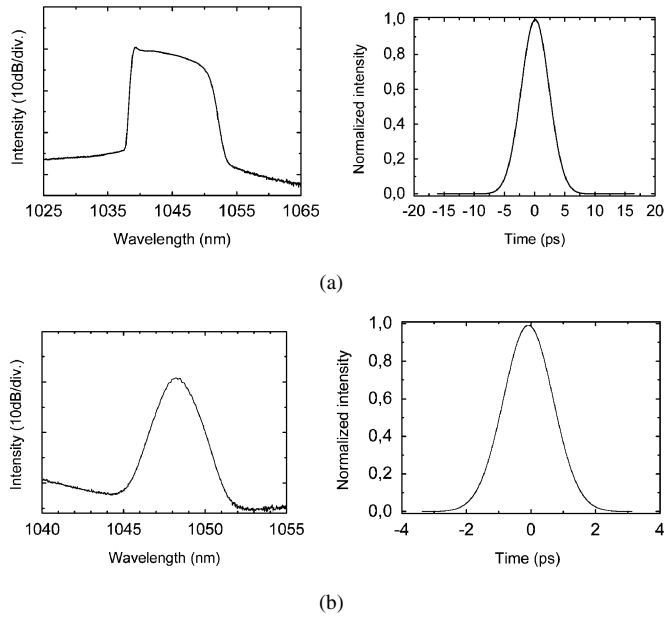

Fig. 5. (a) Optical spectrum and autocorrelation of 3.9-ps pulses obtained without etalon compensator with total cavity dispersion in a normal regime with $\beta_2 = +0.006$ ps^2. The corresponding time-bandwidth product is 10. The contribution to the cavity dispersion from the fiber was reduced, as compared to the geometry presented in Fig. 2. (b) Optical spectrum and autocorrelation of 1.3-ps pulses obtained with dispersion compensated by etalon; corresponding time-bandwidth product is 0.5. Estimated cavity dispersion is $\beta_2 = -0.014$ ps^2 in anomalous regime. Except for the etalon, the cavity is the same as in (a).

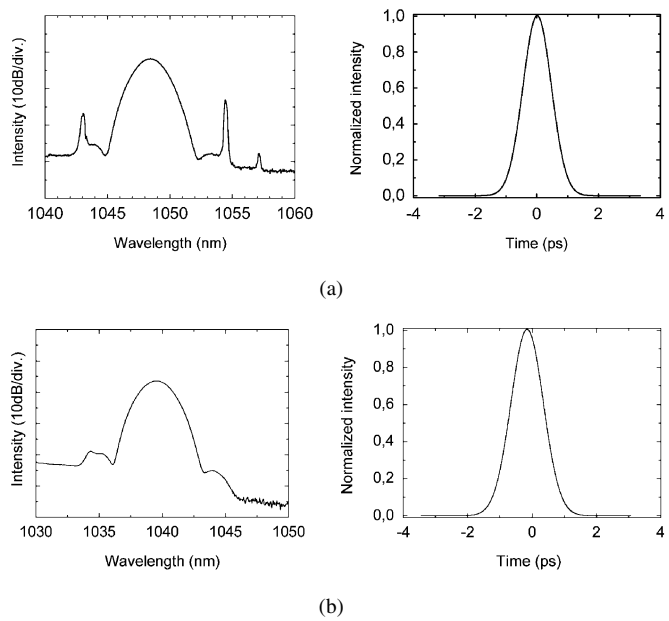

Fig. 6. (a) Optical spectrum and autocorrelation of 0.77-ps pulses with grating pair compensator. The corresponding time-bandwidth product is 0.51. Estimated anomalous dispersion of the cavity is $\beta_2 = -0.13$ ps^2. (b) Optical spectrum and autocorrelation of 0.84-ps pulses obtained with both intracavity etalon and grating pair; corresponding time-bandwidth product is 0.6. Except for the etalon, the cavity is the same as in (a). The solitonic sidebands are filtered out by the etalon.

sidebands. This feature was attributed to the spectral filtering provided by the etalon. This conclusion was further verified by running the laser in soliton regime even without TFE compensation. The cavity dispersion was set to anomalous dispersion regime using transmission grating pair with 1250 lines/mm (not shown in Fig. 2). Fig. 6 shows the output pulse spectra and autocorrelations of the laser with the total cavity dispersion of -0.13 ps^2. Since the dispersion induced by the etalon is low compared to the dispersion of the grating compensator, it could not significantly affect the total cavity dispersion and, consequently, pulsewidth. The duration increases slightly from 0.77 to 0.84 ps indicating that etalon bandwidth is sufficient to support subpicosecond solitons. The solitonic sidebands clearly seen without etalon Fig. 6(a) are strongly suppressed when the etalon is inserted into the cavity Fig. 6(b). Suppression of the spectral sidebands is another positive aspect in using an intracavity etalon for soliton laser [8].

IV. Conclusion

In this letter, we report the first successful implementation of Fabry–Pérot TFE as a dispersion compensator in mode-locked ytterbium fiber laser. The etalon operating in transmission has been rigorously examined in cavities operating in different dispersion regimes. The results show that etalon can generate amount of anomalous dispersion to compensate about 80 cm of fiber at 1 μm in a bandwidth sufficient for supporting subpicosecond pulses. The etalon used in transmission mode generates anomalous dispersion near the low-loss wavelength range and favors pulse operation at this regime without spectral filters. The Fabry–Pérot etalon could be a promising component for ultrafast lasers and can also be used for suppressing solitonic sidebands. In conclusion, we have demonstrated a tunable, compact and easy to align dispersion compensator for ytterbium fiber laser. A self-starting passive mode-locking was ensured with an SESAM. The important conclusion derived from this study shows that there is a tradeoff between amount of dispersion and optical bandwidth provided by the TFE that supports the subpicosecond pulse generation from fiber lasers.

References

[1] F. Gires and P. Tournois, "Interféromètre utilisable pour la compression d'impulsions lumineuses modulées en fréquence," *C. R. Acad. Sci.*, vol. 258, pp. 6112–6115, 1964.

[2] D. Kopf, G. Zhang, R. Fluck, M. Moser, and U. Keller, "All-in-one dispersion-compensating saturable absorber mirror for compact femtosecond laser sources," *Opt. Lett.*, vol. 21, pp. 486–488, 1996.

[3] M. Guina, N. Xiang, and O. G. Okhotnikov, "Stretched-pulse fiber lasers based on semiconductor saturable absorbers," *Appl. Phys. B.*, vol. 74, pp. S193–S200, 2002.

[4] L. Orsila, L. A. Gomes, N. Xiang, T. Jouhti, and O. G. Okhotnikov, "Mode-locked ytterbium fiber lasers," *Appl. Opt.*, vol. 43, pp. 1902–1906, 2004.

[5] H. A. Macleod, *Thin-Film Optical Filters*, 3rd ed. London: Inst. Physics Pub., 2001, pp. 266–280.

[6] U. Keller, K. J. Weingarten, F. X. Kartner, D. Kopf, B. Braun, I. D. Jung, R. Fluck, C. Honninger, N. Matuschek, and J. Aus der Au, "Semiconductor saturable absorber mirrors (SESAMs) for femtosecond to nanosecond pulse generation in solid-state lasers," *IEEE J. Sel. Topics Quantum Electron.*, vol. 2, no. 3, pp. 435–452, Sep. 1996.

[7] R. Herda and O. G. Okhotnikov, "Dispersion compensation-free fiber laser mode-locked and stabilized by high-contrast saturable absorber mirror," *IEEE J. Quantum Electron.*, vol. QE-40, no. 7, pp. 893–899, Jul. 2004.

[8] L. E. Nelson, D. J. Jones, K. Tamura, H. A. Haus, and E. P. Ippen, "Ultrashort-pulse fiber ring lasers," *Appl. Phys. B.*, vol. 65, pp. 277–294, 1997.

Appendix 5

Publication 5

L. Orsila, S. Kivistö, R. Herda and O. G. Okhotnikov, ”Spectroscopy of the relaxation dynamics in Tm-Ho-fiber lasers,” in *Conference Digest of European Conference on Lasers and Electro-Optics 2007,* München, 20–25 June, 2007, p. CE-24-TUE.

Spectroscopy of the relaxation dynamics in Tm-Ho-fiber lasers

L. Orsila, S. Kivistö, R. Herda and O. G. Okhotnikov

Optoelectronics Research Centre, Tampere University of Technology, P.O. Box 692, FIN-33101, Tampere, Finland

Thulium-doped silica fiber proved to be a good solution for light generation near 2 μm. The lasers based on this gain medium were shown to be capable of producing high powers with a broad tuning range and have clear potential for ultra short pulse generation. These features make thulium a promising material for medical and LIDAR applications. Recent studies discover important parameters of thulium doped fiber [1]. Particularly, the dependence of the emission efficiency on the doping level and transition cross section have been determined. Adding holmium as a co-dopant was shown to increase the pump absorption and to extend the thulium gain spectrum to longer wavelengths. The properties of host material and co-doping affect strongly the gain broadening and are used as an instrumental in designing the optical amplifiers, tunable and mode-locked laser systems. Earlier studies have shown that the type of laser transition may evolve across the gain bandwidth [2]. In particular, it has been shown that the transient effects having the form of well-known relaxation oscillations with a characteristic frequency ω_{relax} depend on the operation wavelength.

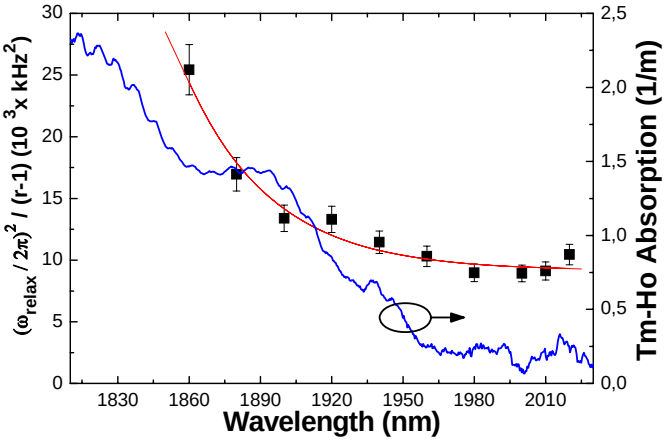

Fig. 1 Wavelength dependence of the relaxation oscillation parameter $(\omega_{relax}/2\pi)^2 / (r-1)$ derived from oscillation frequency vs. normalized pump power (r–1) curves and absorption spectrum of the fiber.

The linear cavity laser containing silica fiber doped with 0.646 wt-% of Tm and 0.040 wt-% of Ho (core diameter of 7.3 μm) was used to investigate Tm-Ho characteristics. The cavity is defined by a 40 % output coupler and a 1/600 mm^{-1} reflection grating operating in a Littrow configuration. The laser was pumped with an 1564-nm single-mode Keopsys laser system supplying up to 6 W of pump power. The relaxation oscillation frequency was determined from the repetition period of the small-amplitude oscillations. The wavelength-resolved relaxation oscillations were measured at room temperature over the entire gain spectrum of Tm-Ho-fiber from 1860 nm to 2020 nm. From Fig. 1 can be seen that at long-wavelength tail of the gain, $\lambda > 1960$ nm, the laser operates as a 4-level scheme at these wavelengths. On the contrary, for the short wavelength range, $\lambda < 1960$ nm, oscillations exhibit significant spectral variation due to thermal population of the terminal energy level at room temperature. This indicates a change in the type of laser transition from four- to three-level type while going to shorter wavelengths. It is generally expected that absorption owing to individual transitions between different Stark sublevels depends on the population of the terminal level and it becomes negligible for the long-wavelength wing of the gain spectrum, where the material operates as a four-level system at room temperature. The behavior correlates with the absorption spectrum of the Tm/Ho fiber. A closer look at longer wavelengths and to Ho properties suggest that Tm-Ho-laser would change back to three-level system around 2020 nm and then can be assumed to change back to four level scheme at longer wavelengths making Tm-Ho-dynamics complicate. This phenomenon affects the transient dynamics and should be accounted in pulsed and tunable lasers.

References

1. J. Wu, S. Jiang, T. Luo, J. Geng, N. Peyghambarian and N. P. Barnes, “Efficient thulium-doped 2-μm germanate fiber laser,” IEEE Photonics Techol. Lett. **18**, 334–336 (2006).

2. L. Orsila and O. Okhotnikov, “Three- and four-level transition dynamics in Yb-fiber laser,” Opt. Express **13**, 3218–3223 (2005).

Appendix 6

Publication 6

L. Orsila, R. Herda and O. G. Okhotnikov, ”Monolithic fiber mirror and photonic crystal technology for high repetition rate all-fiber soliton lasers,” *IEEE Photonics Technology Letters*, vol. 19, no. 24, pp. 2009–2011, 2007.

Monolithic Fiber Mirror and Photonic Crystal Technology for High Repetition Rate All-Fiber Soliton Lasers

Lasse Orsila, Robert Herda, and Oleg G. Okhotnikov

***Abstract*—In this letter, we discuss the technology of a thin-film coating made with electron beam evaporation on a single-mode fiber end facet. A dichroic mirror made of ZrO_2 and SiO_2 was found to provide the necessary selectivity for 980-nm pump and 1040-nm signal wavelengths and enabled us to build a short-cavity mode-locked ytterbium fiber laser. Combined with a photonic crystal fiber dispersion compensator, it allows the realization of a 572-fs soliton all-fiber laser with a fundamental repetition rate of 571 MHz.**

***Index Terms*—Optical fiber lasers, optical films, thin films, ultrafast optics.**

I. Introduction

DESPITE impressive progress in the field of mode-locked fiber lasers, the development of practical sources remains hindered by the lack of appropriate fiber components. Particularly, femtosecond high repetition rate oscillators require dispersion compensators, dichroic elements, and reflectors to assemble an optically pumped laser cavity. These components should preferably be fiber-based to build a low-loss short-length cavity avoiding bulk-optical elements. Recently, dispersion compensators based on photonic crystal fiber (PCF) have been demonstrated, resulting in high-performance systems. However, these still use some bulk elements and intracavity pump couplers that bring in certain constraints as far as shortening of the cavity length [1], [2]. Also, in contrast to the excessively large dispersion of chirped fiber Bragg gratings, PCF provides a proper amount of dispersion to the short laser cavity.

From this perspective, integrated reflectors fabricated by the coating of bare fibers or fiber connectors offer valuable mirrors and pump combiners that allow for extremely short all-fiber cavities. Consequently, the mode-locked oscillator could produce a high fundamental repetition rate with a low timing jitter compared with lasers operated at a higher harmonic [3].

Although simple fiber-end coating is frequently used at present for preventing back-reflections, the technology of the dichroic multilayered coating should address specific issues to control the spectral and mechanical properties of thick structures deposited onto a small-area glass fiber. Here we describe the technology of dichroic reflectors deposited by electron beam evaporation on the fiber-end facets and demonstrate the usefulness of these components together with photonic crystal technology for ultrafast high repetition rate all-fiber lasers.

Manuscript received July 9, 2007; revised September 14, 2007. This work was supported in part by the Academy of Finland, by EU FP6, by the Jenny and Antti Wihuri Foundation, by GETA Graduate School, by The Foundation of Technology in Finland (TES), and by The Finnish Foundation for Economic and Technology Sciences (KAUTE)

The authors are with the Optoelectronics Research Centre, Tampere University of Technology, FIN-33101 Tampere, Finland (e-mail: lasse.orsila@tut.fi).

Color versions of one or more of the figures in this letter are available online at http://ieeexplore.ieee.org.

Digital Object Identifier 10.1109/LPT.2007.909625

II. Fiber End Facet Coatings and Deposition Materials

An obvious strategy in building a compact fiber laser is minimizing the number of intracavity components. Typical mode-locked fiber lasers, however, use an intracavity fiber combiner and output coupler that may essentially contribute to the total cavity length. This can be avoided when the output coupler and pump combiner are designed as the cavity end mirror. In an ytterbium fiber laser, this dichroic mirror should have a high transmission at the pump wavelength of 980 nm and a given reflectivity, typically 50%–80%, at the signal wavelength of 1040–1080 nm. The figure of merit of such a reflector depends primarily on the slope of the spectral response between pump and lasing wavelengths. It is well-known that the sharpness of the edge-type spectral filter increases with the number of layers, which is eventually limited by the material adhesion. It should also be mentioned that for practical implementation, a coating on the fiber, assembled with a standard connector, would be desirable. However, this may limit the temperature that can be used during the coating process because of possible material degradation and thermal expansion in the connector components. On the other hand, the temperature of the coated material cannot be decreased too much because the adhesion of the thin-film to the glass could deteriorate at low temperatures. Finally, the total coating thickness should be kept well below the mode field diameter in a fiber (typically of 4–6 μm around 1 μm wavelength) to avoid excessive optical loss. Therefore, the coating technology should search for a proper trade-off between conflicting requirements.

The materials for fiber coating have been selected based on their refractive index, adhesion, absorption, mechanical properties and heat conductivity. Although TiO_2 has a high refractive index and it is widely used in the thin-film industry, the multilayer coatings on a fiber using TiO_2 films have a tendency to tensile fracturing and delamination [4], [5]. An example of this feature is depicted in Fig. 1 (left). Tantalum pentoxide Ta_2O_5, on the other hand, is susceptible to developing coating defects such as nodules [6], when it is deposited under high oxygen partial pressure and substrate temperatures [7]. In this study, we have

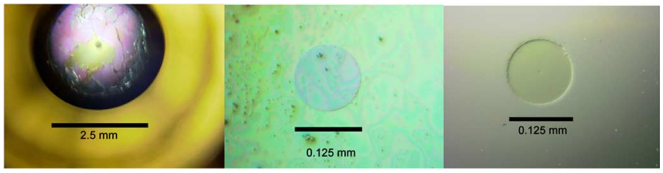

Fig. 1. Examples of fiber end facet coating: coating damaged by poor adhesion and stress (left); material spitting and contamination diminish the surface quality (middle); a successful coating with a smooth surface (right).

found that zirconium oxide ZrO_2 would be an optimal material even though it has a tendency to form inhomogeneous optical layers. The problems that should be addressed with this material include a high temperature required for evaporation and the tendency for the formation of multiple crystal phases within the area exposed to e-beam [8]. However, by tolerating a certain layer inhomogeneity, we could gain a better adhesion to the optical fiber and to low index SiO_2 material. MgF_2 could be another low index material, though it acquires a high tensile stress. This is a general feature of fluorides that limits the thickness of MgF_2 layers [9].

III. Thin-Film Structures and Characteristics

In this work, we tested different materials and temperature regimes to achieve good adhesion to a fiber end facet. The dielectric thin film was deposited onto a single-mode fiber, typically assembled with a FC/PC-connector. We discovered that high temperature ($\sim$150°C and above) has a detrimental effect on the coatings and leads to a poor adhesion and structural defects due to thermal stress, as shown in Fig. 1 (left).

TiO_2 as a high index material, proved to have a weaker adhesion to fiber compared to ZrO_2. However, ZrO_2 tablets have a tendency to spit during the evaporation, as shown in Fig. 1 (middle), unless they are not carefully heated and a spiral e-beam scan is used. Best results have been achieved when the sample was heated to 90 °C with ZrO_2 as a high index material ($n = 1.88$ at 1 μm, evaporation rate 0.1–0.2 nm/s, $1.3 \cdot 10^{-4}$ mbar pressure) and SiO_2 as a low index material ($n = 1.44$ at 1 μm, evaporation rate 0.35 nm/s, pressure around $5 \cdot 10^{-5}$ mbar). Oxygen was added to sustain the pressure. An example of a successful coating is shown in Fig. 1 (right).

Since the exact refractive index and actual evaporation rate depend on various factors, e.g., chamber gas partial pressures, substrate temperature, and evaporation beam shape, a careful calibration of all parameters is needed, while the mirror design should be reasonably tolerant to small perturbations in the evaporation process.

The dichroic mirror aimed at the current application should satisfy quite challenging requirements. The mirror should provide a high throughput at pump wavelength λ_p and have a prescribed reflectivity at signal wavelength λ_s, which determines the output coupling of the laser cavity. An ideal spectral profile for this purpose would be a step-like shape. In practice, however, the mirror quality is largely determined by the spectral slope $dR/d\lambda$ at the range between λ_p and λ_s, as shown in Fig. 2. It is obvious that an increase in the reflectivity slope becomes progressively difficult to achieve for smaller offsets between λ_p and λ_s.

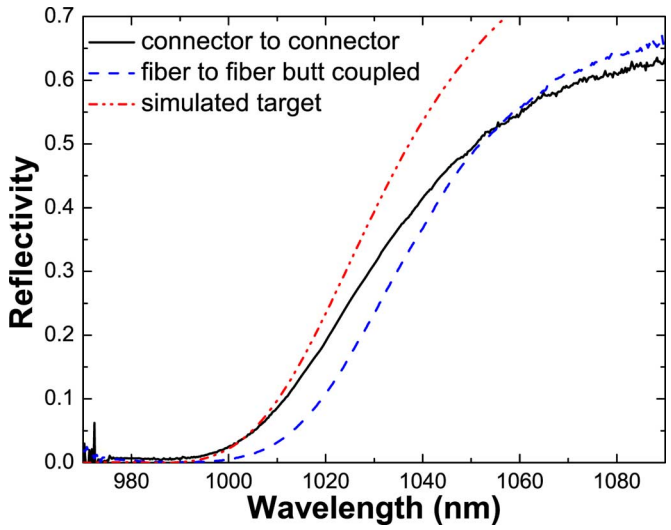

Fig. 2. Reflectivity spectra of typical dichroic coating of the fiber. The current design had 21 layers of ZrO_2 and SiO_2. The variation in the spectral response may originate from small air gaps between the coated fiber and the matched fiber end.

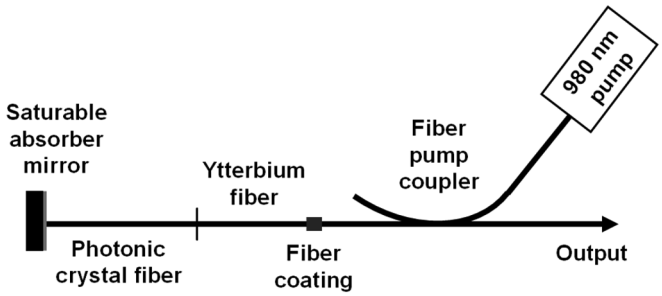

Fig. 3. Passively mode-locked ytterbium fiber laser using an integrated fiber mirror.

In this study, we aim at a dichroic fiber mirror for an ytterbium fiber laser that provides a low reflectivity at the pump wavelength ($R_p < 0.5\%$ at 980 nm) and reflectivity of $R_s \sim 40\%$ at 1040 nm that would ensure an acceptable output coupling. The results of the mirror deposition are presented in Fig. 2. The evaporation process was found to be well controlled and allowed for repeatable results. Since the thicker structures would not improve the overall performance significantly, as expected from numerical modeling, the number of layers was limited to 21–27.

IV. Experimental Results

To take advantage of the fiber mirror in a pulse oscillator, we have built a short ytterbium fiber laser in order to achieve a high fundamental repetition rate. Fig. 3 shows the setup of the mode-locked fiber laser.

The laser cavity comprises 8 cm of highly doped ytterbium fiber with a dispersion of $+0.025$ ps^2/m. The PCF (details in [1]) with a dispersion of -0.025 ps^2/m and a length of 10 cm was spliced to the ytterbium fiber to offset the net cavity dispersion to the anomalous regime. The 980-nm pump light was launched through a 980/1040-nm dichroic fiber coupler, as seen from

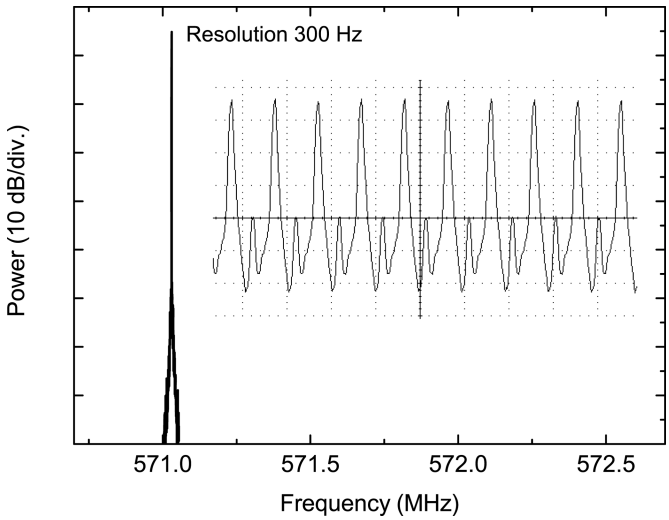

Fig. 4. RF spectrum and scope trace of the pulse train indicate the repetition of 571 MHz corresponding to the fundamental frequency of the laser cavity. The small structures between the pulses are caused by the ringing of the detecting photodiode.

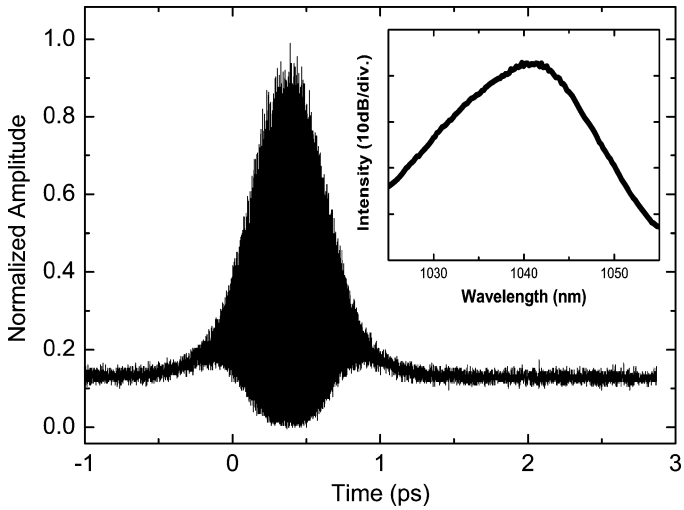

Fig. 5. Interferometric autocorrelation of 572-fs pulse and mode-locked pulse spectrum (inset).

Fig. 3. The essential feature of this cavity defined by the dichroic fiber mirror and semiconductor saturable absorber mirror is that the pumping coupler could be positioned auxiliary to the cavity which in turn allows for length reduction. The pump laser diode provides up to 300 mW of power.

The resonant absorber mirror used in this study is similar to the absorber described in [10]. It was fabricated using solid-source molecular-beam epitaxy on n-type GaAs (100) substrate. The sample had a bottom mirror comprising 30 pairs of AlAs–GaAs quarter-wave layers forming a distributed Bragg reflector (DBR). The DBR's stopband had a center wavelength of 1050 nm and approximately 120-nm bandwidth (990–1110 nm). Throughout this study, we used quantum-well absorber material that consisted of five InGaAs quantum wells with 6-nm thickness and 16-nm GaAs barriers. The quantum-well structure was sandwiched between a $\sim$100-nm GaAs buffer layer and a 100-nm GaAs cap layer. The photoluminescence emission from the quantum wells was picked at 1045 nm. Finally, a postgrowth implantation with heavy ions for decreasing absorber recovery time was applied.

The mode-locking was self-starting at a pump power of 150 mW. Measurements performed with an RF spectrum analyzer and a digital sampling oscilloscope revealed that the short all-fiber cavity enabled a 571.03-MHz fundamental repetition rate with an average power of up to 15 mW, as shown in Fig. 4. To the best of our knowledge, this is the highest fundamental repetition rate reported for an ytterbium fiber laser operating around 1 μm. The autocorrelation of a 572-fs pulses and corresponding spectrum are shown in Fig. 5. The pulses are slightly chirped in the output pigtail.

The higher repetition rate could be further increased by using PCF doped with ytterbium that offers both gain and anomalous dispersion [2] and hence would allow for shorter cavities.

V. Conclusion

The fabrication of a dichroic 980/1040 fiber end mirror as an output coupler and pump combiner simultaneously has been described. Such a configuration assembled with PCF for dispersion compensation enables a 572-fs all-fiber laser with a 571-MHz fundamental repetition rate, which is, to the best of our knowledge, the highest frequency reported for 1-μm ytterbium fiber laser. We expect that dichroic fiber coatings would simplify a number of laser systems and that the increased repetition rate would be useful in high-speed chemical reaction imaging, quasi-continuous-wave inspection systems, high-speed micromachining, and two-photon microscopy.

References

[1] A. Isomäki and O. G. Okhotnikov, "All-fiber ytterbium soliton mode-locked laser with dispersion control by solid-core photonic bandgap fiber," *Opt. Express*, vol. 14, no. 10, pp. 4368–4373, 2006.

[2] A. Isomäki and O. G. Okhotnikov, "Femtosecond soliton mode-locked laser based on ytterbium-doped photonic bandgap fiber," *Opt. Express*, vol. 14, pp. 9238–9243, 2006.

[3] Endo and G. Ghosh, "Estimation of timing jitter in a passively mode-locked tunable fiber laser," in *Tech. Dig. CLEO/Pacific Rim '99*, Seoul, South Korea, 30 Aug.–3 Sep. 1999, vol. 2, pp. 415–416.

[4] K. H. Guenther, "Physical and chemical aspects in the application of thin films on optical elements," *Appl. Opt.*, vol. 23, pp. 3612–3632, 1984.

[5] H. G. Shanbhogue, C. L. Nagendra, M. N. Annapurna, S. A. Kumar, and G. K. M. Thutupalli, "Multilayer antireflection coatings for the visible and near-infrared regions," *Appl. Opt.*, vol. 36, pp. 6339–6351, 1997.

[6] K. H. Guenther, "Microstructure of vapor-deposited optical coatings," *Appl. Opt.*, vol. 23, pp. 3806–3816, 1984.

[7] M. Cesro and G. Carter, "Ion-beam and dual ion-beam sputter deposition of tantalum oxide films," *Opt. Eng.*, vol. 34, pp. 596–606, 1995.

[8] *Cerac Materials News*, vol. 16, no. 1, pp. 2–3, Mar. 2006.

[9] R. Thielsch, J. Heber, T. Feigl, and N. Kaiser, "Stress, microstructure and thermal-elastic properties of evaporated thin MgF2–films," in *Opt. Interference Coatings (OIC), OSA Tech. Dig. Series (Optical Soc. America, 2004)*, Tucson, AZ, Jun. 24, 2004, Paper ThE6.

[10] R. Herda and O. G. Okhotnikov, "Dispersion compensation-free fiber laser mode-locked and stabilized by high-contrast saturable absorber mirror," *IEEE J. Quantum Electron.*, vol. 40, no. 7, pp. 893–899, Jul. 2004.